isvr Institute of Sound and Vibration Research

Harmonic Analysis of Semi-Active Dampers

Y. Liu, T.P. Waters, M.J. Brennan and B.R. Mace

ISVR Technical Memorandum No 900

November 2002

University of Southampton

SCIENTIFIC PUBLICATIONS BY THE ISVR

Technical Reports are published to promote timely dissemination of research results by ISVR personnel. This medium permits more detailed presentation than is usually acceptable for scientific journals. Responsibility for both the content and any opinions expressed rests entirely with the author(s).

Technical Memoranda are produced to enable the early or preliminary release of information by ISVR personnel where such release is deemed to the appropriate. Information contained in these memoranda may be incomplete, or form part of a continuing programme; this should be borne in mind when using or quoting from these documents.

Contract Reports are produced to record the results of scientific work carried out for sponsors, under contract. The ISVR treats these reports as confidential to sponsors and does not make them available for general circulation. Individual sponsors may, however, authorize subsequent release of the material.

UNIVERSITY OF SOUTHAMPTON

INSTITUTE OF SOUND AND VIBRATION RESEARCH

DYNAMICS GROUP

Harmonic Analysis of Semi-Active Dampers

by

Y. Liu, T.P. Waters, M.J. Brennan and B.R. Mace

ISVR Technical Memorandum No: 900

November 2002

Authorised for issue by
Professor M.J. Brennan
Group Chairman

Abstract

Semi-active control strategies can combine the reliability and lower power requirements of passive devices with the versatility, adaptability and higher performance of fully active systems. This report studies the vibration isolation performance of a semi-active single-degree-of freedom (SDOF) system to a pure-tone excitation. The aim is to minimize the response of the system to base excitation in terms of the root-mean-square (RMS) acceleration and RMS relative displacement between the mass and the base. The performance due to a passive damper, a skyhook damper, and five semi-active dampers are compared. Various control algorithms have been suggested in the past. Many are of the on-off variety, which combine a control law together with a condition function. In this report, five control algorithms based on skyhook control, balance control and adaptive damping control are studied. Issues concerning practical implementation are also discussed. Numerical simulations are presented that evaluate the suitability of these algorithms for vibration isolation of harmonic excitation. An experiment was set up to implement semi-active damping using an electromechanical damper. The results show that semi-active systems can reduce the response at resonance without worsening higher frequency isolation performance.

Table of Contents

1. Introduction

The design of passive isolation systems to isolate a vibration sensitive body from base excitation is often achieved by insertion of resilient materials between the sensitive body and the disturbing structure. Considering a single degree of freedom (SDOF) system, such a passive isolator can be modelled at low frequencies as a spring and a damper in parallel. The stiffness is used to determine the corner frequency ω_n, of the isolator, which is where the isolator starts to become affective. For disturbances at frequencies above $\sqrt{2}\omega_n$, the absolute transmissibility of the system is less than unity and vibration isolation occurs. When the disturbance frequency is less than $\sqrt{2}\omega_n$, vibration amplification occurs. For disturbance frequencies much lower than the corner frequency, the absolute transmissibility is unity. When the disturbance frequency approaches the natural frequency of the system, a resonant condition occurs and the transmissibility is unbounded if no damping is present in the isolator. The addition of passive damping reduces the resonance response but must be kept small to provide good high frequency isolation. There is trade-off between the control of vibration at resonance and the higher frequency performance.

Active isolation systems can be used when greater performance is required and passive techniques alone cannot perform adequately. However, the addition of active control makes the system more complex and the number of issues that need to be addressed is increased. Some issues that arise due to the addition of the active system are the selection of actuators and sensors, weight constraints, power requirements, stability, robustness, closed-loop performance and potential situations when the active system fails.

Semi-active vibration control refers to the use of devices with variable properties to control or suppress vibrations of dynamic systems. Semi-active control strategies can combine the reliability and lower power requirements of passive devices with the versatility, adaptability and higher performance of fully active systems. The particular benefits of semi-active methods are that (as with adaptive-passive methods) the system parameters can be changed with time to retain optimal performance and (unlike adaptive-passive methods) higher levels of optimization can be achieved due to the rapid time-variation achievable.

Semi-active dampers and shock absorbers have been in existence for more than two decades. Introduced by Karnopp and Crosby in the early 1970's [1, 2], semi-active dampers have been studied and used in a wide range of applications. Semi-active dampers are a class of dampers

that draw small amounts of energy to operate a valve to adjust the damping level and reduce the amount of energy that is transmitted from the source of vibration to the suspended equipment. Therefore, the force generated by a semi-active damper is directly proportional to the relative velocity across the damper just like a passive damper. Figure 1 shows the schematic of a SDOF system with a passive, active and semi-active damper, where m is the mass of the suspended equipment, k is the spring stiffness, and F_c is the active control force.

The virtues of active and semi-active dampers versus traditional, passive dampers have been addressed in many studies [1-9]. Various control algorithms have been suggested in the past. Many are of the on-off variety, which combine a control algorithm together with a condition function. There exists an abundance of research on the application of semi-active dampers for vehicle primary suspensions and building structural control, but relatively little research has focused on the shock and vibration.

This report is concerned with the use of a simple semi-active isolation system, comprising a semi-active damper together with a passive spring, for vibration isolation of base excitation. The primary purpose of this study is to analyse the behaviour of a simple semi-active SDOF system subjected to a pure-tone input. A base-excited SDOF system is used to compare the vibration isolation due to a conventional passive damper, a skyhook damper, and different types of semi-active dampers. Although more complicated feedback control strategies offer great possibilities in many situations, it is probable that significant performance gains can be realized with basic control strategies. In the initial phases of the numerical simulations, five basic strategies are studied. The semi-active dampers investigated in this study can be classified into three types according to control algorithms: skyhook control dampers, balance control dampers and adaptive damping control dampers, All of which can be further divided into on-off and continuously variable semi-active dampers. The second purpose is to evaluate the benefits of various semi-active control algorithms that are commonly considered.

The main body of this report consists of 6 sections. Following this introduction, section 2 gives a detailed description of the five semi-active control algorithms of interest. Section 3 describes the model development. The numerical problems met when doing simulations with semi-active dampers are discussed in this section. The conditions for chatter and jerk problems are presented and anti-jerk semi-active control methods are suggested. The controllers are implemented in Matlab/Simulink. In Section 4, a simple SDOF system with semi-active dampers subjected to a pure-tone excitation is evaluated. The vibration isolation performances of semi-active systems are compared with passive and skyhook systems. It is

established that similar to a skyhook damper, both the on-off and continuously variable dampers exhibit the ability to lower the resonance peak without worsening the isolation at higher frequencies. Section 5 describes the experimental work on semi-active vibration isolation using an electromechanical damper. The electromechanical device is a Colossus 12MB Loudspeaker Driver. Physical parameters of the device were measured and an adaptive damping semi-active control algorithm was implemented using the experimental setup. A summary and some conclusions are drawn in section 6. There are three appendixes to this report. Appendix A discusses the isolation properties of semi-active dampers. The reason why semi-active dampers are able to isolate at frequencies well below those for passive dampers, even though they do not add any energy to the system is investigated using its passive equivalent. The effects of non-zero off state damping on the isolation performance are also discussed. Appendix B is a list of the equipment used for the experiment. Appendix C is the specification of the Colossus 12 MB Loudspeaker Driver.

2. Nonlinear Control Strategies for Semi-Active Damping

This section introduces five semi-active control algorithms for a SDOF system, which are continuous skyhook control, on-off skyhook control, continuous balance control, on-off balance control and adaptive damping control. Detailed information on each control algorithm is presented.

In both passive and semi-active dampers, the magnitude of the damper force is dependent on the relative velocity across the damper. However, the force versus velocity curve of each type is not identical. In passive damping, the damper has a pre-defined characteristic in units of force/velocity as shown in Figure 2. A change in the relative velocity across the damper, $\dot{x} - \dot{x}_0$, will change the force exerted by the damper, F_d. Referring to Figure 2, the magnitude and direction of the force exerted depend only on the relative velocity across the damper. In many applications, the slope of the force versus velocity is nonlinear, and tends to decrease as the velocity increases [10]. However, in the passive model considered in this report, the slope of the curve is constant.

Although the direction of the damper force in semi-active dampers still depends on the relative velocity across the damper, the magnitude of the damper force is adjustable. The damping value is adjusted by a controller that can be programmed to any type of control algorithm.

Semi-active dampers may be of the on-off type or of the continuously variable type. A damper of the first type is switched, in accordance with a suitable control algorithm, between alternate on and off damping states. In its on state, the damping coefficient is of a pre-selected relatively high magnitude. The term "damping coefficient" means the ratio of the damper force generated by the damper to the relative velocity across the damper, which is not necessarily linear. In its off state, the damping coefficient and corresponding damper force of the damper is of relatively low magnitude. This may be almost zero, but in many practical applications, a magnitude greater than zero is desired. A continuously variable semi-active damper is also switched during operations between an on and off state. In the off state, its damping coefficient and corresponding damper force is approximately zero or of other low magnitude. However, when a continuously variable damper is in its on state, the damping coefficient and corresponding damper force may be changed over a range of different magnitudes. The concept of semi-active damping concept is illustrated in Figure 3. The shaded part of the graph represents the range of damping coefficients. The damping

coefficient of a semi-active on-off type damper is a discontinuous function in the time domain, which can be seen in Figure 4 (a). The damping coefficient of a semi-active continuous type damper is a continuous function as shown in Figure 4 (b).

2.1 Continuous Skyhook Control

The initial semi-active system was based on skyhook semi-active control, which was invented by Karnopp in reference [2] to emulate the skyhook damper. This scheme does not require hydraulic power. Forces were generated in a damper by modulating its fluid-flow orifices. The name "skyhook" is derived from the fact it was a passive damper hooked to an imaginary sky. Considering the SDOF system with a skyhook damper in Figure 5, it can be realized using active control by programming the active force as

$$F_c = c_{sky}\dot{x} + k(x - x_0) \tag{2.1}$$

Where F_c is the active control force, k is the spring stiffness, and c_{sky} is the skyhook damping.

The semi-active continuous skyhook control algorithm was designed to modulate the force generated by a passive device to approximate the force that would be generated by a damper connected to ground. The SDOF system with a semi-active damper is schematically shown in Figure 6. The semi-active device is installed in the place of the conventional damper, and the device is passive, but the force generated by the device is controllable. The excitation and response signals are fed into a controller to produce a desired damping force. The passive device can only absorb vibration energy, so the product of the damper force, F_{sa}, and the relative velocity, $\dot{x} - \dot{x}_0$, must great equal than zero

$$F_{sa}(\dot{x} - \dot{x}_0) \geq 0 \tag{2.2}$$

i.e., the power associated with the semi-active damper force, F_{sa}, is always dissipated. Thus, if the relative velocity is increasing, $(\dot{x} - \dot{x}_0) > 0$, F_{sa} must be positive, and if $(\dot{x} - \dot{x}_0) < 0$, F_{sa} must be negative.

Defining the up direction as positive and down as negative, consider first the case when the mass is moving upwards separating from the base. Under the ideal skyhook configuration, the desired value of F_{sky} is

$$F_{sky} = -c_{sky}\dot{x} \tag{2.3}$$

Where F_{sky} is the skyhook damper force. For the semi-active equivalent model, the damper force due to the semi-active damper is

$$F_{sa} = -c_{sa}(\dot{x} - \dot{x}_0) \tag{2.4}$$

Where F_{sa} is the semi-active force, and c_{sa} is the semi-active damping coefficient. In order for the semi-active equivalent model to perform like the skyhook model, the damper forces must be equal. The semi-active damping constant can thus be found by setting equation (2.3) to be equal to equation (2.4) in terms of the skyhook damping. The semi-active damper force can then be found for the case when both $\dot{x}$ and $\dot{x} - \dot{x}_0$ are positive, which gives

$$c_{sa} = \frac{c_{sky}\dot{x}}{\dot{x} - \dot{x}_0} \tag{2.5}$$

and

$$F_{sa} = \frac{c_{sky}\dot{x}}{\dot{x} - \dot{x}_0}(\dot{x} - \dot{x}_0) \tag{2.6}$$

Next, consider the case when both $\dot{x}$ and $\dot{x} - \dot{x}_0$ are negative. Now the mass is moving downwards. The skyhook damper force would be in the positive direction, hence

$$F_{sky} = c_{sky}\dot{x} \tag{2.7}$$

Following the same procedure as the first case, equating the damper forces reveals the same semi-active damper force as the first case. Thus it can be concluded that when the product of the $\dot{x}$ and $\dot{x} - \dot{x}_0$ is positive, the semi-active damping coefficient is defined by equation (2.5) and the semi-active damper force is defined by equation (2.6).

Now consider the case when the mass is moving upwards and the mass and base are moving towards each other. The skyhook damper would again apply a force on the mass in the negative direction. In this case, the semi-active damper cannot apply a force in the same direction as the skyhook damper. For this reason, the damping should be set to zero thus minimizing the force acting on the mass.

The final case to consider is the case when the mass is moving downwards and is separating from the base. Again, in this condition, the skyhook damper force and the semi-active damper force are not in the same direction. The skyhook damper force is in the positive direction,

while the semi-active damper force is in the negative direction. The best that can be achieved is to set the damping in the semi-active damper to zero.

Summarizing these four conditions, the well-known semi-active skyhook control algorithm is given by

$$F_{sa} = \begin{cases} c_{sky}\dot{x} & \dot{x}(\dot{x}-\dot{x}_0) \geq 0 \\ 0 & \dot{x}(\dot{x}-\dot{x}_0) < 0 \end{cases} \tag{2.8}$$

Whenever it is required to supply energy to the system, the best the device can do is to supply no force at all. Otherwise the device provides a force proportional to the absolute velocity of the mass. The switching of the device can be controlled by the term $\dot{x}(\dot{x}-\dot{x}_0)$, which is called the condition function. If the product of the absolute velocity of the mass, $\dot{x}$, and the relative velocity $\dot{x}-\dot{x}_0$ between the mass and the base is positive, the damper is switched on, so that a force is generated to reduce the acceleration of the mass. If this term is negative, the damper is switched off so that no force is generated. This control scheme intends to closely simulate an ideal skyhook damper. The theoretical semi-active damping required to produce the damping force, F_{sa}, is given by

$$c_{sa} = \begin{cases} \dfrac{c_{sky}\dot{x}}{\dot{x}-\dot{x}_0} & \dot{x}(\dot{x}-\dot{x}_0) \geq 0 \\ 0 & \dot{x}(\dot{x}-\dot{x}_0) < 0 \end{cases} \tag{2.9}$$

Figure 7 is the three-dimensional plot of the semi-active damping required by continuous variable skyhook damper in the above equation. It can be seen from the figure that when the relative velocity $\dot{x}-\dot{x}_0$ is very small, the required damping increases abruptly and tends to infinity, which cannot be provided by practical hardware. The damper constant, c_{sa}, is limited by the physical parameters of the conventional damper. This means that there is both an upper bound, $c_{\max}$, and a lower bound, $c_{\min}$, on c_{sa}. Considering the limitation of the practical hardware, the damping in equation (2.9) can be rewritten as

$$c_{sa} = \begin{cases} \max\left[c_{\min}, \min\left[\dfrac{c_{sky}\dot{x}}{\dot{x}-\dot{x}_0}, c_{\max}\right]\right] & \dot{x}(\dot{x}-\dot{x}_0) \geq 0 \\ c_{\min} & \dot{x}(\dot{x}-\dot{x}_0) < 0 \end{cases} \tag{2.10}$$

2.2 On-Off Skyhook Control

The control algorithm given in equation (2.8) requires a continuous modification of the damper orifice area. To simplify the operation, a simple on-off scheme has been proposed [4]. The on-off damper operates between the sprung mass and the base. It acts as a conventional passive damper during the vibration attenuation portion of the vibration cycle, but a zero damping coefficient is assumed when a passive damper would normally accelerate the mass. The damper force generated is proportional to the relative velocity between the mass and the base, instead of the absolute velocity of the sprung mass. In this case, the damper force and the control logic are governed by

$$F_{sa} = \begin{cases} c_{on}(\dot{x} - \dot{x}_0) & \dot{x}(\dot{x} - \dot{x}_0) \geq 0 \\ 0 & \dot{x}(\dot{x} - \dot{x}_0) < 0 \end{cases} \tag{2.11}$$

where c_{on} is the on state damping constant of the on-off damper.

In practice, zero damping coefficients are impossible when the damper is switched off. Therefore, the damping coefficient is actually switched between a high value and a low value. Considering the non-zero off state damping, the control algorithm in equation (2.11) can be restated as

$$c_{sa} = \begin{cases} c_{\max} & \dot{x}(\dot{x} - \dot{x}_0) \geq 0 \\ c_{\min} & \dot{x}(\dot{x} - \dot{x}_0) < 0 \end{cases} \tag{2.12}$$

where $c_{\max}$ and $c_{\min}$ are the maximum and minimum coefficients of the on-off damper respectively. Usually the on state damping $c_{\max}$ is much greater than off state damping $c_{\min}$, and $c_{\min}$ should as small as possible.

Figure 8 shows the velocity relationship of the two skyhook control algorithms. If the product of the absolute velocity of the mass and the relative velocity between the mass and the base is positive, the damper is switched on, so that a force is generated to attenuate the acceleration. Otherwise, the damper is switched off. When the relative velocity across the damper is positive, the damper force acts to pull down on the suspended mass; when the relative velocity is negative, the damper force acts to push up on the mass. Thus when the absolute velocity of the mass is negative, it is travelling downwards and the on state damping is desired to push up on the mass; while minimum damping is desired to continue pulling down on the mass. However, if the absolute velocity of the body mass is positive and the mass is

travelling upwards, the on state damping is desired to pull down on the mass, while the minimum value of damping is desired to further push the mass upwards.

Both the continuous skyhook control and on-off skyhook control algorithms intend to produce the effect of skyhook damping. However, there are differences between them, which can be found by interpreting the damping force in terms of phase and amplitude. The original expression for the continuous skyhook control in equation (2.8) can provide the same amplitude and phase in its on state as those of a skyhook damper. Due to the practical limitation of physical systems, however it can only provide the same amplitude and phase during part of the on state period. In addition, there are non-zero off state damping effects. The on-off skyhook control can only ensure that the semi-active damping force is the same sign of the desired skyhook damping force. The magnitude is not representative of the skyhook damper force anymore, although it is shown that it gives similar results. It is not, however, "skyhook" anymore in some sense.

2.3 On-Off Balance Control

Considering a passive SDOF system subject to base excitation, the acceleration response of the suspended mass due to the base excitation can be expressed as

$$\ddot{x} = -\frac{1}{m}(F_k + F_d) \tag{2.13}$$

where F_k and F_d are the spring and damper forces respectively, which are given by

$$\begin{aligned} F_k &= k(x - x_0) \\ F_d &= c(\dot{x} - \dot{x}_0) \end{aligned} \tag{2.14}$$

and k and c are the constant spring rate and damping coefficients respectively. The amplitude of the acceleration of the mass due to harmonic base excitation can be expressed in terms of the spring and damper forces[5]

$$|\ddot{x}| = (|F_k| + |F_d|)/m \quad \begin{cases} t_0 < t < t_0 + \dfrac{\tau}{4} \\ t_0 + \dfrac{\tau}{2} < t < t_0 + \dfrac{3\tau}{4} \end{cases} \tag{2.15}$$

$$|\ddot{x}| = (|F_k| - |F_d|)/m \quad \begin{cases} t_0 + \dfrac{\tau}{4} < t < t_0 + \dfrac{\tau}{2} \\ t_0 + \dfrac{3\tau}{4} < t < t_0 + \tau \end{cases} \tag{2.16}$$

where t_0 is the start time, and τ is the period of vibration. Figure 9 shows the inertial force ($m\ddot{x}$), spring force and damper force of a passive SDOF system subject to harmonic base excitation. Most of the time, it is desired for the acceleration of the mass to be small, but it is evident from equation (2.15) and Figure 9 that the damper force tends to increase the acceleration amplitude of the mass during a part of vibration cycle. In the remaining part of a vibration cycle, the mass acceleration response due to the damper force would be attenuated, which can demonstrated by equation (2.16) and Figure 9. Poor vibration isolation performance of heavily damped passive systems is attributed to this phenomenon. Isolation performance of passive isolators due to fixed damping deteriorates at high excitation frequencies, when the magnitude of the damper force is dominant.

An analogous phenomenon also exists in shock isolation systems[11]. Due to the inherent limitations of passive shock isolators, specifically with constant damping, various dual phase damper concepts have been proposed and analyzed [12, 13]. In dual phase dampers, the damping coefficient varies as a function of the relative velocity across the damper. The damper assumes a high damping value corresponding to low relative velocity, and the damping coefficient is reduced considerably at high relative velocity. For intermediate relative velocities there is a linear transition between high and low values of damping.

An on-off damping mechanism may be realized, which operates as a conventional passive damper during the part of the cycle to reduce the acceleration of the mass as demonstrated in equation (2.16) and Figure 9. The damping mechanism assumes zero damping during the portion of the cycle when a passive damper would normally increase the amplitude of the acceleration of the mass. In reference [5], an on-off hydraulic damper realized using a two position valve operated by a solenoid relay was described.

Based on the above discussion, the damper force will cause an increase in the acceleration of the mass whenever forces due to the spring and the damper have the same sign, or equivalently when the relative velocity and relative displacement have the same sign. A control algorithm to ensure that this does not occur is [5]

$$F_{sa} = \begin{cases} c_{on}(\dot{x} - \dot{x}_0) & (x - x_0)(\dot{x} - \dot{x}_0) \le 0 \\ 0 & (x - x_0)(\dot{x} - \dot{x}_0) > 0 \end{cases} \tag{2.17}$$

where c_{on} is the on state damping constant of the on-off damper.

The control algorithm shows that whenever the damper force accelerates the mass, it is switched off. Whenever the damper force reacts with the spring force so as to decelerate the mass, the damper is switched on. Since the purpose of the damping force in this algorithm is to cancel the spring force, it is termed "balance control". This control algorithm is relatively easy to implement in some applications such as vehicle suspensions, as the relative displacement and the relative velocity can be easily measured.

The corresponding semi-active damping considering non-zero off state damping is given by

$$c_{sa} = \begin{cases} c_{\max} & (x - x_0)(\dot{x} - \dot{x}_0) \le 0 \\ c_{\min} & (x - x_0)(\dot{x} - \dot{x}_0) > 0 \end{cases} \tag{2.18}$$

where $c_{\max}$ and $c_{\min}$ are the maximum and minimum coefficients of the on-off damper.

2.4 Continuous Balance Control

The control algorithm in equation (2.17) has the potential for improvement. During the on state of the damper, the instantaneous damper force is seldom exactly equal in magnitude to the instantaneous spring force. Consequently, the surplus force will still accelerate the mass. In reference [14], a continuously variable control policy has been proposed, which can be considered as a further development of the preceding control algorithm in equation (2.17). In this control algorithm, the damping coefficient is continuously variable, depending on the relative displacement and the relative velocity

$$F_{sa} = \begin{cases} -k(x - x_0) & (x - x_0)(\dot{x} - \dot{x}_0) \le 0 \\ 0 & (x - x_0)(\dot{x} - \dot{x}_0) > 0 \end{cases} \tag{2.19}$$

This control algorithm shows that if the spring force and the damper force exerted on the mass are in the same direction, to reduce the sprung mass acceleration, the damper force should be minimum. On the other hand, if the spring force and the damper force are in opposite direction, then the damper force should be adjusted in such a way that it equals the spring force in magnitude so as to produce zero acceleration of the sprung mass. The semi-active damping required for this control algorithm is given by

$$c_{sa} = \begin{cases} \dfrac{-k(x - x_0)}{\dot{x} - \dot{x}_0} & (x - x_0)(\dot{x} - \dot{x}_0) \le 0 \\ 0 & (x - x_0)(\dot{x} - \dot{x}_0) > 0 \end{cases} \tag{2.20}$$

Figure 10 shows the three-dimensional plot of the damping coefficient defined by equation (2.20). It can be seen from the figure that the damping coefficient goes to infinity at $\dot{x}-\dot{x}=0$, which cannot be implemented in practice. Similarly to equation (2.10), the damper constant c_{sa} saturates at the upper and lower bounds imposed by the physical parameters of the damper. Considering the practical hardware constraints, the damping coefficient can be rewritten as

$$c_{sa}=\begin{cases}\max\left[c_{\min},\min\left[\dfrac{-k(x-x_0)}{\dot{x}-\dot{x}_0},c_{\max}\right]\right] & (x-x_0)(\dot{x}-\dot{x}_0)\le 0\\ c_{\min} & (x-x_0)(\dot{x}-\dot{x}_0)>0\end{cases} \tag{2.21}$$

Both on-off and continuous two balance control algorithms program the damping force so that it can cancel the spring force whenever the damping force and the spring force have the same sign. According to equation (2.17) and (2.18), since the on-off balance damper can only produce a damping force proportional to the relative velocity across the damper in its on state, it cannot ensure the damping force is exactly equal to the spring force. Depending on the dynamics of the system and the damping, $c_{\max}$, the spring force can partly be cancelled or even sometimes the spring force can be over cancelled which might change the static equilibrium of the system. The continuous balance can cancel the spring force in theory, but due to the hardware limitations, it might only be able to realise this during part of the on state period.

2.5 Adaptive Damping Control

The last control algorithm considered in this report for harmonic analysis is a adaptive damping method, which is to adapt the damping constant according to the disturbance frequency. The idea of this control algorithm is quite straightforward. The passive system can only provide isolation at the frequency range $\omega/\omega_n>\sqrt{2}$, where ω is the excitation frequency and ω_n is the natural frequency. Increasing the damping coefficient in the frequency range $\omega/\omega_n\le\sqrt{2}$ will reduce the resonance peak, while the isolation performance in the frequency range $\omega/\omega_n>\sqrt{2}$ will be degraded. As illustrated in Figure 11, the ideal case for harmonic vibration isolation is that when $\omega/\omega_n\le\sqrt{2}$, the damping coefficient should have a larger value, and when $\omega/\omega_n>\sqrt{2}$, then the damping coefficient should have small value. To realize this, the following control algorithm has been established

$$c_{sa} = \begin{cases} c_{\max} & \text{RMS}(\ddot{x}) \geq RMS(\ddot{x}_0) \\ c_{\min} & \text{RMS}(\ddot{x}) \geq RMS(\ddot{x}_0) \end{cases} \tag{2.22}$$

The terms $RMS(\ddot{x})$ and $RMS(\ddot{x}_0)$ are calculated over a time period much longer than the natural period of the system. The control algorithm uses the Root-Mean-Square (RMS) value of the response as the condition function to adjust the damping. When the RMS value of the response $\ddot{x}$ is greater than the RMS of the base acceleration, no isolation occurs and the damper is switched to its maximum value. Otherwise, the damper is switched off so that no damping is presented in the system. For this semi-active control algorithm, the damper works in a bi-state (on-off) manner. It works as a common passive damper, which can be switched from one value to the other. This is the simplest and cheapest way to implement a control algorithm since it does not need the damper to switch alternately between the on and off states from during one period. It is very useful for vibration isolation of rotating machines such as washing machines: the high damping value $c_{\max}$ is used when the drum is at low speed, i.e., during acceleration or deceleration, while the low damping value $c_{\min}$ is used for high speed. The disadvantage of this control algorithm is that it can only applicable to harmonic vibration isolation.

2.6 Summary

Details of five semi-active control algorithms of interest have been presented in this section. The original control algorithms and the theoretical semi-active damping coefficient required for the desired damping force discussed in this section are summarized in Table 1. Considering the constraints by the physical parameters of the conventional damper, the damping coefficient of the semi-active damper must lay in the range $[c_{\min}, c_{\max}]$. For the continuous skyhook control and continuous balance control, the denominator in the expressions of the damping equation will introduce high nonlinearity into the system. There are two issues need to be addressed when considering implementation of the semi-active dampers: practical available damping and jerk caused by sudden changes in damping force. These will be studied in the next section.

3. Numerical Model

This section is concerned with the model development for simulations of a SDOF system with semi-active damper. The numerical problems encountered when doing simulations with semi-active dampers are first discussed. A phenomenon often referred to as chatter occurs with semi-active dampers at low excitation frequencies. The conditions for chatter to occur are demonstrated by studying the dynamics of the system, and a modified control scheme is suggested to avoid the chatter problem. Jerk is associated with chatter which is caused by switching between different states of the damping. A detailed description of an anti-jerk implementation is presented and anti-jerk controllers are developed. Both chatter and jerk can be suppressed using anti-jerk semi-active control algorithms.

3.1 Chatter of Semi-Active Damper

When doing numerical simulations with semi-active dampers, the so-called chatter problem occurs under certain dynamic conditions. To observe the onset and persistence of chatter in semi-active on-off systems, consider the SDOF system shown in Figure 6 and assume that at some time t, the spring is compressed, the damper is off, and the base velocity, $\dot{x}_0$, is large and negative (downward). Since there is currently no damper force, the compressed spring will begin to push the mass upward, and $\dot{x}$ will become positive. With $\dot{x} > 0$ and $\dot{x} - \dot{x}_0 > 0$, the control strategy in equation (2.11) indicates that the damper will turn on to a fixed value. The damper force is tensile, and if the damper force pulling down is greater than the spring force, then the damper force will decelerate the mass and reverse its direction. The mass velocity will become negative while the relative velocity $\dot{x} - \dot{x}_0$ is still positive. The damper will turn off with the process repeating itself as long as the spring is in compression. This switching between on the off state, with $\dot{x}$ remaining near zero is called chatter.

For the semi-active on-off systems, the damper switches due to changes in the sign of the mass velocity, $\dot{x}$, are defined as "$\dot{x}$ switches", while those due to changes in the sign of $\dot{x} - \dot{x}_0$ are called "$\dot{x} - \dot{x}_0$ switches". It is noted that only $\dot{x}$ switches are important with respect to the potential of chatter. This is because $\dot{x}$ switches can be associated with large relative velocity, $\dot{x} - \dot{x}_0$, and thus large damper forces, while $\dot{x} - \dot{x}_0$ switches are always associated with small damper forces. Also, chatter can only occur if the damper and spring force are in opposition, and if the on state damper force is of larger magnitude than the instantaneous spring force. If the damper force is not larger than the spring force, then the damper would not

change the direction of the acceleration and would not initiate chatter. Figure 12 shows a typical damping and spring force when chatter occurs. The conditions for the chatter are summarized in Table 2. If these three conditions are met, chatter will be initiated and will continue until an $\dot{x}-\dot{x}_0$ switch takes place; or either condition (2) or (3) in Table 2 is not met.

Following the analysis in [15], a modified logic is used to eliminate the chatter, which is given in Table 3. When $\dot{x}$ has just changed its sign, if the damper force is of different sign to the spring force, and the magnitude of the damper force is bigger than that of spring force, do not switch the damper until the two conditions are not met.

The same phenomenon can also occur in continuous variable skyhook dampers at lower excitation frequencies. The forces take the form

$$F_k = k(x-x_0) \tag{3.1}$$

$$F_{sa} = \begin{cases} c_{sky}\dot{x} & \dot{x}(\dot{x}-\dot{x}_0) \geq 0 \\ 0 & \dot{x}(\dot{x}-\dot{x}_0) < 0 \end{cases} \tag{3.2}$$

For the expression $\dot{x}(\dot{x}-\dot{x}_0)$ in the condition function, there are two special cases that may arise. In the first case, when $\dot{x}=0$, the desired damper force is $F_{sa}=0$; in the second case, $\dot{x}\neq 0$ but $\dot{x}-\dot{x}_0=0$, and in this case the damper force is $c_{sky}\dot{x}$. In this case, chatter might occur.

Suppose $\dot{x}-\dot{x}_0 \approx 0$, then $x-x_0 \approx$ constant; consider two cases:

(a) $\dot{x}>0$

(b) $\dot{x}<0$

(a) $\dot{x}>0$, the mass is moving up. The acceleration of the mass can be expressed as

$$\ddot{x} = \begin{cases} -\frac{k}{m}(x-x_0) - \frac{c_{sky}}{m}\dot{x} & \dot{x}(\dot{x}-\dot{x}_0) > 0 \\ -\frac{k}{m}(x-x_0) & \dot{x}(\dot{x}-\dot{x}_0) < 0 \end{cases} \tag{3.3}$$

where $-\frac{k}{m}(x-x_0)$ is nearly a constant, which can be denoted as B, so the acceleration can be further expressed as

$$\ddot{x} = \begin{cases} B - \frac{c_{sky}}{m}\dot{x} & \dot{x}(\dot{x} - \dot{x}_0) > 0 \\ B & \dot{x}(\dot{x} - \dot{x}_0) < 0 \end{cases} \tag{3.4}$$

- When $\dot{x}(\dot{x} - \dot{x}_0) < 0$, $\dot{x} - \dot{x}_0 < 0, B > 0$, the velocity takes the form of $\dot{x} \approx D + Bt$, and is increasing;

- When $\dot{x}(\dot{x} - \dot{x}_0) > 0$, $\dot{x} - \dot{x}_0 > 0, B < 0$, the velocity takes the form of $\dot{x} \approx E + Bt - \frac{c}{m}x$, which is increasing when $B - \frac{c}{m}\dot{x} > 0$, and decreasing when $B - \frac{c}{m}\dot{x} < 0$.

where D and E are constants associated with the velocity. If $\dot{x}$ continues to increase when $\dot{x} - \dot{x}_0$ passes through zero, no chatter occurs. If $\dot{x}$ decreases when $\dot{x} - \dot{x}_0$ passes through zero, chatter might occur. However $\dot{x}$ decreases when $B - \frac{c}{m}\dot{x} < 0$, which indicates that $B < \frac{c}{m}\dot{x}$, that is the damper force is greater than the spring force in amplitude.

(b) $\dot{x} < 0$, and the mass is moving up. The acceleration of the mass can still be expressed by equation (3.3) and (3.4).

- When $\dot{x}(\dot{x} - \dot{x}_0) < 0$, $\dot{x} - \dot{x}_0 > 0, B < 0$, the velocity takes the form of $\dot{x} \approx D + Bt$, and is decreasing;

- When $\dot{x}(\dot{x} - \dot{x}_0) > 0$, $\dot{x} - \dot{x}_0 < 0, B > 0$, the velocity takes the form of $\dot{x} \approx E + Bt - \frac{c}{m}x$, which is increasing when $B - \frac{c}{m}\dot{x} > 0$, and decreasing when $B - \frac{c}{m}\dot{x} < 0$.

If $\dot{x}$ continues to decrease when $\dot{x} - \dot{x}_0$ passes through zero, no chatter occurs. However if $\dot{x}$ increases when $\dot{x} - \dot{x}_0$ passes through zero, chatter might occur.

In general, chatter occurs when B and $B - \frac{c}{m}\dot{x}$ have different signs when $\dot{x} - \dot{x}_0$ is nearly zero. When the damper force is turned on, the relative velocity is driven through zero so that the damper force drops to zero, the relative velocity again passes through zero, F_d begins to build up, and so on. A limit cycle oscillation can exist when $\dot{x} - \dot{x}_0$ is nearly zero.

3.2 Jerk of Semi-Active Control

Jerk is defined as sharp changes in the acceleration response of the system. It can be seen from the discussion in section 3.1 that chatter will induce sharp changes in the damping force, thus it will result in jerk. No matter what control algorithm is used, the damper force exhibits discontinuities at the time of switching. Thus a significant change in acceleration may be experienced by the suspended mass, which is undesirable. Figures 13-16 show three-dimensional control surface plots of damping force F_{sa} as a function of the variables in the condition function defined by equations (2.8), (2.11), (2.17) and (2.19). A surface discontinuity is present in the control surface at $\dot{x}-\dot{x}_0=0$ in Figure 13, a surface discontinuity in the control surface at $\dot{x}=0$ in Figure 14, a surface discontinuity in the control surface at $x-x_0=0$ in Figure 15, and a surface discontinuity in the control surface at $\dot{x}-\dot{x}_0=0$ in Figure 16. All these surface discontinuities may lead to an undesirable jerk.

3.3 Anti-jerk Control

To reduce the jerk induced by the switching of semi-active dampers, the method discussed in US patent 6,115,658 [16] is adopted. Figure 17 is a block diagram of the continuous skyhook control algorithm defined by equation (2.8). This control algorithm requires measurements of the velocity of the suspended mass, $\dot{x}$, and relative velocity, $\dot{x}-\dot{x}_0$ across the damper. $\dot{x}$ is scaled by a predefined damping coefficient c_{sky} to form the on state desired damping force $c_{sky}\dot{x}$, which is the first input to the switch block. The second input to the switch block is the product of $\dot{x}$ and $\dot{x}-\dot{x}_0$, $\dot{x}(\dot{x}-\dot{x}_0)$ is tested in the switch block to decide whether is the first input $c_{sky}\dot{x}$ or a zero constant force is passed through. If $\dot{x}(\dot{x}-\dot{x}_0)\geq 0$, then $c_{sky}\dot{x}$ is passed through, else, a constant zero force is passed through.

To reduce the jerk, a shaping function is introduced according to the discussion in reference [16]. Figure 18 is the block diagram of the proposed anti-jerk algorithm for continuous skyhook control. The absolute velocity of the mass, $\dot{x}$, is scaled by a positive gain factor, G, in a gain block. $\dot{x}$ is also multiplied by the relative velocity signal, $\dot{x}-\dot{x}_0$, in a multiplier block to form a velocity product signal, i.e., $\dot{x}(\dot{x}-\dot{x}_0)$, which is input to a switch block. The first input to the switch block has become the product of $G\dot{x}$ and a shaping function F, which depend on the relative velocity, $\dot{x}-\dot{x}_0$. Optionally, the shaping function may also

depend on the absolute velocity $\dot{x}$, and relative displacement, $x-x_0$, as well. So the shaping function can be written as $F(x-x_0,\dot{x},\dot{x}-\dot{x}_0)$, which is a function of the variables defining the condition function and may be implemented as a mathematical equation.

The shaping function $F(x-x_0,\dot{x},\dot{x}-\dot{x}_0)$ will define the overall shape of the three-dimensional control surface. Table 4 lists the guidelines that should be observed in selecting the shaping function $F(x-x_0,\dot{x},\dot{x}-\dot{x}_0)$[16].

Three different shaping functions have been described in reference [16] for continuous skyhook control. The first one of interest has a shaping function given by

$$F(x-x_0,\dot{x},\dot{x}-\dot{x}_0)=|\dot{x}-\dot{x}_0| \tag{3.5}$$

For this shaping function the control strategy becomes:

$$F_{sa}=\begin{cases} G\cdot|\dot{x}-\dot{x}_0|\cdot\dot{x} & \dot{x}(\dot{x}-\dot{x}_0)\geq 0 \\ 0 & \dot{x}(\dot{x}-\dot{x}_0)<0 \end{cases} \tag{3.6}$$

Figure 19 is the three-dimensional control surface plot showing the resulting control surface of the control algorithm described in equation (3.6). It can be seen that this control algorithm is devoid of any surface discontinuity at $\dot{x}-\dot{x}_0=0$ compared with Figure 13, thus it can reduce the acceleration jerk. This anti-jerk control method is used in the implementation of the semi-active control method in this report.

3.4 Controller Development

This section is concerned with the development of the semi-active control algorithms considering anti-jerk and practical hardware implementation. In the original control algorithms shown in Table 1, zero damping is assumed when the damper is switched off, which is not true in practice. When implementing the damping force required by each control algorithm in Table 1 using a conventional damper, which can only provide a damping force proportional to the relative velocity across it, there exists an upper and lower limit of the damping coefficients, c_{max} and c_{min}. All the damping the practical semi-active damper can provide should be in the range $[c_{min},c_{max}]$. Continuous skyhook control, on-off skyhook, continuous balance control, on-off balance control and adaptive damping control are employed. Each control algorithm is implemented using Matlab/Simulink.

3.4.1 Continuous Skyhook Control

Recalling the anti-jerk method described in equation (3.6), and the control surface plot in Figure 19, the semi-active damping required is given by

$$c_{sa} = \begin{cases} \dfrac{G \cdot |\dot{x} - \dot{x}_0| \cdot \dot{x}}{\dot{x} - \dot{x}_0} & \dot{x}(\dot{x} - \dot{x}_0) \geq 0 \\ 0 & \dot{x}(\dot{x} - \dot{x}_0) < 0 \end{cases} \tag{3.7}$$

Notice that the damper is switched to its on state whenever $\dot{x}$ and $\dot{x} - \dot{x}_0$ have the same sign, when $\dot{x} - \dot{x}_0 \geq 0$, $\dot{x}$ also needs to be greater equal than zero, thus

$$\frac{G \cdot |\dot{x} - \dot{x}_0| \cdot \dot{x}}{\dot{x} - \dot{x}_0} = G\dot{x} = G|\dot{x}| \tag{3.8}$$

When $\dot{x} - \dot{x}_0 \leq 0$, $\dot{x} \leq 0$

$$\frac{G \cdot |\dot{x} - \dot{x}_0| \cdot \dot{x}}{\dot{x} - \dot{x}_0} = -G\dot{x} = G|\dot{x}| \tag{3.9}$$

Following this discussion and taking into consideration the constraints of practical implementation, the following algorithm is developed to implement the continuously variable skyhook control algorithm

$$c_{sa} = \begin{cases} \max\left[c_{\min}, \min\left[G|\dot{x}|, c_{\max}\right]\right] & \dot{x}(\dot{x} - \dot{x}_0) \geq 0 \\ c_{\min} & \dot{x}(\dot{x} - \dot{x}_0) < 0 \end{cases} \tag{3.10}$$

It can be seen from equation (3.10) that the semi-active damping coefficient c_{sa} is a function of gain factor G, and velocity $\dot{x}$, which makes sure it has finite value and is proportional to $\dot{x}$. The maximum and minimum damping coefficients $c_{\max}$ and $c_{\min}$ are applied as a constraint to semi-active damping. Figure 20 shows the control algorithm block diagram for the new controller defined by equation (3.10). If the product of $\dot{x}$ and $\dot{x} - \dot{x}_0$ is greater than or equal to zero, the damper force is proportional to $\dot{x}$; otherwise, the damper force has the minimum value.

3.4.2 On-Off Skyhook Control

Recalling the algorithm defining the on-off skyhook damper in (2.11), it is a simplified control algorithm to the continuously skyhook control. Using the anti-jerk method described in the previous section, the shaping function for this control algorithm can be chosen as

$$F(x-x_0,\dot{x},\dot{x}-\dot{x}_0)=|\dot{x}| \tag{3.11}$$

Correspondingly, the damping force is given by

$$F_{sa}=\begin{cases} G\cdot|\dot{x}|\cdot(\dot{x}-\dot{x}_0) & \dot{x}(\dot{x}-\dot{x}_0)\geq 0 \\ c_{\min}(\dot{x}-\dot{x}_0) & \dot{x}(\dot{x}-\dot{x}_0)<0 \end{cases} \tag{3.12}$$

and the damping coefficient can be written in the same form as in equation (3.10) for continuously variable skyhook damper, i.e. this control algorithm is no longer on-off, but is continuously variable and identical to the anti-jerk control algorithm for continuous skyhook control after the anti-jerk modification. The control surface plot of equation (3.12) is the same as in Figure 19. One can see there are no surface discontinuities at areas near $\dot{x}=0$ compared to Figure 14. The anti-jerk control algorithm block diagram for on-off skyhook controller is the same as in shown in Figure 20.

After the anti-jerk modification, both the on-off skyhook and continuous skyhook control can be implemented using the same control algorithm as described by equation (3.10). The gain factor G, which has an unit of $N/(m/s)^2$, is introduced, which has no apparent relationship with c_{sky}. In the anti-jerk control algorithm, the semi-active damping force retains the same phase information as that of the desired skyhook damping force when at their on states. However, the amplitude does not resemble that of the skyhook damping although the damping force is still proportional to the absolute velocity.

Although jerk might occur with the simple on-off skyhook control algorithm, it is much simpler and easier to implement since only two states of damping are assumed. Also, the effects of delays in the controller and mechanical components may suppress the occurrence of chatter. For these reasons, it is implemented numerically and studied in this report. Figure 21 shows the block diagram for on-off skyhook control algorithm without anti-jerk modification.

3.4.3 On-Off Balance Control

Recalling the on-off balance control algorithm defined by equation (2.18), the control surface exhibits discontinuities at $x-x_0=0$ as shown in Figure 15. The shaping function to avoid the control surface discontinuities is chosen as

$$F(x-x_0,\dot{x},\dot{x}-\dot{x}_0)=|x-x_0| \tag{3.13}$$

The damping force for this control algorithm is given by

$$F_{sa}=\begin{cases} G\cdot|x-x_0|\cdot(\dot{x}-\dot{x}_0) & (x-x_0)(\dot{x}-\dot{x}_0)\le 0 \\ c_{\min}(\dot{x}-\dot{x}_0) & (x-x_0)(\dot{x}-\dot{x}_0)>0 \end{cases} \tag{3.14}$$

Figure 22 shows the control surface plot of equation (3.14). The surface discontinuity at areas $x-x_0=0$ is therefore avoided by the introduction of the shaping function compared to Figure 15. The damping coefficient corresponding to equation (3.14) can be written as

$$c_{sa}=\begin{cases} \max\left[c_{\min},\min\left[G|x-x_0|,c_{\max}\right]\right] & (x-x_0)(\dot{x}-\dot{x}_0)\le 0 \\ c_{\min} & (x-x_0)(\dot{x}-\dot{x}_0)>0 \end{cases} \tag{3.15}$$

As for the on-off skyhook control algorithm, the anti-jerk control algorithm defined by equation (3.15) for on-off balance control is no longer "on-off". The damping coefficient becomes continuous variable. Figure 23 shows the control algorithm block diagram for this controller. It will be used in the analysis of the vibration isolation performance of the damper, and it will be seen in section 3.4.4 that for the continuous balance control, the anti-jerk controller has the same form. For the same reason as discussed about for the skyhook semi-active damper, the control algorithm described in equation (2.18) is much more simple and easy to implement since only two states of damping are assumed. It is also implemented numerically and studied in this report. The block diagram of the on-off balance control algorithm is defined by equation (2.18) is shown in Figure 24.

3.4.4 Continuous Balance Control

Recalling the algorithm defining the continuous balance control in equation (2.19), and as shown in Figure 16, there exists surface discontinuities at $\dot{x}-\dot{x}=0$. When the anti-jerk control is used, the shaping function is chosen as

$$F(x-x_0,\dot{x},\dot{x}-\dot{x}_0)=|\dot{x}-\dot{x}_0| \tag{3.16}$$

The damping force therefore can be written as

$$F_{sa} = \begin{cases} -G \cdot |\dot{x} - \dot{x}_0| \cdot (x - x_0) & (x - x_0)(\dot{x} - \dot{x}_0) \le 0 \\ c_{\min}(\dot{x} - \dot{x}_0) & (x - x_0)(\dot{x} - \dot{x}_0) > 0 \end{cases} \tag{3.17}$$

and the damping coefficient is given by

$$c_{sa} = \begin{cases} \dfrac{-G \cdot |\dot{x} - \dot{x}_0| \cdot (x - x_0)}{\dot{x} - \dot{x}_0} & (x - x_0)(\dot{x} - \dot{x}_0) \le 0 \\ c_{\min} & (x - x_0)(\dot{x} - \dot{x}_0) > 0 \end{cases} \tag{3.18}$$

The damper is switched to its on state whenever $x - x_0$ and $\dot{x} - \dot{x}_0$ have different signs, i.e. when $\dot{x} - \dot{x}_0 \ge 0$, $x - x_0 \le 0$, we have

$$\frac{-G \cdot |\dot{x} - \dot{x}_0| \cdot (x - x_0)}{\dot{x} - \dot{x}_0} = -G(x - x_0) = G|x - x_0| \tag{3.19}$$

when $\dot{x} - \dot{x}_0 \le 0$, $x - x_0 \ge 0$

$$\frac{-G \cdot |\dot{x} - \dot{x}_0| \cdot (x - x_0)}{\dot{x} - \dot{x}_0} = G(x - x_0) = G|x - x_0| \tag{3.20}$$

Thus the damping coefficient can be further simplified as the same form as in equation (3.15).

As with the two skyhook control algorithms, both on-off balance and continuous balance control algorithms share the same anti-jerk implementation algorithm as shown in equation (3.15). The gain factor G for balance control has the unit of $N/m^2/s$, which is different to the unit for skyhook control. The resulting semi-active damping force after anti-jerk modification has the opposite sign of the spring force when in the on state, and it is proportional to the relative displacement.

3.4.5 Adaptive Damping Control

For the adaptive damping control algorithm, the damper works in a bi-state manner. It works as a common passive damper, which can be switched from one value to the other. Since the switch time can be chosen as when the damping force equals zero, there is no jerk associated with this control algorithm. The block diagram for this control algorithm is shown in Figure 25. A Math Function is used to get the RMS values of the excitation acceleration and the system acceleration response. Then the two RMS values are compared with each other to decide which damping state to choose.

3.5 Summary

Matlab/Simulink models for the five control algorithms of interest are established for numerical simulations of semi-active dampers. Both chatter and jerk associated with the switches between on and off states of semi-active dampers have been studied. Modified logic to avoid chatter and anti-jerk control algorithms have been proposed. As a summary, Table 5 lists the five control algorithms used to study the vibration isolation performance of semi-active dampers, which are numbered from SA-1 to SA-5 semi-active damper (SA means semi-active). It can be seen from the previous discussion that both the two skyhook semi-active dampers can be implemented by the same anti-jerk control strategy, which is referred to as SA-1 damper. A conventional on-off damper without anti-jerk is referred to as SA-2 damper. The anti-jerk implementation of the two balance control algorithms is referred to SA-3 damper. The simple on-off balance controlled damper is referred to as SA-4 damper. It should be pointed out that SA-2 and SA-4 damper are conventional on-off damper without anti-jerk treatment. Although they might cause jerk during operation, they are studied here since they are less complex and can provide comparison with anti-jerk control algorithms. Vibration isolation performance of a SDOF system comprising the four semi-active dampers together with the adaptive damping method is studied in the next section.

4. Harmonic Analysis of Semi-Active Dampers

This section presents an evaluation of the five semi-active control algorithms under harmonic excitation. The computer programs used to do the numerical simulations are first introduced. The input excitation used for performance evaluation and performance indices are described. These are followed by an evaluation of each control algorithm. The section ends with comparison and critical comments on each control algorithm.

4.1 Model Formulation

Consider the semi-active system in Figure 6. The equation of motion describing this system is

$$m\ddot{x}(t)+c(t)\left(\dot{x}(t)-\dot{x}_0(t)\right)+k\left(x(t)-x_0(t)\right)=0 \tag{4.1}$$

Equation (4.1) is solved for harmonic excitation to establish the vibration isolation performance. The response of the system can be obtained by directly integrating equation (4.1). The fourth order Runge-Kutta method was chosen to integrate the differential equation.

Numerical models of passive and semi-active SDOF systems subjected to base excitation have been established in Matlab m files and Matlab/Simulink model to carry out the numerical simulation. Figure 26 shows the Matlab/Simulink model for the simulation. The model comprises fours parts. The first one is the signal generator, which produces the excitation input into the system. The second part is the representation of the system and the third part is the semi-active controller, which produces the damper force according to different control algorithms. The block diagrams shown in Figures 20 to 24 can be inserted into this part to program a desired semi-active damping force. The last part is the displaying and the post processing the results according to the performance indices defined.

The organization of the main program for simulation is shown in the flow chart of Figure 27. As detailed in this flow chart, the program begins with a definition of the constants of the system parameters. Next, the initial conditions (all zero for this study) and inputs of the system are assigned. The time step of each iteration and final time of the program are now defined, setting the total number of iterations to be performed by the calculation loop of the program.

The first part of the calculation loop determines the value of damper force of the semi-active damper. If passive damping is applied, the damper is set to a constant, not changing within the loop. If semi-active damping is applied, a subroutine is called to calculate the current damper

value based on the control algorithm applied. Once the damping values have been determined, the definition of all components of the model will be completed.

The next stage is calculating the responses of the system from the differential equation. This computation is performed using fourth order Runge-Kutta method [17]. By defining $x_1 = x$ and $x_2 = \dot{x}$, the above second order differential equation can be written as two first order equations

$$\begin{aligned} \dot{x}_1 &= x_2 \\ \dot{x}_2 &= f(x_1, x_2, t) \end{aligned} \tag{4.2}$$

By defining

$$\mathbf{x} = \begin{Bmatrix} x_1 \\ x_2 \end{Bmatrix} \quad \text{and} \quad \mathbf{F(t)} = \begin{Bmatrix} x_2 \\ f(x_1, x_2, t) \end{Bmatrix} \tag{4.3}$$

the following recurrence formula is used to find the values of $\mathbf{x}(t)$ at different times t_i according to the fourth order Runge-Kutta method

$$\mathbf{x}(t+\tau) = \mathbf{x}(t) + \tau[\mathbf{K}_1 + 2\mathbf{K}_2 + 2\mathbf{K}_3 + \mathbf{K}_4]/6 \tag{4.4}$$

where

$$\begin{aligned} \mathbf{K}_1 &= \mathbf{F}(\mathbf{x}, t) \\ \mathbf{K}_2 &= \mathbf{F}(\mathbf{x} + 0.5\tau\mathbf{K}_1, t + 0.5\tau) \\ \mathbf{K}_3 &= \mathbf{F}(\mathbf{x} + 0.5\tau\mathbf{K}_2, t + 0.5\tau) \\ \mathbf{K}_4 &= \mathbf{F}(\mathbf{x} + \tau\mathbf{K}_1, t + \tau) \end{aligned}$$

The next loop of the program is now ready to be calculated, continuing for a predefined number of iterations until the calculation loop is completed and the program is halted.

4.2 The Harmonic Excitation and Performance Indices

The base excitation used for numerical simulations for this report takes the form

$$x_0 = X_0 \sin \omega t \tag{4.5}$$

where ω is the excitation frequency, and ω_n is the natural frequency of the system. All the simulations are run in the time-domain with discrete frequency excitation over a range from $0.5\omega_n$ to $10\omega_n$.

The equation of motion for the base excited SDOF system with any type of damper can be generalized as

$$m\ddot{x}(t)+a\left(\dot{x}(t)-\dot{x}_0(t)\right)+k\left(x(t)-x_0(t)\right)=0 \tag{4.6}$$

where a is the damping parameter given as follows:

Passive damper: $a=c_{pass}$

Skyhook damper: $a=c_{sky}$

SA-1 damper: $a=\begin{cases}\max\left[c_{\min},\min\left[G|\dot{x}|,c_{\max}\right]\right] & \dot{x}(\dot{x}-\dot{x}_0)\geq 0\\ c_{\min} & \dot{x}(\dot{x}-\dot{x}_0)<0\end{cases}$

SA-2 damper: $a=\begin{cases}c_{\max} & \dot{x}\left(\dot{x}-\dot{x}_0\right)\geq 0\\ c_{\min} & \dot{x}\left(\dot{x}-\dot{x}_0\right)<0\end{cases}$

SA-3 damper: $a=\begin{cases}\max\left[c_{\min},\min\left[G|x-x_0|,c_{\max}\right]\right] & (x-x_0)(\dot{x}-\dot{x}_0)\leq 0\\ c_{\min} & (x-x_0)(\dot{x}-\dot{x}_0)>0\end{cases}$

SA-4 damper: $a=\begin{cases}c_{\max} & (x-x_0)(\dot{x}-\dot{x}_0)\leq 0\\ c_{\min} & (x-x_0)(\dot{x}-\dot{x}_0)>0\end{cases}$

SA-5 damper: $a=\begin{cases}c_{\max} & \mathrm{RMS}(\ddot{x})\geq RMS(\ddot{x}_0)\\ c_{\min} & \mathrm{RMS}(\ddot{x})<RMS(\ddot{x}_0)\end{cases}$

The performance of the semi-active dampers depend on the gain factor G and the minimum and maximum damping coefficients $c_{\min}$ and $c_{\max}$. For a given system, there is a maximum value of the damping term $G|\dot{x}|$ for SA-1 damper and $G|x-x_0|$ for SA-3 damper if G is set to a constant. To make a relatively "fair" comparison between different types dampers, a trial and error method is used such that the equivalent damping ratio corresponding to the maximum value of $G|\dot{x}|$ or $G|x-x_0|$ is equal to $0.25, 0.5, 0.707, 1$ for each control algorithm.

The performance of the semi-active damper due to harmonic excitation is evaluated in terms of the following response parameters:

Absolute Acceleration Transmissibility Since the semi-active system is nonlinear with step changes in damper force, the acceleration response will have discontinuities. Previous researchers have used displacement transmissibility to characterize the isolator performance.

Since the human body or suspended mass is sensitive to inertial forces, the characterization in terms of acceleration would be more appropriate. In this study, the ratio of the RMS value of the response acceleration to the RMS value of the input acceleration is used as a performance index to evaluate vibration isolation performance. The absolute acceleration transmissibility is given by

$$TR = \frac{RMS(\ddot{x})}{RMS(\ddot{x}_0)} \tag{4.7}$$

Relative Displacement Transmissibility The relative transmissibility is a measure of the clearance required in an isolator. It is defined as the ratio of the RMS value of relative displacement between the mass and the base to the RMS value of the displacement of foundation, and given by

$$TR = \frac{RMS(x - x_0)}{RMS(x_0)} \tag{4.8}$$

The results presented in this section are based on the assumption that the off state damping, $c_{\min} = 0$. However, it is impossible to achieve a damping coefficient of zero when working with actual hardware. Therefore the active damping coefficients will actually switch between a higher value and a lower value. Since the objective of the off state damping is to minimize the acceleration of the mass, the lower value of the damping coefficient should be as low as physically practical. Because some energy is being transferred to the mass in the off state, the performance of the semi-active damper will be slightly degraded from the ideal theoretical performance. This has been pointed out in reference [18] and will be shown in the results of this report.

4.3 Passive and Skyhook System

A passive SDOF system isolation model subjected to base excitation is shown in Figure 28. It consists of a spring and a viscous damper. The differential equation describing the motion of the passive system can be written as

$$m\ddot{x}(t) + c(\dot{x} - \dot{x}_0) + k(x - x_0) = 0 \tag{4.9}$$

where m is the mass of the system, c is the damping coefficient, k is the spring stiffness, x is instantaneous displacement, and x_0 is the base displacement.

Defining the damping ratio $c/m = 2\zeta\omega_n$, natural frequency $\omega_n = \sqrt{k/m}$, and dividing equation (4.9) through by the mass, the governing equation becomes

$$\ddot{x} + 2\zeta\omega_n\dot{x} + \omega_n^2 x = 2\zeta\omega_n\dot{x}_0 + \omega_n^2 x_0 \tag{4.10}$$

Its vibration isolation can be characterized by absolute acceleration transmissibility and relative displacement transmissibility. Since the system is linear, it does not matter whatever acceleration or displacement transmissibility is used. For the passive SDOF system, the absolute transmissibility is given by [17]

$$T = \frac{X}{X_0} = \frac{\sqrt{1+\left(2\zeta\dfrac{\omega}{\omega_n}\right)^2}}{\sqrt{\left[1-\left(\dfrac{\omega}{\omega_n}\right)^2\right]^2 + \left[2\zeta\dfrac{\omega}{\omega_n}\right]^2}} \tag{4.11}$$

and the relative transmissibility can be expressed as

$$T_{rel} = \frac{X - X_0}{X_0} = \frac{\left(\dfrac{\omega}{\omega_n}\right)^2}{\sqrt{\left[1-\left(\dfrac{\omega}{\omega_n}\right)^2\right]^2 + \left[2\zeta\dfrac{\omega}{\omega_n}\right]^2}} \tag{4.12}$$

The transmissibility amplitudes of the acceleration and relative displacement are shown in Figure 29 (a) and (b) respectively. In general, Figure 29 (a) indicates attenuation of excitation at frequencies $\omega > \sqrt{2}\omega_n$, amplification at resonance and unity at low frequencies. The isolation region can be extended by decreasing the spring stiffness, k, or by increasing the mass m. Since the mass is usually predetermined, the designer selects k to yield the desired natural frequency.

Control of the resonant amplitude is achieved by the damper. This reduction is accompanied by decreased isolation above the resonance frequency in the isolation region. Increasing damping reduces the resonance response, but it increases transmissibility in the isolation range $\omega/\omega_n \geq \sqrt{2}$. If no damping were present, the amplitude at resonance would be infinite. The high frequency amplitude would be asymptotic to a slope of $-40dB/decade$, giving superior isolation there. This represents the well-known compromise between better control at the resonance and poor vibration isolation at high frequencies due to damping. Studying the

relative displacement transmissibility curves in Figure 29 (b) , it can be seen that a higher value of damping gives lower values of relative displacement transmissibility.

When active systems are used, the suspension force can be generated based on any control strategy. Using optimal control theory and the commonly used quadratic performance criterion it has been shown that an optimum SDOF isolator must generate a suspension force given by[2]

$$\frac{F_c}{m} = -2\zeta\omega_n\dot{x} - \omega_n^2(x - x_0) \tag{4.13}$$

where F_c is the suspension force. The above equation leads to the equation of motion of the mass as

$$\ddot{x} + 2\zeta\omega_n\dot{x} + \omega_n^2(x - x_0) = 0 \tag{4.14}$$

The linear control strategy in equation (4.13) can be realized using an ordinary spring and a skyhook as shown in Figure 5. The transmissibility of the SDOF system with a skyhook damper is given by

$$T = \frac{1}{\sqrt{\left[1 - \left(\frac{\omega}{\omega_n}\right)^2\right]^2 + \left[2\zeta\frac{\omega}{\omega_n}\right]^2}} \tag{4.15}$$

and the relative transmissibility is

$$T = \frac{\sqrt{\left(\frac{\omega}{\omega_n}\right)^4 + \left(2\zeta\frac{\omega}{\omega_n}\right)^2}}{\sqrt{\left[1 - \left(\frac{\omega}{\omega_n}\right)^2\right]^2 + \left[2\zeta\frac{\omega}{\omega_n}\right]^2}} \tag{4.16}$$

The transmissibility and relative transmissibility of a SDOF system with a skyhook damper are shown Figure 30 (a) and 30(b). From Figure 30 (a) it can be seen that the compromise between resonance control and isolation that is inherent in conventional passive system does not exist for the skyhook damper system. Increasing the damping reduces both the resonance response and the transmissibility in the isolation range. Studying the relative displacement transmissibility curves in Figure 30 (b), it can be seen that an increase in damping leads to smaller relative displacement transmissibility for a skyhook damper at frequencies

$\omega/\omega_n \geq \frac{1}{\sqrt{2}}$. The cross over point for the relative transmissibility curves in Figure 30 (b) is 0.707.

4.4 Semi-Active Dampers

This part of the work concerns the vibration isolation performance analysis of the five semi-active dampers defined in Table 5 and by equation (4.6). The vibration isolation performances of the five semi-active systems are compared with those of passive and skyhook systems.

4.4.1 SA-1 Semi-Active Damper

Figure 31 (a), (b) and (c) show the time history plot of the damping force, the condition function and the acceleration response with $G = 185$. For the plots in Figure 31 (a), the normalized excitation frequency is $\omega/\omega_n = 0.5$, in Figure 31 (b) $\omega/\omega_n = 1.0$, and in Figure 31(c) $\omega/\omega_n = 3.0$. The system was allowed to run until steady state was reached although only the last few cycles are plotted in the figures. Note that the damper forces in the figure are not to the same scale. The plots of damper force versus time show that the damper force switches between zero and on state damper force. The acceleration plots show the somewhat nonlinear mass acceleration due to the nonlinear force generated by the semi-active damper. When $\omega/\omega_n = 3.0$ as shown in Figure 31(c), the acceleration plot shows significant attenuation of the base induced acceleration disturbance.

The RMS acceleration transmissibility and RMS relative displacement transmissibility of SA-1 system to various gain G under the same maximum damping $c_{\max}$, are shown in Figure 32 (a) and (b). As shown in Figure 32 (a), the acceleration transmissibility of a SDOF system with an SA-1 damper is quite similar and approaches the skyhook isolation system. Increasing G improves the RMS acceleration transmissibility without worsening the high frequency isolation. For the higher G, the base disturbance can be attenuated below and through the system resonance. Furthermore, the high frequency attenuation provides superior isolation to that of passive isolation system at the same damping level. There is no compromise between the resonance control and the high frequency isolation. The attenuation at and below resonance gives the system characteristics similar to that of a lower natural frequency isolator, which is highly desirable. This is achieved without reducing the spring rate, which is favourable from a static deflection point of view. However, there are limits to the

performance improvement. It was noted by Karnopp that as $\zeta \to \infty$, the high frequency performance approached that of a skyhook system with $\omega_n = 0.6\sqrt{k/m}$ and $\zeta = 1.0$ [2].

Studying the relative displacement transmissibility in Figure 32 (b) shows that increasing G improves the relative displacement transmissibility. Comparing Figure 32 (b) with Figure 30 (b) shows that there are no crossing points in Figure 32 (b). This is due to the fact that the damper is turned off during part of the vibration period and the amplitude of the damper force is not exactly the same as the ideal skyhook damper when it is on.

It can be seen from equation (3.10) that the performance of SA-1 damper depends on the gain, G, besides the minimum, $c_{\min}$, and maximum damping, $c_{\max}$. There is a maximum damping, $\max\left[G|\dot{x}|\right]$ needed by each gain, which may vary with excitation frequencies. The best performance that the SA-1 damper can provide under each gain solely depends on this maximum value. If the maximum value $\max\left[G|\dot{x}|\right]$ is greater than $c_{\max}$, increasing $c_{\max}$ will improve the performance until $c_{\max}$ is greater than $\max\left[G|\dot{x}|\right]$, after which the performance will not improve. This relationship has been shown in Figure 33 (a) and (b) with $G = 185$. The damping ratio corresponding to $\max\left[G|\dot{x}|\right]$ when $G = 185$ is 1.0. If we define the damping ratio corresponding to $c_{\max}$ as $\zeta_{\max}$, when the maximum damping ratio $\zeta_{\max} < 1.0$, increasing $\zeta_{\max}$ will improve the performance. When $\zeta_{\max} \geq 1.0$, the performance reaches its best and does not increase with $\zeta_{\max}$. The same is true for any other value of G.

4.4.2 SA-2 Semi-Active Damper

Figures 34 (a), (b) and (c) show the time history plot of the condition function, the damper force and the acceleration responses for SA-2 control algorithm with the on-state damping ratio $\zeta_{\max} = 1$. For the plots in Figure 34 (a), the normalized excitation frequency is $\omega/\omega_n = 0.5$, in Figure 34 (b) $\omega/\omega_n = 1.0$, and in Figure 34(c) $\omega/\omega_n = 3.0$. The acceleration response of the on-off damper consistently reveals two peaks during each vibration cycle irrespective the excitation frequency. The two peaks are associated with high and zero values of damping. With the increase of excitation frequency, the duration of the off cycle of SA-2 system increases. This can be explained by studying the phase relationship between the variable of the condition function, i.e. $\dot{x}$ and $\dot{x} - \dot{x}_0$. Considering the passive system in Figure 28, it is straightforward to derive the transfer function relating $\dot{x}$ to $\dot{x}_0$, as

$$\frac{\dot{X}}{\dot{X}_0} = \frac{1+2i\zeta\dfrac{\omega}{\omega_n}}{1-\dfrac{\omega^2}{\omega^2{}_n}+2i\zeta\dfrac{\omega}{\omega_n}} \tag{4.17}$$

where ζ is the damping ratio. Since

$$\frac{\dot{X}-\dot{X}_0}{\dot{X}_0} = \frac{\dot{X}}{\dot{X}_0} - 1 \tag{4.18}$$

and using equation (4.17), we have

$$\frac{\dot{X}-\dot{X}_0}{\dot{X}_0} = \frac{\dfrac{\omega^2}{\omega^2{}_n}}{1-\dfrac{\omega^2}{\omega^2{}_n}+2i\zeta\dfrac{\omega}{\omega_n}} \tag{4.19}$$

Finally,

$$\frac{\dot{X}-\dot{X}_0}{\dot{X}_0} = \frac{2i\zeta\dfrac{\omega}{\omega_n}+1}{\dfrac{\omega^2}{\omega_n{}^2}} \tag{4.20}$$

For frequency response, the phase angle between i.e. $\dot{x}$ and $\dot{x}-\dot{x}_0$ is

$$\angle\frac{\dot{X}-\dot{X}_0}{\dot{X}_0} = \tan^{-1}\left(2\zeta\frac{\omega}{\omega_n}\right) \tag{4.21}$$

For low frequency excitation, the phase angle in equation (4.21) is nearly zero, and $\dot{x}$ and $\dot{x}-\dot{x}_0$ are in phase. As ω increases, the phase difference increases and approaches 90^o as $\omega \to \infty$. For an on-off system, we would expect the damper to be on most of the time for low frequencies since $\dot{x}$ and $\dot{x}-\dot{x}_0$ are of the same sign most of the time (see Figure 34 (a)). As the excitation frequency increases, the damper would be on less time.

The RMS acceleration and RMS relative displacement transmissibility of the SA-2 semi-active system are shown in Figure 35 (a) and (b). It can be seen from Figure 35(a) that the performance of the SDOF system with the SA-2 damper is very similar to the performance of the system with the SA-1 damper. As the on state damping ratio $\zeta_{\max}$ increases, the suspension controls the resonance peak better with a slightly worse isolation at higher

frequencies. Figure 35(b) shows that increasing the damping reduces the RMS relative displacement transmissibility of the system.

Both on-off and continuously variable skyhook control semi-active dampers exhibited the ability to lower the resonance peak without worsening isolation at higher frequencies. However, there is some difference between the performances of these two semi-active dampers. The RMS acceleration and relative displacement transmissibility of the velocity skyhook controlled semi-active dampers are compared with those of passive and skyhook dampers. The results are shown in Figure 36 (a), (b), (c) and (d). Studying the RMS acceleration transmissibility curves in Figure 36, it can be seen that both the two semi-active dampers can provide better performance at higher frequencies than passive dampers and their performance is comparable to the skyhook damper at even higher frequencies. In the higher frequency range, the performance of SA-1 damper is better than SA-2 damper, which meets the expectation that it can more closely emulate the skyhook damper when this control algorithm was developed. However, one can see from the figure that both of the semi-active dampers exhibit a larger resonance peak than the passive damper at a same damping level, which is a disadvantage of the two dampers. Examining the relative transmissibility curves, one can find that there are larger peaks with both skyhook and SA-1 dampers. Even the skyhook damper cannot simultaneously reduce the acceleration transmission and relative displacement transmission. As for relative displacement transmissibility, the SA-2 damper provides smaller relative transmissibility than SA-1 damper.

4.4.3 SA-3 Semi-Active Damper

Figure 37 (a), (b), and (c) show the steady-state response of an SA-3 system at three different frequencies for $G = 140$. For the plots in Figure 37 (a), the normalized excitation frequency is $\omega/\omega_n = 0.5$, in Figure 37 (b) $\omega/\omega_n = 1.0$, and in Figure 37 (c) $\omega/\omega_n = 3.0$. From the figure we can see that whenever the relative displacement and the relative velocity bears different sign, the semi-active damper is switched on to partially cancel the spring force.

Figures 38 (a) and (b) show the RMS acceleration and relative displacement transmissibility for various values of the gain G. As G is increased, the resonant peak decreases and the isolation performance improves. At higher frequencies, the transmissibility jumps to very large values for larger G. The same trend can be found in the relative displacement transmissibility. The reason for the discontinuity of the transmissibility curves is that, although the on state damping force has the opposite sign as the spring force and is

proportional to the relative displacement, it cannot exactly cancel the spring force. At high frequencies, a large value of G may over-cancel the spring force and effectively change the stiffness of the system. The mass vibrates about a new equilibrium position. Since the transmissibility is calculated and expressed in terms of RMS value, the change of the equilibrium position makes the transmissibility inconsistent.

4.4.4 SA-4 Semi-Active Damper

The steady state response of the SA-4 system is shown in Figure 39 (a), (b) and (c) for three different excitation frequencies with $\zeta_{\max} = 1.0$. It can be seen that the damper assumes a low damper force whenever the spring and the damper forces bear the same sign. The acceleration response reveals two peaks associated with the two states of the damping level. It can be seen from Figure 39 (c) that at higher frequencies, the SA-4 system changes from its equilibrium position. The mass vibrates about a new equilibrium position. Under this circumstance, the relative displacement does not change sign, such that the switch of the semi-active damper is determined solely by the sign of relative velocity.

Figures 40 (a) and (b) show the acceleration transmissibility of SA-4 system with different on state damping ratios, $\zeta_{\max}$. It can be seen from Figure 40(a) that with the increase of the on state damping, the resonant responses are reduced, but the high frequency isolation performance is also degraded. Increasing the damping reduces the relative transmissibility at resonance, but the isolation performance at higher frequencies is dramatically increased due to the offset of the equilibrium position.

A comparison of the acceleration and relative transmissibility of SA-3 and SA-4 system with passive and skyhook system is shown in Figures 41 (a), (b), (c) and (d). Compared to the passive system, the SA-3 system has a far superior performance at higher frequencies. The acceleration transmissibility curves show that a SA-3 system can even provide a better performance than a very lightly damping system or even an undamped system at higher frequencies. However, there is a price to be paid in terms of inferior low frequency performance and relative displacement transmissibility. The SA-4 damper system can also provide better performance at higher frequencies when compared with the passive damper with the same damping level. However, the performance at lower frequencies and around resonance is worse than the passive system. Both SA-3 and SA-4 damper were developed to minimize the RMS acceleration of the system instead of the relative displacement. It was

shown from the simulations that these strategies might lead to the mass vibration about a new position, which indicates an offset of the displacement.

4.4.5 SA-5 Semi-Active Damper

Figures 43 (a) and (b) show the RMS acceleration and relative displacement transmissibility of a SDOF system with an SA-5 semi-active damper respectively. It can be seen from the two figures that the response of the SA-5 system is identical to the passive system with the damping ratio $\zeta = \zeta_{\max}$ at frequencies $\omega/\omega_n \leq \sqrt{2}$, and the response is identical to undamped passive system at frequencies $\omega/\omega_n > \sqrt{2}$. The control of vibration at resonance is achieved by the on state damping $\zeta_{\max}$, while higher frequency isolation is not affected. It retains the best performance of the undamped passive system. Studying the relative transmissibility in Figure 42 (b) , it can be seen that relative displacement transmissibility of the SA-5 system is independent of the on state damping $\zeta_{\max}$ at the frequencies $\omega/\omega_n > \sqrt{2}$, the transmissibility at this range is the same as a passive system with zero damping. The SA-5 control algorithm makes the relative displacement worse beyond a frequency ratio of $\sqrt{2}$.

4.5 Discussion and Conclusions

Figures 42 (a) and (b) are a comparison of the RMS acceleration transmissibilities of the passive, skyhook and semi-active dampers. It can be established that:

1. The semi-active system almost always provides a better isolation than a conventional passive system. As the damping ratio increases, the difference between the two systems becomes more obvious. Whereas a conventional passive suspension can never provide isolation at frequency ratios of ω/ω_n less than $\sqrt{2}$, a semi-active isolator can in principle isolate at frequencies well below that.
2. The compromise between resonance control and isolation that is inherent in a conventional passive system does not exist for the semi-active systems. The reduction in the resonance peak does not necessarily occur at the cost of reduced isolation at high frequencies. In fact, with a sufficiently large damping ratio, one can completely eliminate the resonance peak and actually achieve better isolation across the whole impact frequency spectrum. This is particularly useful for sensitive machinery that cannot tolerate any overshoot in power-up or power-down, and yet must have good

isolation during normal operation. Conventional passive systems offer one of the two, whereas the semi-active offers both.

3. From Figure 43 we can see that with the increase of damping of semi-active dampers, both the high frequency isolation and resonance response are improved. However, this also leads to deterioration at very low frequencies due to the abrupt discontinuities in the damper force.

4. The acceleration jerk in the conventional on-off system can be significantly reduced by the anti-jerk implementation.

5. The skyhook damper system always provides the best performance but it is only an ideal case. SA-1 and SA-2 provide similar performance and in terms of relative transmissibility, SA-2 system is even better than SA-1 system, and is much simpler.

6. SA-3 system can provide superior isolation performance at higher frequencies at the cost of a large resonance peak and large relative displacement transmissibility. Both SA-3 and SA-4 systems are not good for relative displacement transmissibility reduction.

7. SA-5 is possibly the simplest and cheapest way to implement a control algorithm for harmonic vibration isolation, but is not applicable to random excitations.

5. Experimental Work

This section presents the experiment work on vibration isolation evaluation of a semi-active base isolated system using an electromechanical damper. An experiment was setup to investigate the use of an electromechanical device as a semi-active damper for vibration isolation. The experiment was conducted with the following objectives:

- ◊ To measure and verify the physical parameters of the experimental rig
- ◊ To investigate the effectiveness of electromechanical damping
- ◊ To implement semi-active control algorithms discussed in the previous sections and compare with theoretical analysis

5.1. Introduction

Linear electromechanical devices consisting of coils of metal wire interacting with magnetic fields produced by a permanent magnet or an electromagnet can be used to construct electromechanical dampers with a variable damping coefficient. The damping coefficient can be rapidly varied by changing the external resistance connected to the coil. In the open circuit state the electromechanical damping effect vanishes, while when the coil is short circuited the damping coefficient reaches a maximum value. Since the effective resistance can be rapidly varied electrically, an electromechanical damper can function as a semi-active damper in vibration isolation systems.

Figure 44 shows the SDOF base isolation system model using an electromechanical damper. In the model, the magnet and the iron core is arranged to move together with the base and the coil is attached to and moves together with the mass to be controlled. When the coil is moving in the magnet field, a voltage called the *back emf* – electromotive force is induced in the coil, which is governed by Lenz's Law. If the strength of the magnetic field is B, the coil moves with a velocity of $\dot{x}$ and the base velocity is $\dot{x}_0$, then the induced voltage in the coil can be expressed as

$$E_{bemf} = BL(\dot{x} - \dot{x}_0) \tag{5.1}$$

Where $L = ln$ is the effective length of the wire; l is the length of the coil per turn and n is the number of effective coil turns.

If the circuit is closed, there will be a current flowing in the coil, and there will be an electromechanical force F_{em} on the coil. This force is developed by the interaction between the magnetic field of strength B that exists across the gap and the magnetic field due to current flowing in the coil. The resulting force is

$$F_{em} = BLI \tag{5.2}$$

Assuming the resistance of the coil is R_c and is connected to an external resistance R_{ext}, then the current related to the induced *back emf* is given by

$$I = \frac{E_{bemf}}{R_c + R_{ext}} \tag{5.3}$$

The electromechanical force F_{em} therefore can be written as

$$F_{em} = \frac{(BL)^2}{R_c + R_{ext}}(\dot{x} - \dot{x}_0) \tag{5.4}$$

For the SDOF system with an electromechenical damper subject to base excitation, the equation of the motion can be written as

$$m\ddot{x} + c_{me}(\dot{x} - \dot{x}_0) + k(x - x_0) + F_{em} = 0 \tag{5.5}$$

where k is a spring constant and c_{me} is the mechanical damping coefficient of the system. Substituting equation (5.4) into (5.5), gives

$$m\ddot{x} + (c_{me} + c_{em})(\dot{x} - \dot{x}_0) + k(x - x_0) = 0 \tag{5.6}$$

Where $c_{em} = \frac{(BL)^2}{R_c + R_{ext}}$ is the electromechanical damping due to the electromechanical damper.

It can be seen from equation (5.6) that the damping of the system consists of two parts, one is the mechanical damping c_{me}, and the other is the electromechanical damping c_{em}. The mechanical damping if fixed for a given system, while the electromechanical damping can be changed by varying the external resistance or simply opening or closing the circuit. The maximum damping coefficient of the system occurs when $R_{ext} = 0$, which is given by

$$c_{\max} = c_{me} + \frac{(BL)^2}{R_c} \tag{5.7}$$

The damping ratios corresponding to the mechanical damping and electromechanical damping can be expressed as

$$\zeta_{me} = \frac{c_{me}}{2m\omega_n}; \zeta_{em} = \frac{c_{em}}{2m\omega_n} = \frac{(BL)^2}{R_c + R_{ext}} \frac{1}{2m\omega_n} \tag{5.8}$$

5.2 Experimental Setup

Figure 45 shows the experimental setup for semi-active vibration isolation (a complete list of the equipment used can be found in Appendix B). In this setup, a SDOF using a passive spring-damper isolator together with an electromechanical damper is set on a vibrator table. The passive isolator consists of a stiffness coefficient k and a mechanical damping coefficient c_{me}. The coil-magnet system of the electromechanical damper was provided from a Colossus 12MB loudspeaker driver. The specification of the Colossus 12MB loudspeaker driver is listed in Appendix C. A switch was connected in series with the coil resistance to close or open the electrical circuit. Maximum and minimum damping can be obtained when the switch is switched on and off respectively. An 8-channel HP analyzer was used to generate the excitation signal, measure and analyze the response of the system. Two B&K 4393 accelerometers were used to measure the response of the mass and the base respectively. The measured signals were fed into the HP analyzer for processing after being amplified by charge amplifiers. Two Wavetek DM25XT Digital Volt Meters were used measure the root-mean-square (RMS) values of the measured signals.

5.3 Experimental Procedure and Results

The first measurement conducted using the experimental setup was to measure the frequency response of the system with the switch was set to on and off respectively. When the switch was in the off state, the electrical circuit was open. Thus there was no electromagnetic force exerted by the electromechanical damper. The damping coefficient of the system was a minimum and was equal to the mechanical damping of the system. When the switch was in the on state, electromechanical damping was added to the system. The damping coefficient of the system was of maximum value and was equal to the sum of the mechanical damping of the system and the electromechanical damping. The maximum value of the damping can be determined by equation (5.7).

Figure 46 shows the measured acceleration transmissibility between the mass and the base when the switch was on and off. It can be seen that when the switch was off, there was a

certain mechanical damping in the system. When the switch was on, electromechanical damping was added to the system. The system resonance response was greatly reduced by the added electromechanical damping. It can also be seen from the measurement that the natural frequency of the system was at about $60Hz$. From the peak value of the acceleration transmissibility when the switch was off, the mechanical damping ratio of the system was calculated to be $\zeta_{me} = 0.245$, and the electromechanical damping of the system was calculated to be $\zeta_{em} = 1.276$ using the physical parameters of the system according to equation (5.8). To validate the measured parameters and the characteristics of the system, a comparison was made between the measured data and the theoretical numerical simulations. The comparison is also shown in Figure 46. It can be seen that the measurement results agree reasonably well with the theoretical numerical simulation results.

The second measurement was conducted to implement the SA-5 control algorithm using the experimental setup. Recalling the equation defining the SA-5 adaptive damping control algorithm, the control algorithm for the current case can be defined as

$$c_{sa} = \begin{cases} c_{me} + c_{em} & RMS(\ddot{x}) \geq RMS(\ddot{x}_0) \\ c_{me} & RMS(\ddot{x}) < RMS(\ddot{x}_0) \end{cases} \tag{5.9}$$

The condition function is the comparison of the RMS values of the acceleration response of the mass and the base. The RMS values of the two acceleration signals were measured using two Wavetek DM25XT digital volt meters. The operation of the switch was conducted by hand. Figure 47 shows the result of the acceleration transmissibility with SA-5 semi-active control algorithm and compared with the on and off state responses of the system. It can be seen from the figure that the system behaves as a heavily damped system at frequencies when the excitation frequency ω is smaller than $\sqrt{2}\omega_n$, while it behaves as a light damped system at higher frequencies. The adaptive damping control algorithm can greatly reduce the response at resonance while retaining the higher frequency isolation performance.

5.4 Conclusion

An experiment was conducted to investigate the use of an electromechanical device as semi-active damper for vibration and shock isolation. The electromechanical damper is adopted from the coil magnet system of a Colossus 12MB loudspeaker driver. The physical parameters are validated by measurement. The electromechanical damper is effective in adding damping into the system, and the measurement results agree reasonably well with the numerical simulations. The SA-5 semi-active control algorithm is implemented using the experimental setup. The results show that the control algorithm can greatly reduce the system response at resonance while retaining the higher frequency isolation performance.

6. Conclusions

A simple SDOF system subject to harmonic base excitation has been used to study the vibration isolation performance of passive, skyhook and semi-active dampers. Five semi-active control algorithms have been studied, which are based on skyhook control, balance controlled, and adaptive damping control. The chatter and jerk problems met when doing numerical simulations with semi-active dampers have been investigated and anti-jerk semi-active control algorithms have been suggested. With the suggested control algorithm, the sharp changes and the discontinuities of the damper force can be smoothed, thus jerk can be significantly reduced. The system and controller models have been built using Matlab/Simulink. Using the established model, the vibration isolation performance of the five semi-active systems have been analyzed and compared with passive and skyhook systems. It has been concluded from the results that the semi-active system almost always provides better isolation than a conventional passive system. As the damping ratio increases, the difference between the two systems becomes more obvious. The Skyhook damper system always provides the best performance but it is only an ideal case. The SA-1 and SA-2 systems provide similar performance and in terms of relative transmissibility, the SA-2 system is even better than SA-1 system. Furthermore, the SA-2 system is much simpler than the SA-1 system. The SA-3 and SA-4 systems are good at reducing acceleration response at higher frequencies, but not relative displacement transmissibility. SA-5 is the simplest and cheapest control algorithm. To better understand the isolation properties of semi-active dampers, the semi-active system has been studied using its passive equivalent. The effects of non-zero off state damping have also been studied. The insertion of off-state damping has two effects compared to the system without off-state damping, (a) it reduces the RMS acceleration ratio at and around the natural frequency; and (b) it increase the RMS acceleration transmissibility at frequencies greater than natural frequency.

Reference

1. Crosby, M.J. and D.C. Karnopp, The Active Damper: A New Concept for Shock and Vibration Control. Shock and Vibration Bulletin, 1973. 43: p. 119-133.
2. Karnopp, D.C., M.J. Crosby, and R.A. Harwood, Vibration Control using Semi-Active Force Generators. ASME Journal of Engineering for Industry, 1974. 96(2): p. 619-626.
3. Krasnicki, E.J., Comparison of Analytical and Experimental Results for a Semi-Active Vibration Isolator. Shock and Vibration Bulletin, 1980. 50: p. 69-76.
4. Krasnicki, E.J. The Experimental Performance of an "On-Off" Active Damper. in Proceedings of the 51st Shock and Vibration Symposium. 1980. San Diego, USA.
5. Rakheja, S. and S. Sankar, Vibration and Shock Isolation Performance of a Semi-Active "On-Off" Damper. ASME Journal of Vibration, Acoustics, Stress, and Reliability in Design, 1985. 107: p. 398-403.
6. Miller, L.R. Tuning Passive, Semi-Active, and Fully Active Suspension Systems. in Proceeding of the 27th Conference on Decision and Control. 1988. Austin, Texas.
7. Franchek, M.A., M.W. Ryan, and R.J. Bernhard, Adaptive Passive Vibration Control. Journal of Sound and Vibration, 1995. 189(5): p. 565-585.
8. Onoda, J., H.-U. Oh, and K. Minesugi, Semi-Active Vibration Suppression with Electrorheological-Fluid Dampers. AIAA Journal, 1997. 35(12): p. 1844-1852.
9. Wu, X. and M.J. Griffin, A Semi-Active Control Policy to Reduce the Occurrence and Severity of End-Stop Impacts in a Suspension Seat with an Electrorheological Fluid Damper. Journal of Sound and Vibration, 1997. 203(5): p. 781-793.
10. Harris, C.M., Shock and Vibration Handbook. 1987: McGRAW-HILL.
11. Snowdon, J.C., Vibration and Shock in Damped Mechanical Systems. 1968: John Wiley & Sons.
12. Guntur, R.R. and S. Sankar, Performance of Different Kinds of Dual Phase Damping Shock mounts. Journal of Sound and Vibration, 1982. 84(2): p. 253-267.
13. Sankar, S., A.K. Ahmed, and S. Venkatesh, Analytical and Experimental Evaluation of Displacement Dependent Dual-Phase Dampers in Vibration Isolation. Journal of Sound and Vibration, 1994. 169(1): p. 55-69.

14. Alanoly, J. and S. Sankar, A New Concept in Semi-Active Vibration Isolation. ASME Journal of Mechanisms, Transmissions, and Automation in Design, 1987. 109: p. 242-247.

15. Donald, L.M. and G. Mehrnaz, The Chatter of Semi-Active On-Off Suspensions and its Cure. Vehicle System Dynamics, 1984. 13: p. 129-144.

16. Ahmadian, M., R. Brian, and X. Song, No-Jerk Semi-Active Skyhook Control Method and Apparatus, in United States patent. 2000: USA.

17. Rao, S.S., Mechanical Vibrations. Third Edition ed. 1995: Addison-Wesley Publishing Company.

18. Oueslati, F. and S. Sankar, A Class of Semi-Active Suspension Schemes for Vehicle Vibration Control. Journal of Sound and Vibration, 1994. 172(3): p. 391-411.

Tables

Table 1 Damping characteristics of semi-active dampers

Damper Type	Original Control Algorithm	Semi-Active Damping Required	Semi-Active Damping in Practice
Continuous skyhook	$F_{sa}=\begin{cases}c_{sky}\dot{x} & \dot{x}(\dot{x}-\dot{x}_0)\geq 0\\ 0 & \dot{x}(\dot{x}-\dot{x}_0)<0\end{cases}$	$c_{sa}=\begin{cases}\dfrac{c_{sky}\dot{x}}{\dot{x}-\dot{x}_0} & \dot{x}(\dot{x}-\dot{x}_0)\geq 0\\ 0 & \dot{x}(\dot{x}-\dot{x}_0)<0\end{cases}$	$c_{sa}=\begin{cases}\max\left[c_{\min},\min\left[\dfrac{c_{sky}\dot{x}}{\dot{x}-\dot{x}_0},c_{\max}\right]\right] & \dot{x}(\dot{x}-\dot{x}_0)\geq 0\\ c_{\min} & \dot{x}(\dot{x}-\dot{x}_0)<0\end{cases}$
On-off skyhook	$F_{sa}=\begin{cases}c_{on}(\dot{x}-\dot{x}_0) & \dot{x}(\dot{x}-\dot{x}_0)\geq 0\\ 0 & \dot{x}(\dot{x}-\dot{x}_0)<0\end{cases}$	$c_{sa}=\begin{cases}c_{on} & \dot{x}(\dot{x}-\dot{x}_0)\geq 0\\ 0 & \dot{x}(\dot{x}-\dot{x}_0)<0\end{cases}$	$c_{sa}=\begin{cases}c_{\max} & \dot{x}(\dot{x}-\dot{x}_0)\geq 0\\ c_{\min} & \dot{x}(\dot{x}-\dot{x}_0)<0\end{cases}$
On-off balance	$F_{sa}=\begin{cases}c_{on}(\dot{x}-\dot{x}_0) & (x-x_0)(\dot{x}-\dot{x}_0)\leq 0\\ 0 & (x-x_0)(\dot{x}-\dot{x}_0)>0\end{cases}$	$c_{sa}=\begin{cases}c_{on} & (x-x_0)(\dot{x}-\dot{x}_0)\leq 0\\ 0 & (x-x_0)(\dot{x}-\dot{x}_0)>0\end{cases}$	$c_{sa}=\begin{cases}c_{\max} & (x-x_0)(\dot{x}-\dot{x}_0)\leq 0\\ c_{\min} & (x-x_0)(\dot{x}-\dot{x}_0)>0\end{cases}$
Continuous balance	$F_{sa}=\begin{cases}-k(x-x_0) & (x-x_0)(\dot{x}-\dot{x}_0)\leq 0\\ 0 & (x-x_0)(\dot{x}-\dot{x}_0)>0\end{cases}$	$c_{sa}=\begin{cases}\dfrac{-k(x-x_0)}{\dot{x}-\dot{x}_0} & (x-x_0)(\dot{x}-\dot{x}_0)\leq 0\\ 0 & (x-x_0)(\dot{x}-\dot{x}_0)>0\end{cases}$	$c_{sa}=\begin{cases}\max\left[c_{\min},\min\left[\dfrac{-k(x-x_0)}{\dot{x}-\dot{x}_0},c_{\max}\right]\right] & (x-x_0)(\dot{x}-\dot{x}_0)\leq 0\\ c_{\min} & (x-x_0)(\dot{x}-\dot{x}_0)>0\end{cases}$
Adaptive damping	$F_{sa}=\begin{cases}c_{on}(\dot{x}-\dot{x}_0) & \mathrm{RMS}(\ddot{x})\geq RMS(\ddot{x}_0)\\ 0 & \mathrm{RMS}(\ddot{x})<RMS(\ddot{x}_0)\end{cases}$	$c_{sa}=\begin{cases}c_{on} & \mathrm{RMS}(\ddot{x})\geq RMS(\ddot{x}_0)\\ 0 & \mathrm{RMS}(\ddot{x})<RMS(\ddot{x}_0)\end{cases}$	$c_{sa}=\begin{cases}c_{\max} & \mathrm{RMS}(\ddot{x})\geq RMS(\ddot{x}_0)\\ c_{\min} & \mathrm{RMS}(\ddot{x})<RMS(\ddot{x}_0)\end{cases}$

Table 2 Conditions for the chatter of a semi-active on-off damper

(1)	An $\dot{x}$ switch has taken place;
(2)	The damper force, F_d, if on, is of opposition sign to the spring force;
(3)	The damper force is of larger amplitude than the instantaneous spring force.

Table 3 Modified logic for cure of chatter in semi-active on-off dampers

(1)	$\dot{x}$ has just changed sign;
(2)	If the damper force is of the same sign as the spring force, then switch the damper according to the switch condition. Otherwise, use (3);
(3)	If the damper force magnitude, if on, is smaller than the spring force, then switch the damper according to switch function. Otherwise, use (4)
(4)	Do not switch the damper until (2) or (3) are not met

Table 4 Guidelines for selecting shaping function

(1)	$F(x-x_0, \dot{x}, \dot{x}-\dot{x}_0)$ is a continuous function;
(2)	$F(x-x_0, \dot{x}, \dot{x}-\dot{x}_0)$ is equal to 0 at the points whenever a variable in the condition function results in surface discontinuities ;
(3)	$F(x-x_0, \dot{x}, \dot{x}-\dot{x}_0)$ and the control surface both include continuous first derivatives for all values of $x-x_0$, $\dot{x}$ and $\dot{x}-\dot{x}_0$, where the condition defined in equation (2.8), (2.11), (2.17) and (2.19) are met;
(4)	$F(x-x_0, \dot{x}, \dot{x}-\dot{x}_0)$ and the control surface both are devoid of discontinuities

Table 5 Anti-jerk control algorithms for semi-active control

Damper Type	Original Control Algorithm	Semi-Active Damping In Practice	Anti-jerk Implementation
Continuous skyhook	$F_{sa}=\begin{cases} c_{sky}\dot{x} & \dot{x}(\dot{x}-\dot{x}_0)\geq 0 \\ 0 & \dot{x}(\dot{x}-\dot{x}_0)<0 \end{cases}$	$c_{sa}=\begin{cases} \max\left[c_{\min},\min\left[\dfrac{c_{sky}\dot{x}}{\dot{x}-\dot{x}_0},c_{\max}\right]\right] & \dot{x}(\dot{x}-\dot{x}_0)\geq 0 \\ c_{\min} & \dot{x}(\dot{x}-\dot{x}_0)<0 \end{cases}$	$c_{sa}=\begin{cases} \max\left[c_{\min},\min\left[G\lvert\dot{x}\rvert,c_{\max}\right]\right] & \dot{x}(\dot{x}-\dot{x}_0)\geq 0 \\ c_{\min} & \dot{x}(\dot{x}-\dot{x}_0)<0 \end{cases}$ (SA-1)
On-off skyhook	$F_{sa}=\begin{cases} c_{on}(\dot{x}-\dot{x}_0) & \dot{x}(\dot{x}-\dot{x}_0)\geq 0 \\ 0 & \dot{x}(\dot{x}-\dot{x}_0)<0 \end{cases}$	$c_{sa}=\begin{cases} c_{\max} & \dot{x}(\dot{x}-\dot{x}_0)\geq 0 \\ c_{\min} & \dot{x}(\dot{x}-\dot{x}_0)<0 \end{cases}$ (SA-2)	
On-off balance	$F_{sa}=\begin{cases} c_{on}(\dot{x}-\dot{x}_0) & (x-x_0)(\dot{x}-\dot{x}_0)\leq 0 \\ 0 & (x-x_0)(\dot{x}-\dot{x}_0)>0 \end{cases}$	$c_{sa}=\begin{cases} c_{\max} & (x-x_0)(\dot{x}-\dot{x}_0)\leq 0 \\ c_{\min} & (x-x_0)(\dot{x}-\dot{x}_0)>0 \end{cases}$ (SA-4)	$c_{sa}=\begin{cases} \max\left[c_{\min},\min\left[G\lvert x-x_0\rvert,c_{\max}\right]\right] & (x-x_0)(\dot{x}-\dot{x}_0)\leq 0 \\ c_{\min} & (x-x_0)(\dot{x}-\dot{x}_0)>0 \end{cases}$ (SA-3)
Continuous balance	$F_{sa}=\begin{cases} -k(x-x_0) & (x-x_0)(\dot{x}-\dot{x}_0)\leq 0 \\ 0 & (x-x_0)(\dot{x}-\dot{x}_0)>0 \end{cases}$	$c_{sa}=\begin{cases} \max\left[c_{\min},\min\left[\dfrac{-k(x-x_0)}{\dot{x}-\dot{x}_0},c_{\max}\right]\right] & (x-x_0)(\dot{x}-\dot{x}_0)\leq 0 \\ c_{\min} & (x-x_0)(\dot{x}-\dot{x}_0)>0 \end{cases}$	
Adaptive damping	$F_{sa}=\begin{cases} c_{on}(\dot{x}-\dot{x}_0) & \mathrm{RMS}(\ddot{x})\geq RMS(\ddot{x}_0) \\ 0 & \mathrm{RMS}(\ddot{x})<RMS(\ddot{x}_0) \end{cases}$	$c_{sa}=\begin{cases} c_{\max} & \mathrm{RMS}(\ddot{x})\geq RMS(\ddot{x}_0) \\ c_{\min} & \mathrm{RMS}(\ddot{x})<RMS(\ddot{x}_0) \end{cases}$ (SA-5)	

Figures

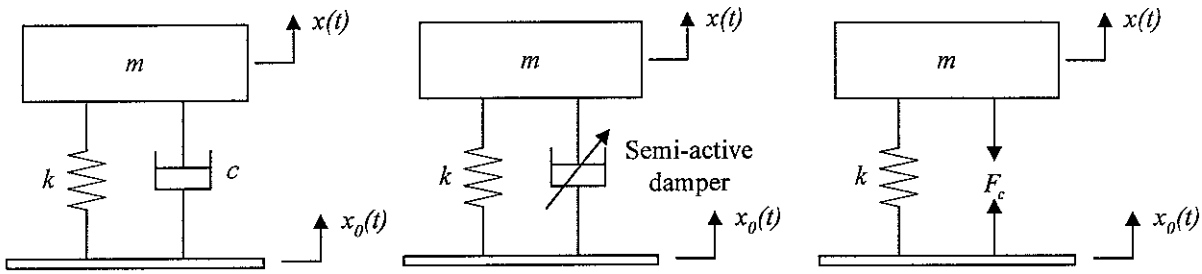

Figure 1 Schematic of a SDOF system with a (a) passive; (b) semi-active; and (c) active damper

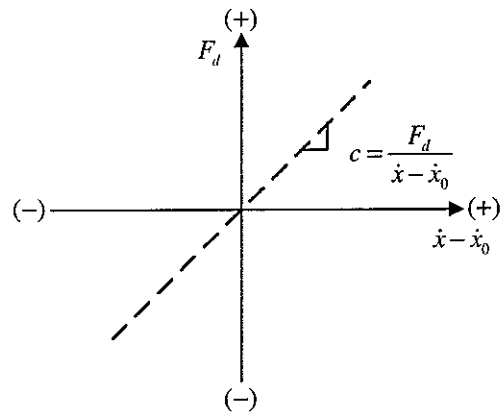

Figure 2 Passive damping concept

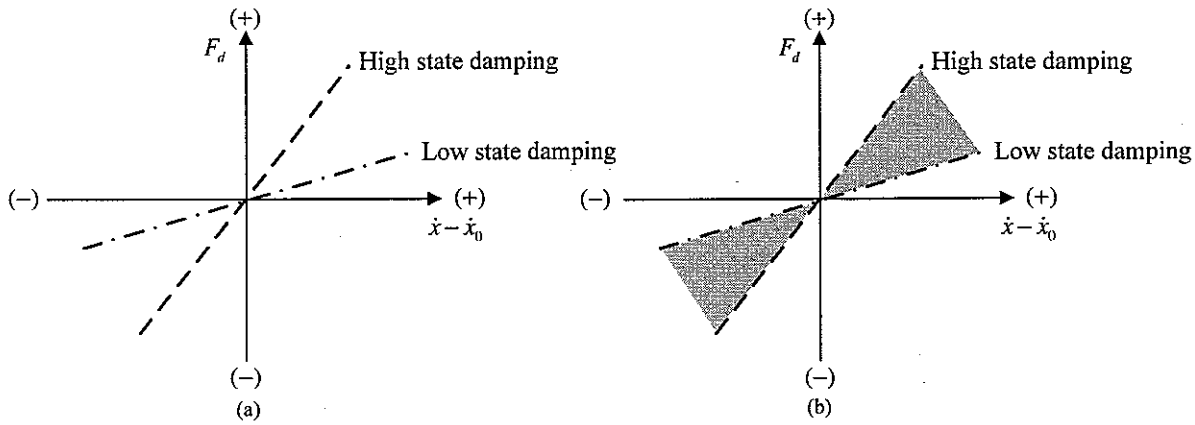

Figure 3 Semi-active damping concept of (a) on-off damper; (b) continuously variable damper

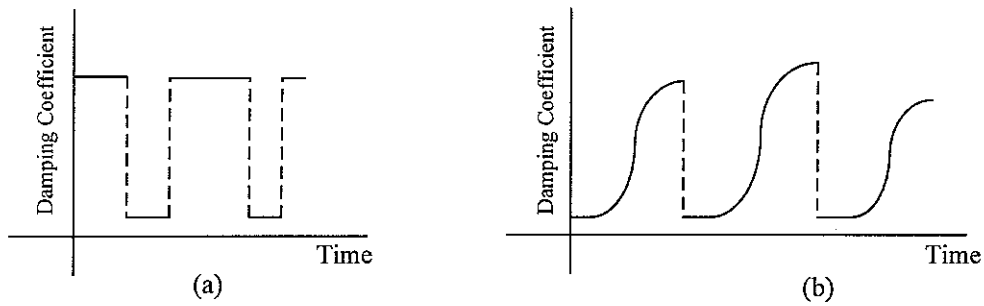

Figure 4 Semi-active damper characteristics in the time domain (a) on-off damper; (b) continuously variable damper

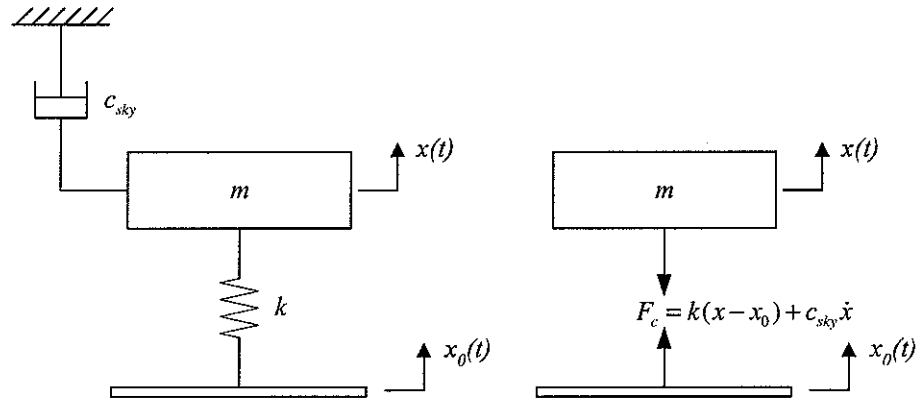

Figure 5 Skyhook system and its active equivalent

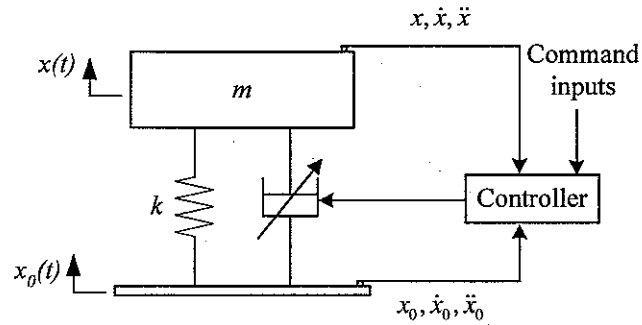

Figure 6 Semi-active SDOF system

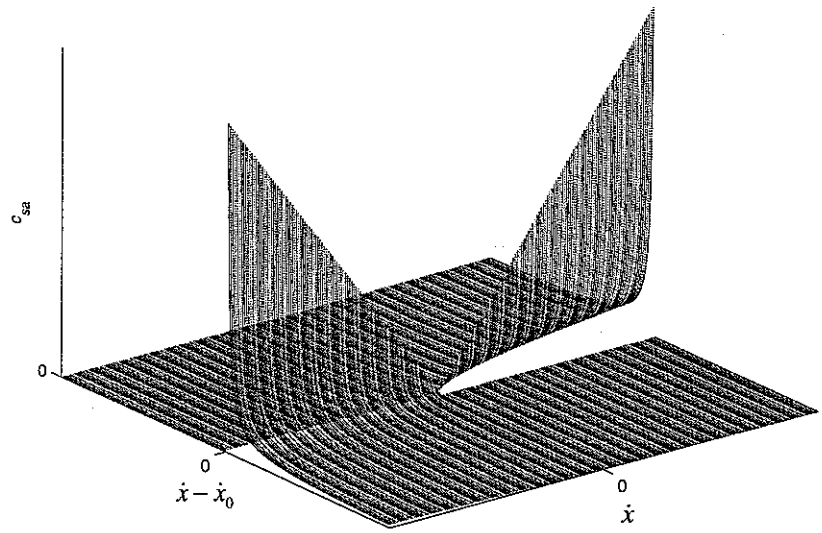

Figure 7 Required damping coefficient for continuous skyhook damping as a function of absolute and relative velocity (equation (2.9))

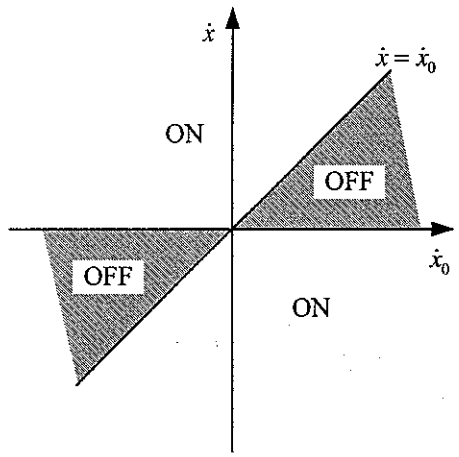

Figure 8 Velocity relationship of skyhook control algorithm

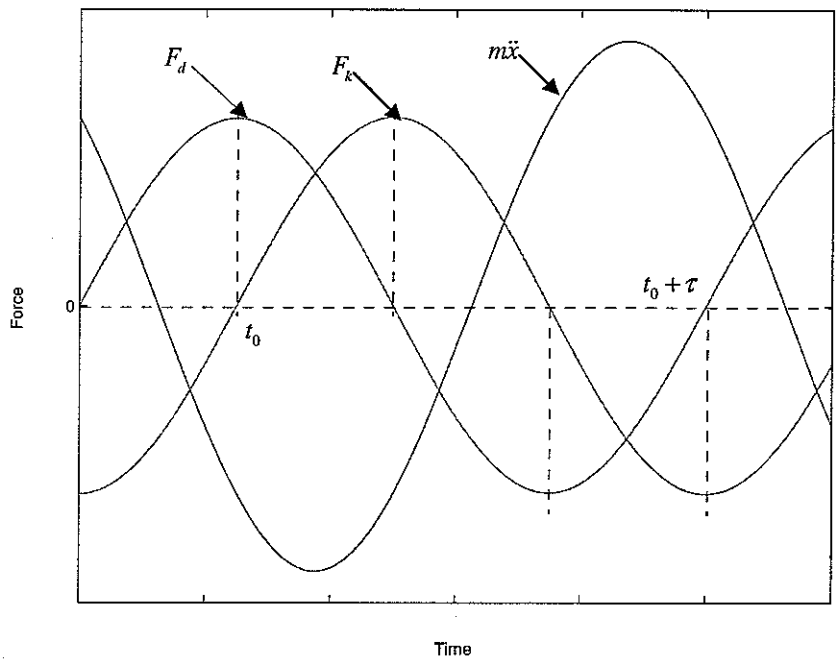

Figure 9 Inertial, spring and damper force of a passive SDOF system

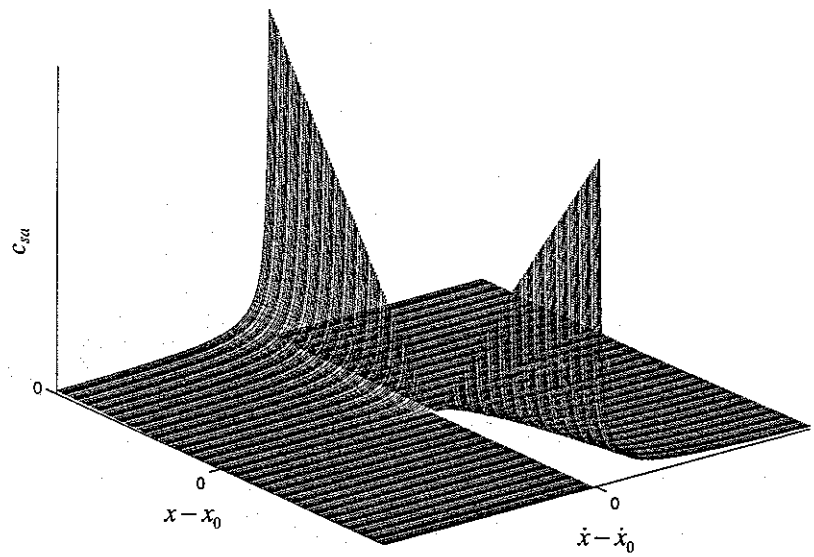

Figure 10 Required damping coefficient for continuous balance semi-active damping as a function of relative displacement and relative velocity (equation (2.20))

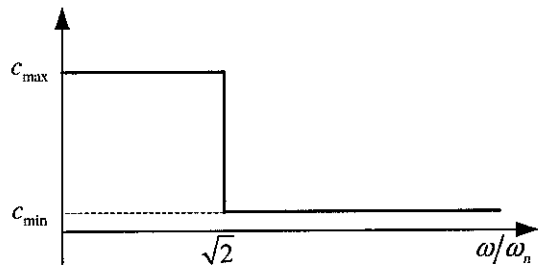

Figure 11 Ideal damping characteristics for harmonic vibration isolation

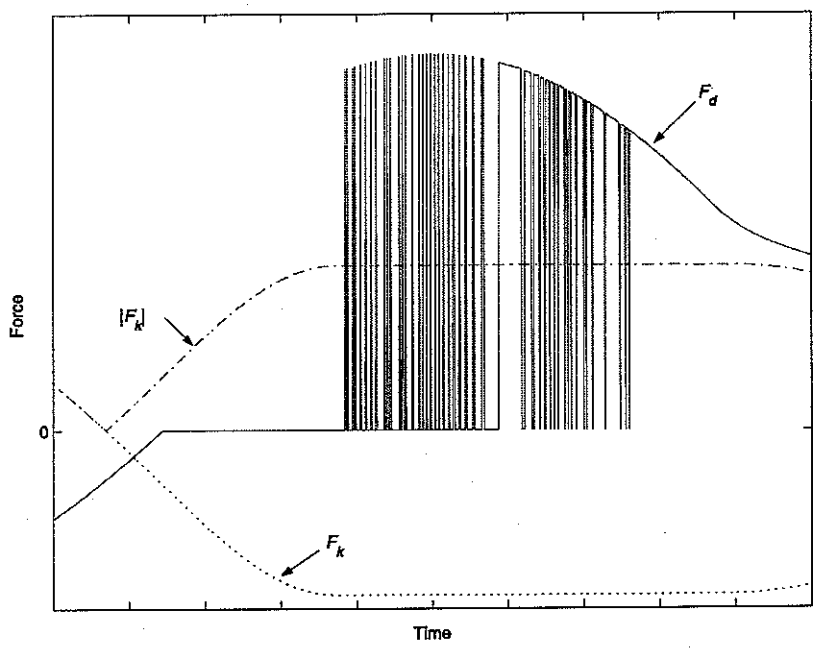

Figure 12 Spring and damping force during chatter period

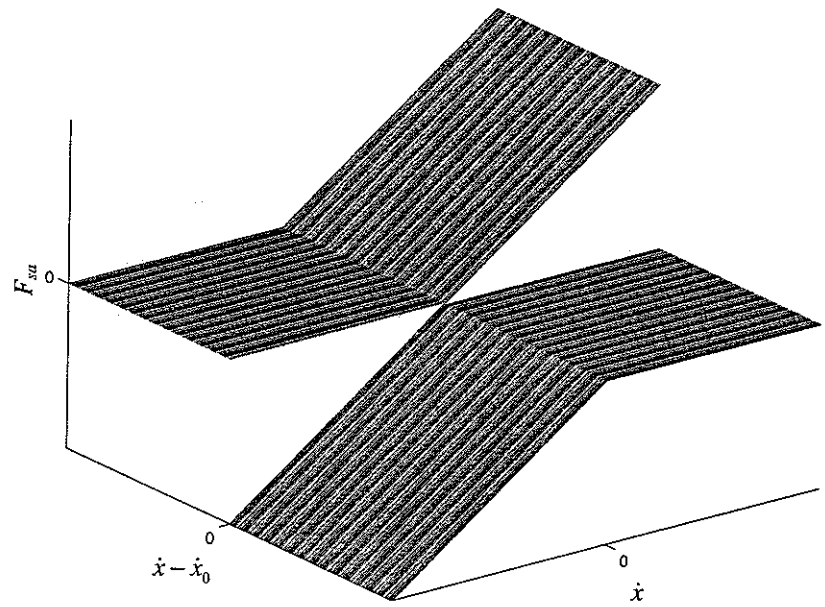

Figure 13 Three-dimensional control surface plot of desired force for continuous skyhook control (equation (2.8))

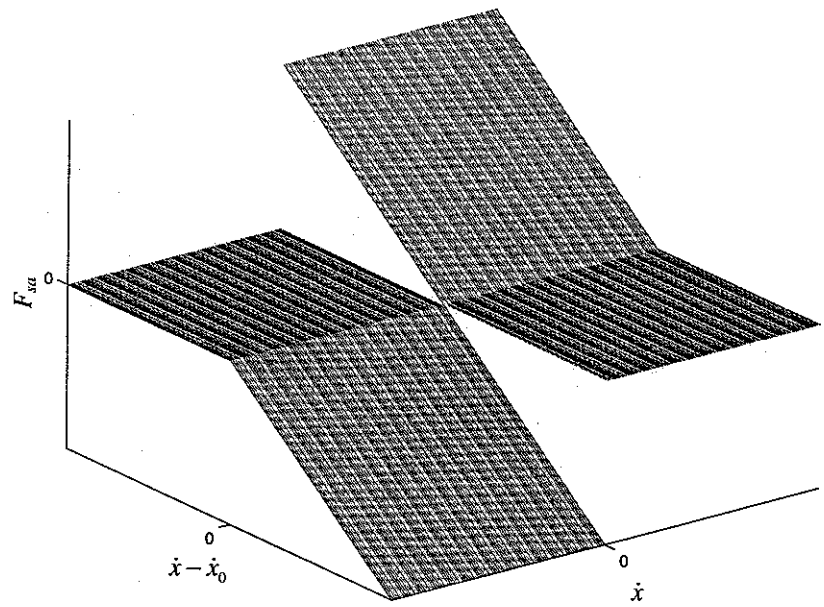

Figure 14 Three-dimensional control surface plot of desired force for on-off skyhook control (equation (2.11))

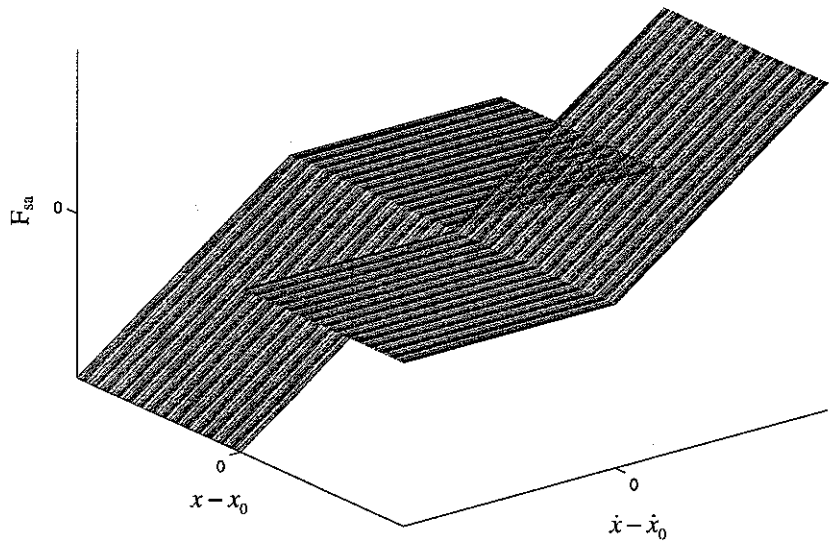

Figure 15 Three-dimensional control surface plot of desired force for on-off balance control (equation (2.17))

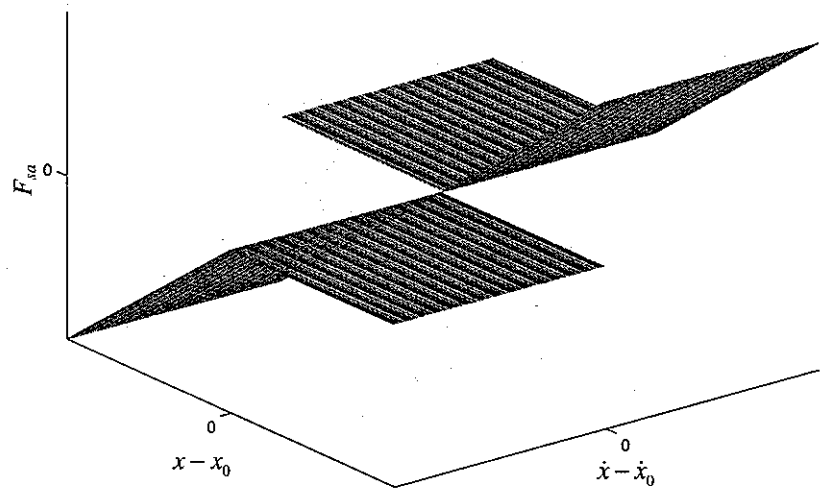

Figure 16 Three-dimensional control surface plot of desired force for on-off balance control (equation (2.19))

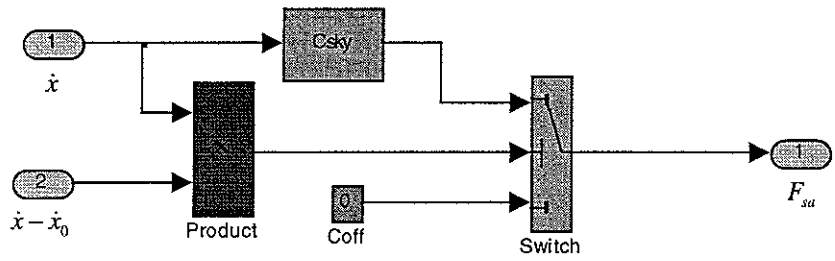

Figure 17 Block diagram of conventional continuous skyhook control

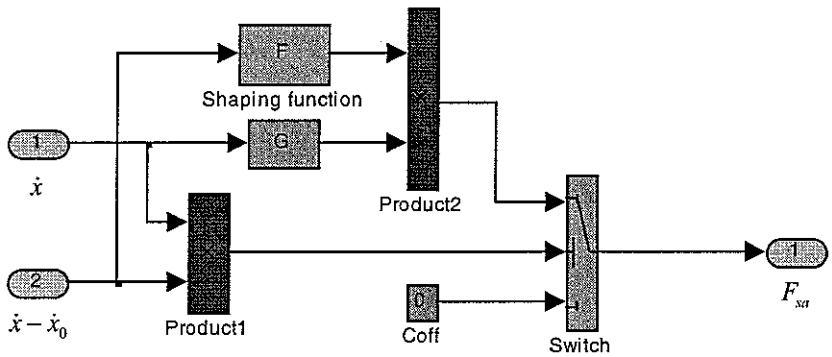

Figure 18 Block diagram of anti-jerk continuous skyhook control

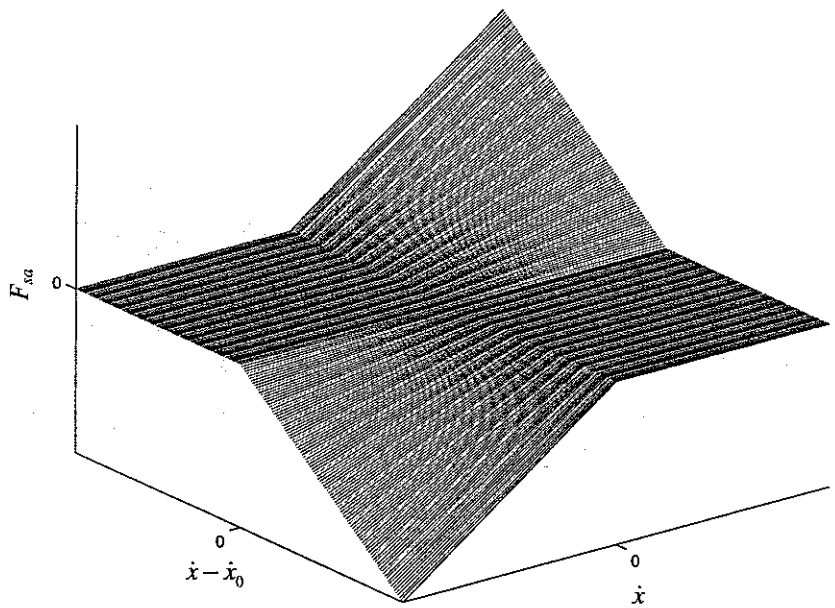

Figure 19 Three-dimensional control surface plot of the desired damping force for continuous variable skyhook control with anti-jerk modification (equation (3.6))

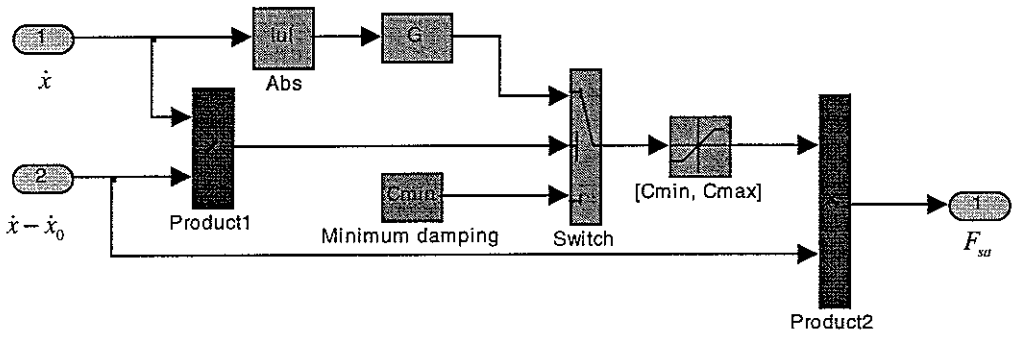

Figure 20 Block diagram of continuous skyhook control algorithm with anti-jerk modification

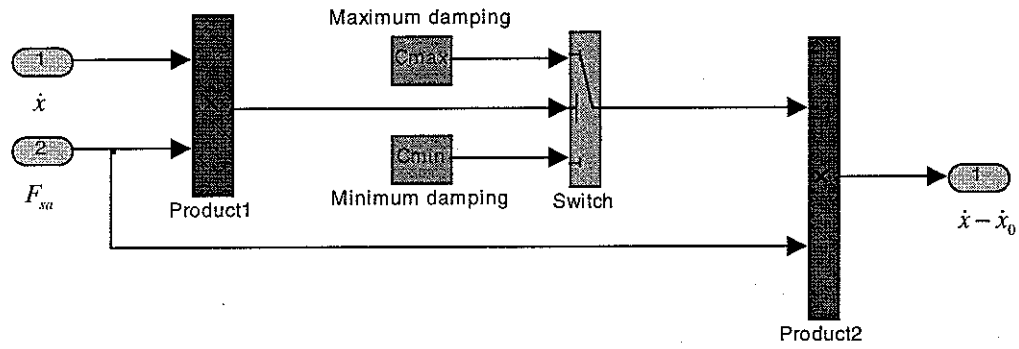

Figure 21 Block diagram of on-off skyhook control algorithm without anti-jerk modification

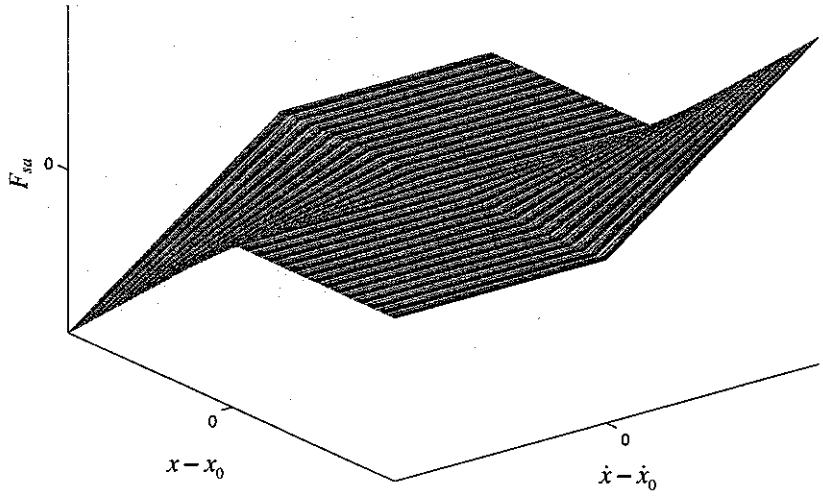

Figure 22 Three-dimensional control surface plot of desired damping force for on-off balance control with anti-jerk modification (equation (3.14))

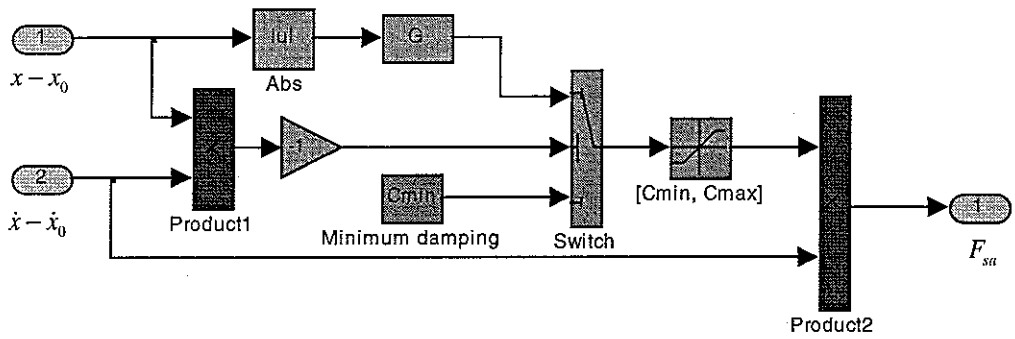

Figure 23 Block diagram of on-off balance control algorithm with anti-jerk modification (equation (3.14))

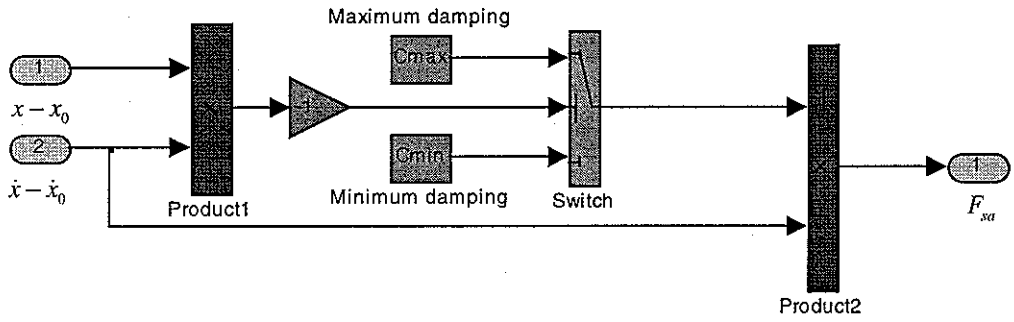

Figure 24 Block diagram of on-off balance algorithm without anti-jerk modification (equation (2.18))

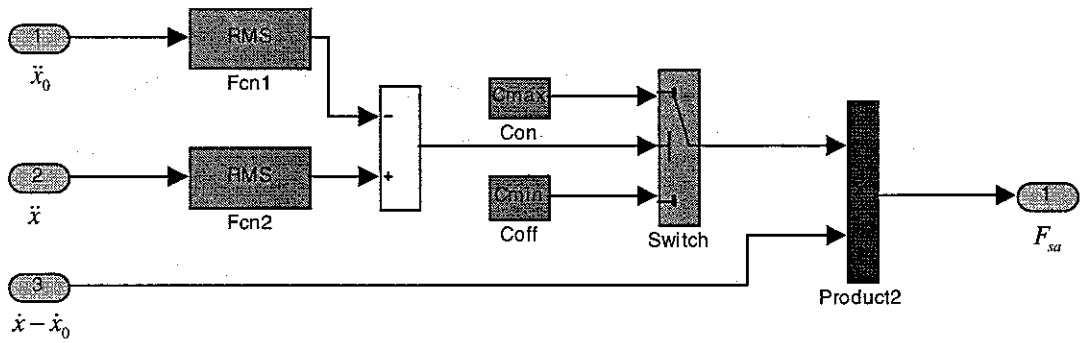

Figure 25 Block diagram of adaptive damping control algorithm

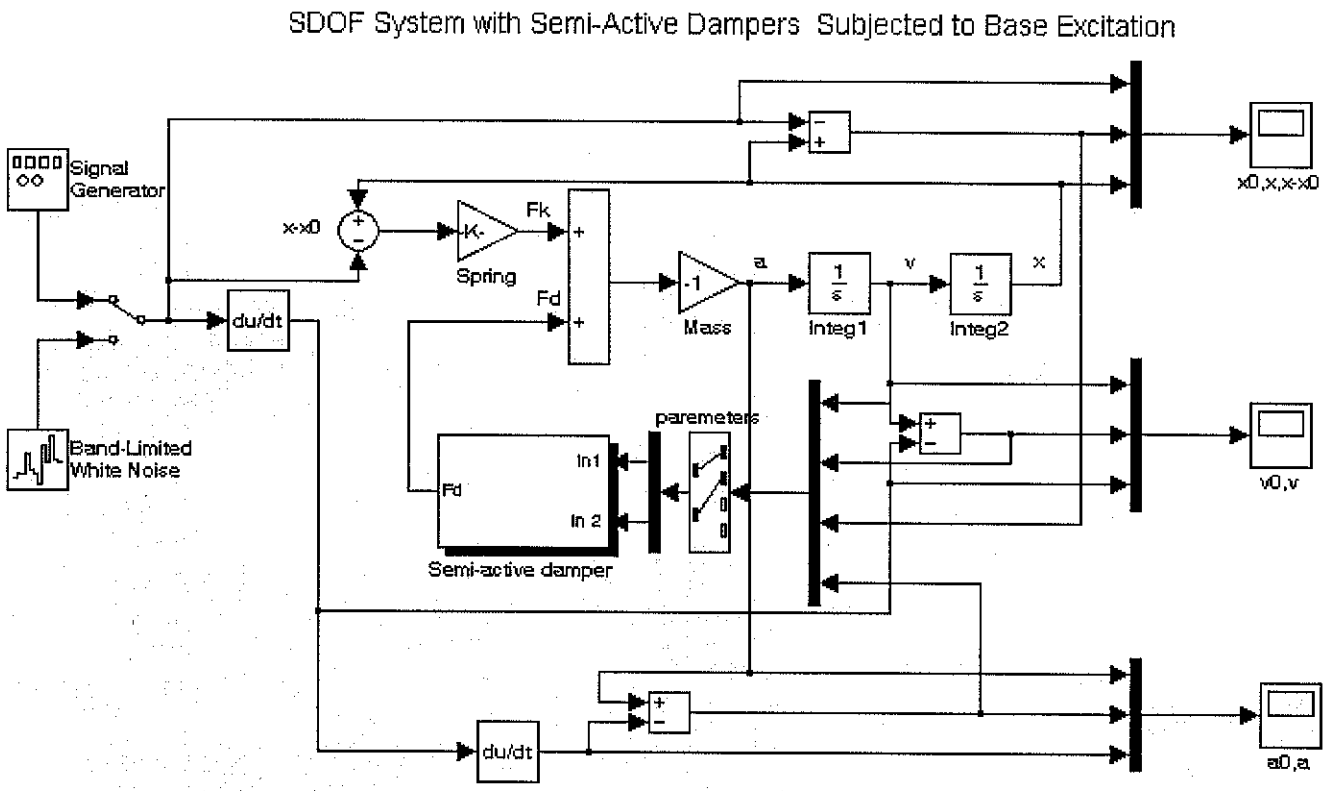

Figure 26 Matlab/Simulink Semi-Active SDOF System Model

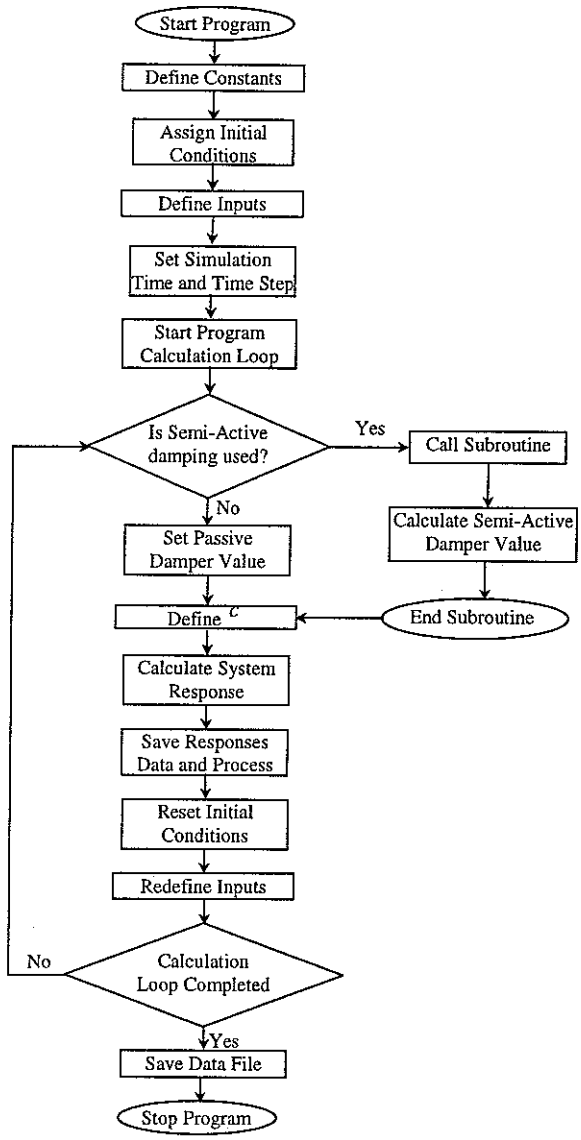

Figure 27 Flow chart of the simulation model

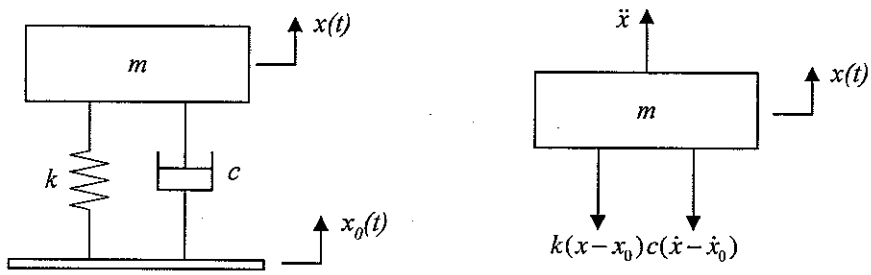

Figure 28 Schematic of SDOF system with a passive damper

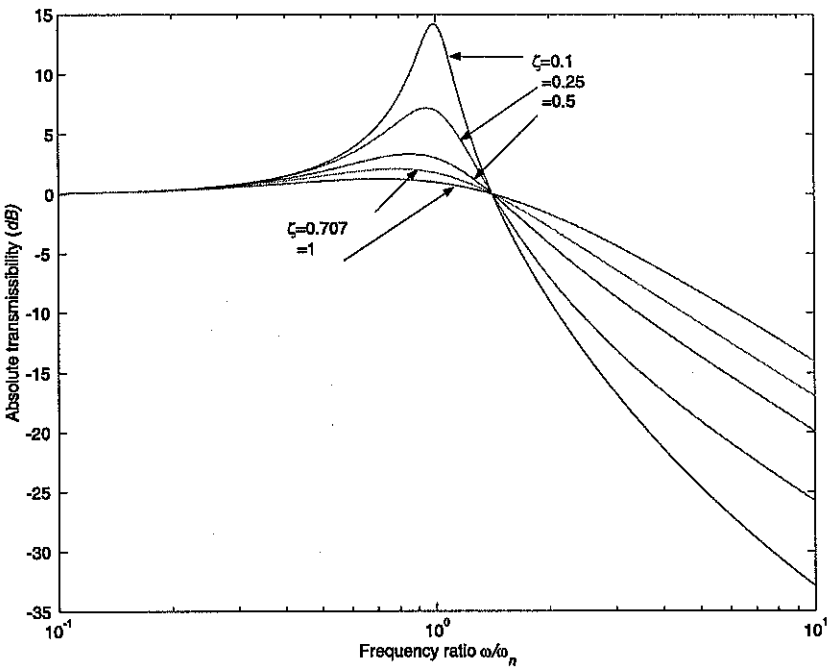

(a)

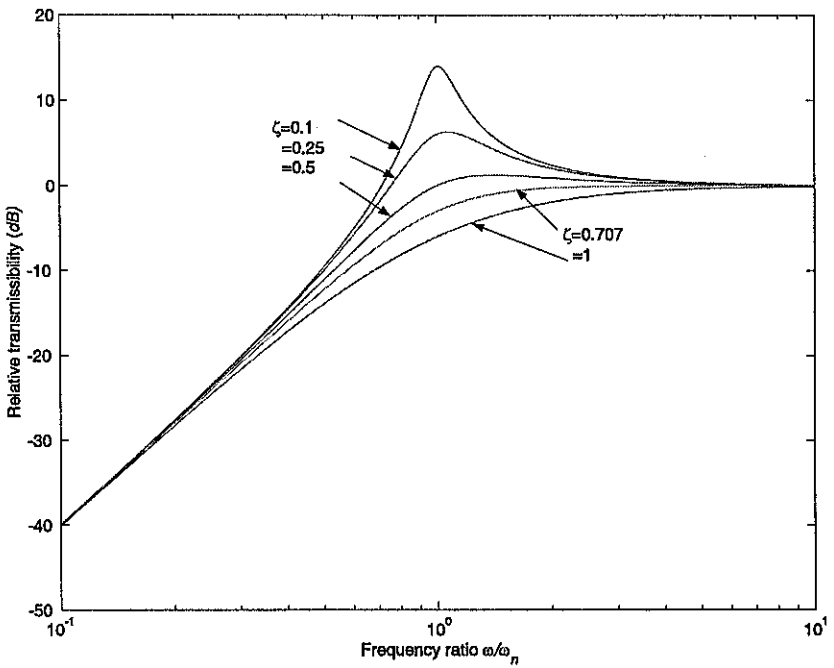

(b)

Figure 29 Transmissibility of passive SDOF system (a) absolute transmissibility; (b) relative transmissibility

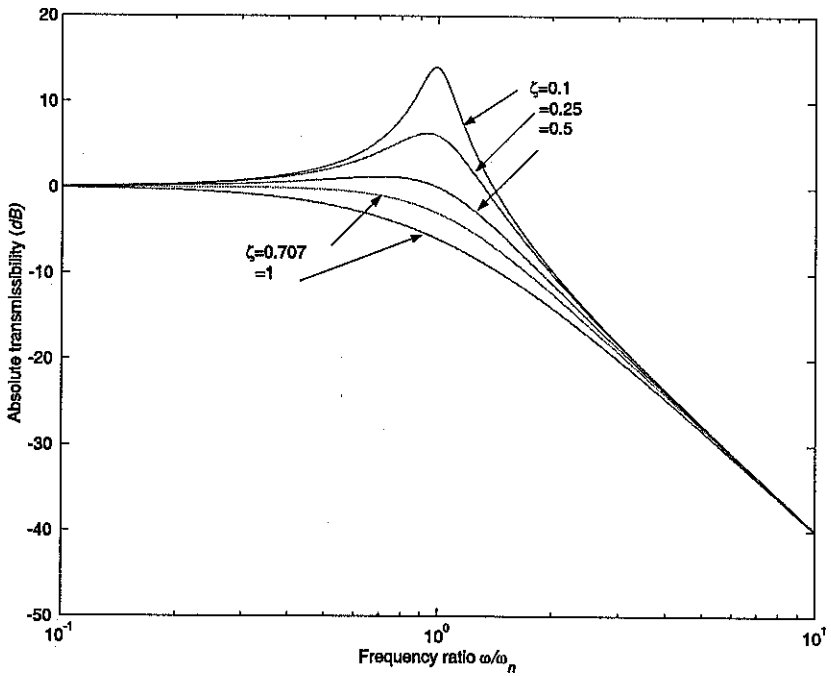

(a)

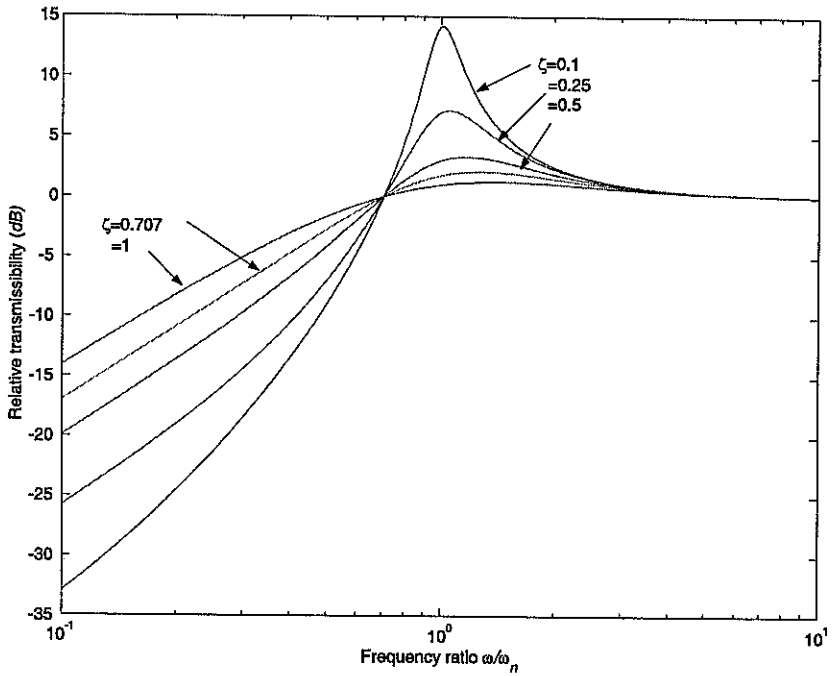

(b)

Figure 30 Transmissibility of skyhook SODF system (a) absolute transmissibility; (b) relative transmissibility

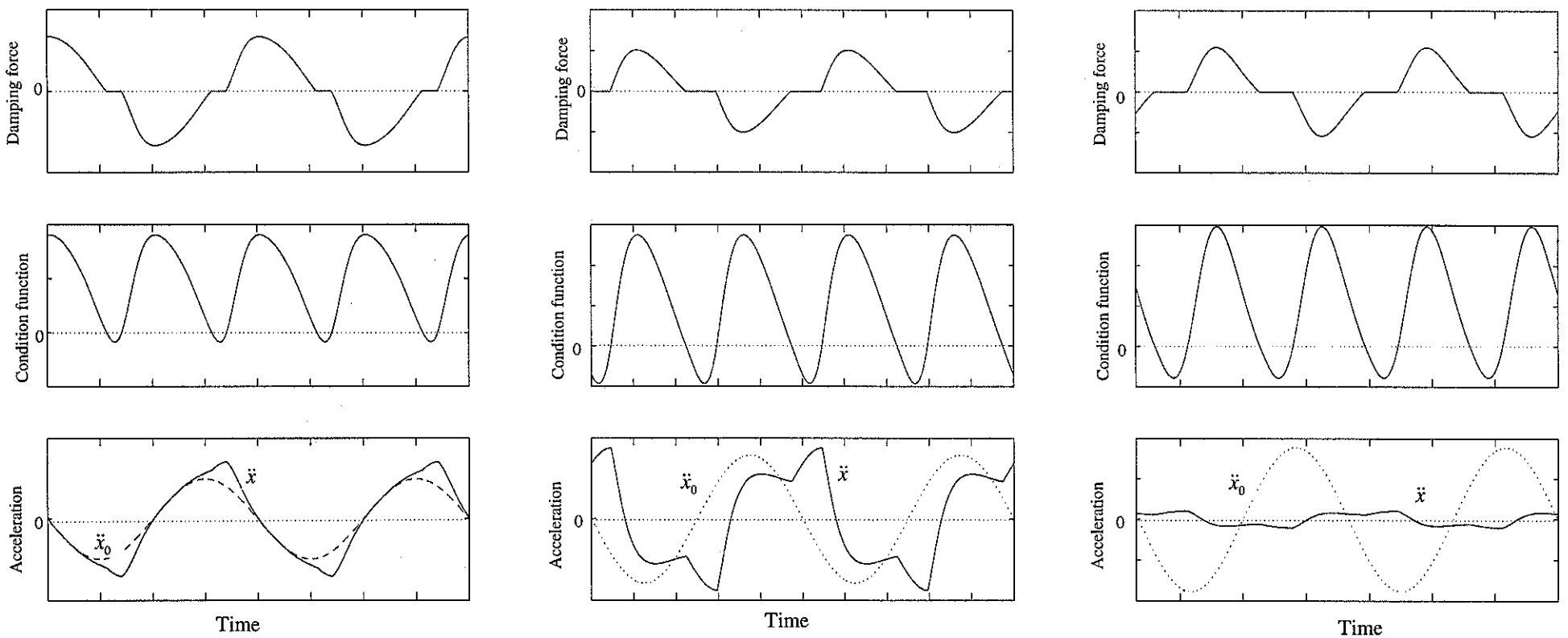

Figure 31 Steady-state response of SA-1 SDOF system (a) $\omega/\omega_n = 0.5$; (b) $\omega/\omega_n = 1$; (c) $\omega/\omega_n = 3$

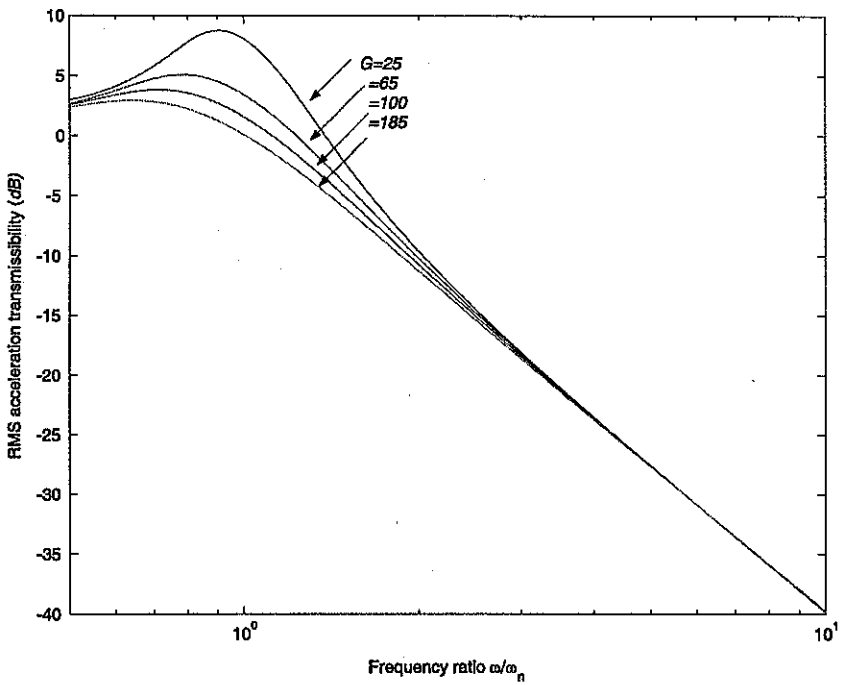

(a)

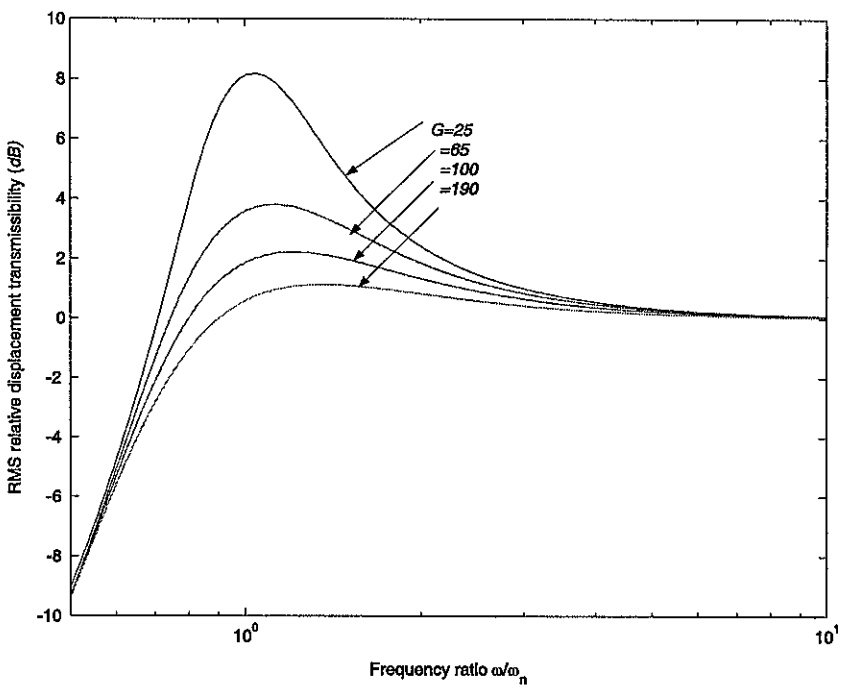

(b)

Figure 32 Transmissibility of SA-1 SDOF system (a) acceleration transmissibility; (b) relative transmissibility

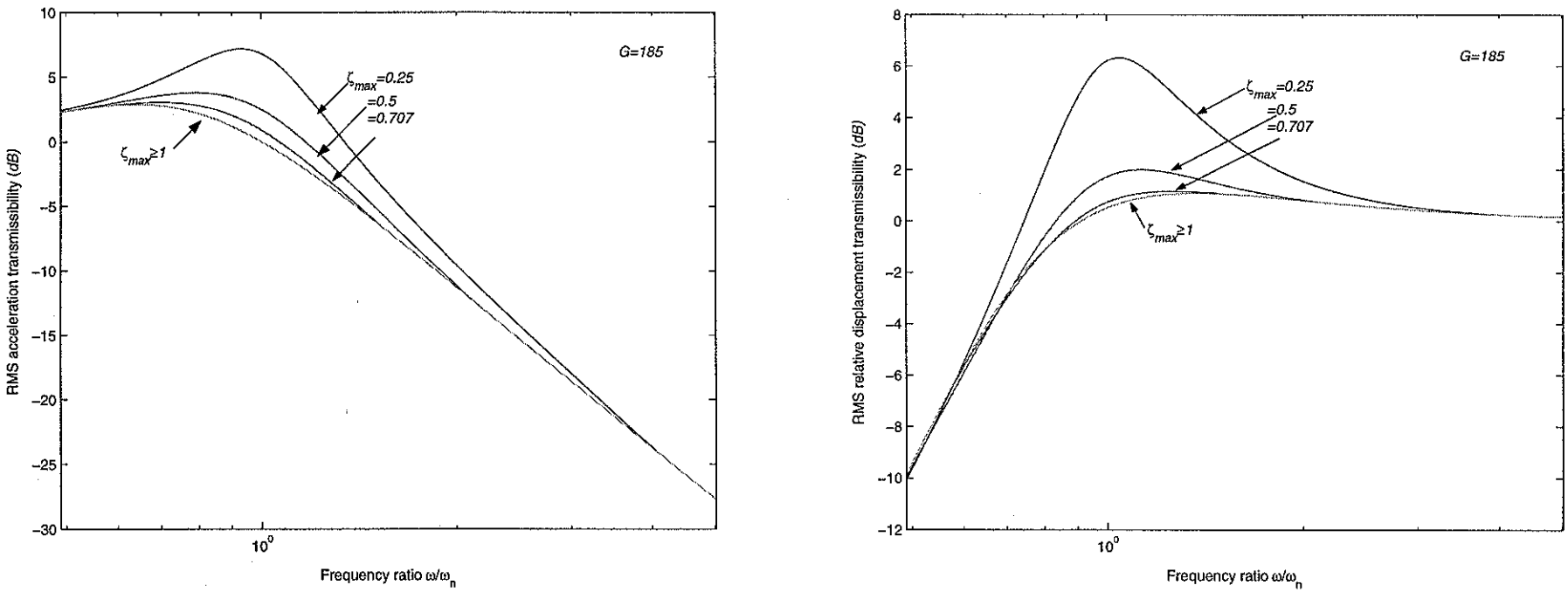

(a) (b)

Figure 33 Transmissibility of SA-1 SDOF system for various c_{max} with same G

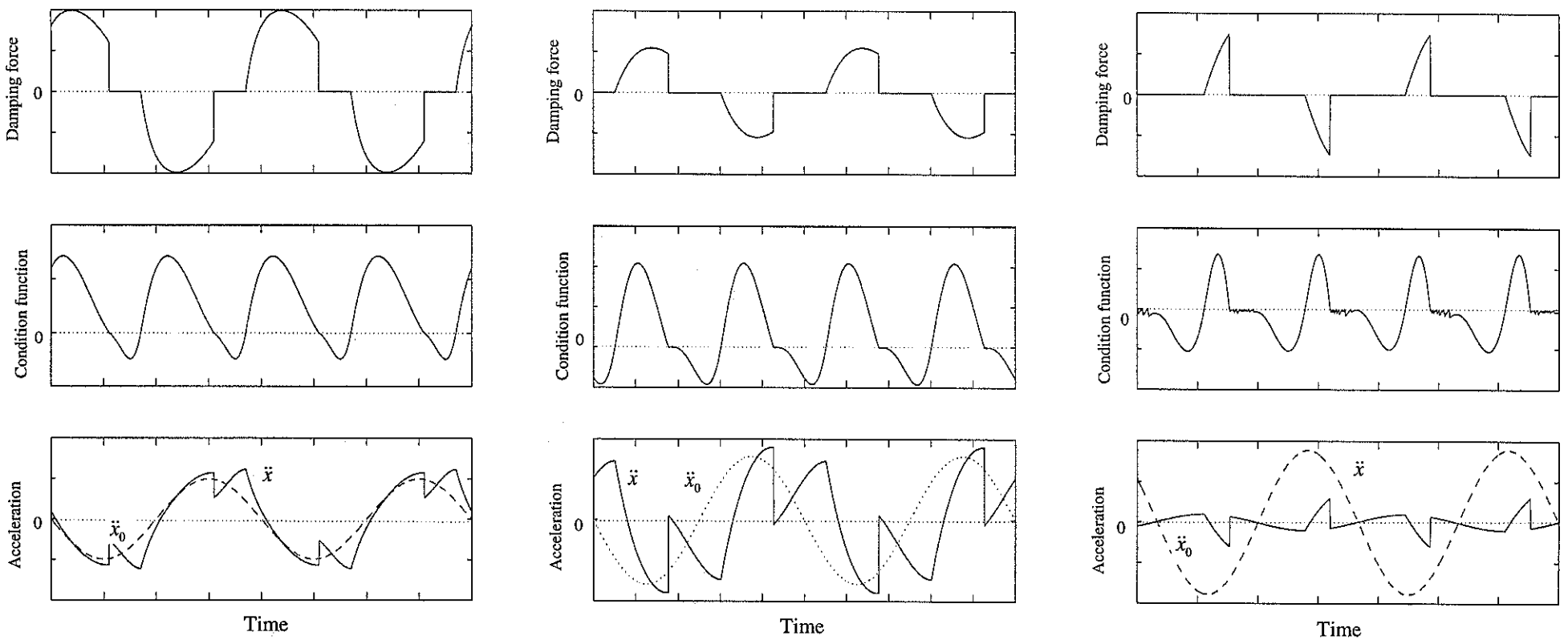

Figure 34 Steady-state response of SA-2 SDOF system at (a) $\omega/\omega_n = 0.5$; (b) $\omega/\omega_n = 1$; (c) $\omega/\omega_n = 3$

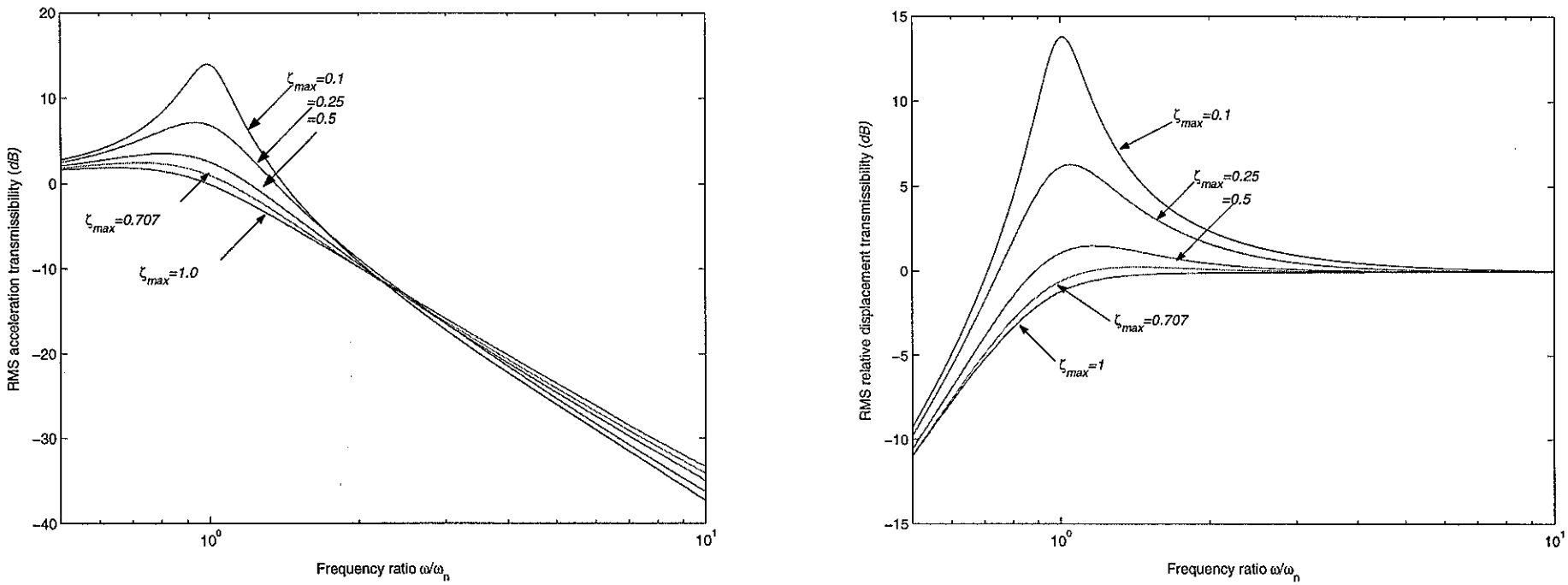

(a) (b)

Figure 35 Transmissibility of SA-2 SDOF system (a) acceleration transmissibility; (b) relative displacement transmissibility

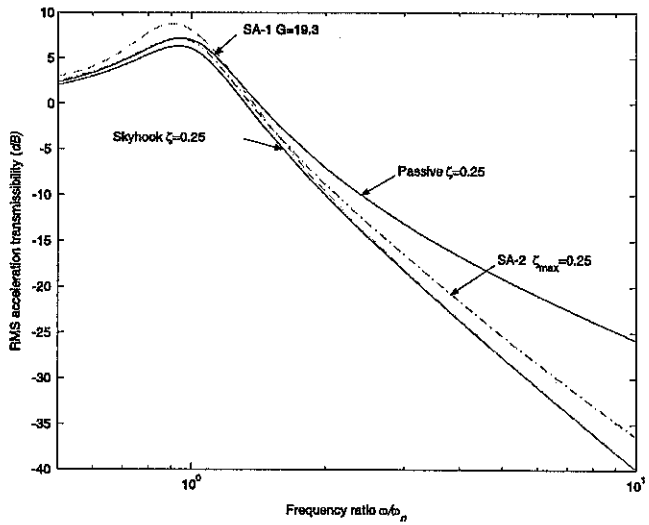
SA-1 G=19.3
Skyhook ζ=0.25
Passive ζ=0.25
SA-2 ζmax=0.25
RMS acceleration transmissibility (dB)
Frequency ratio ω/ωn

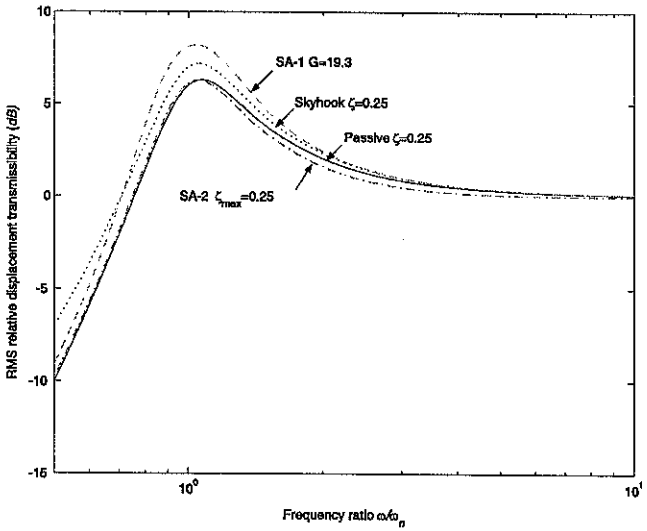
SA-1 G=19.3
Skyhook ζ=0.25
Passive ζ=0.25
SA-2 ζmax=0.25
RMS relative displacement transmissibility (dB)
Frequency ratio ω/ωn

(a)

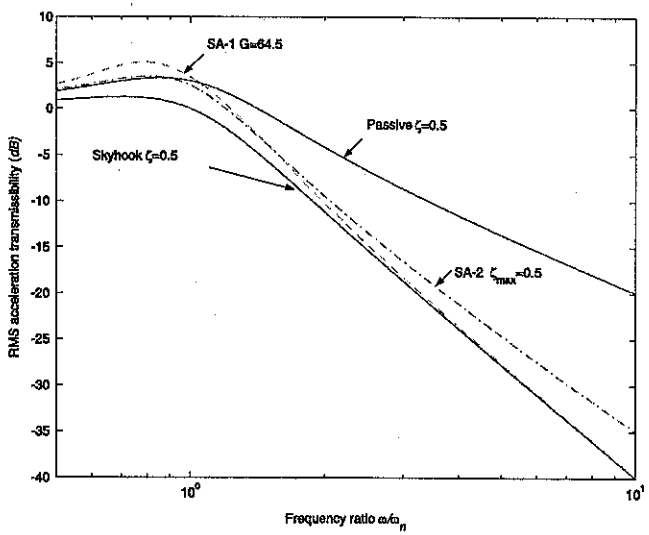
SA-1 G=64.5
Passive ζ=0.5
Skyhook ζ=0.5
SA-2 ζmax=0.5
RMS acceleration transmissibility (dB)
Frequency ratio ω/ωn

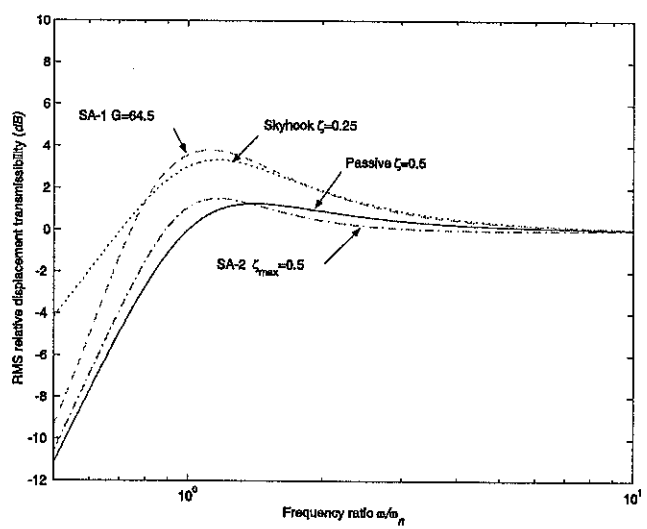
SA-1 G=64.5
Skyhook ζ=0.25
Passive ζ=0.5
SA-2 ζmax=0.5
RMS relative displacement transmissibility (dB)
Frequency ratio ω/ωn

(b)

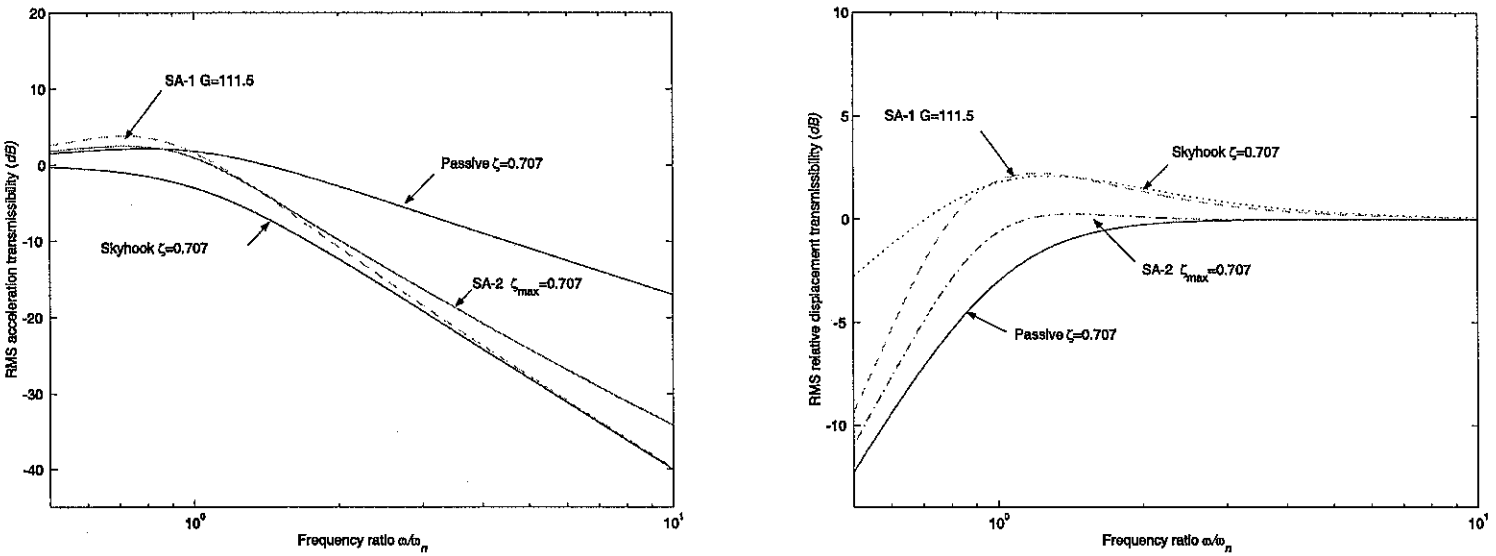

(c)

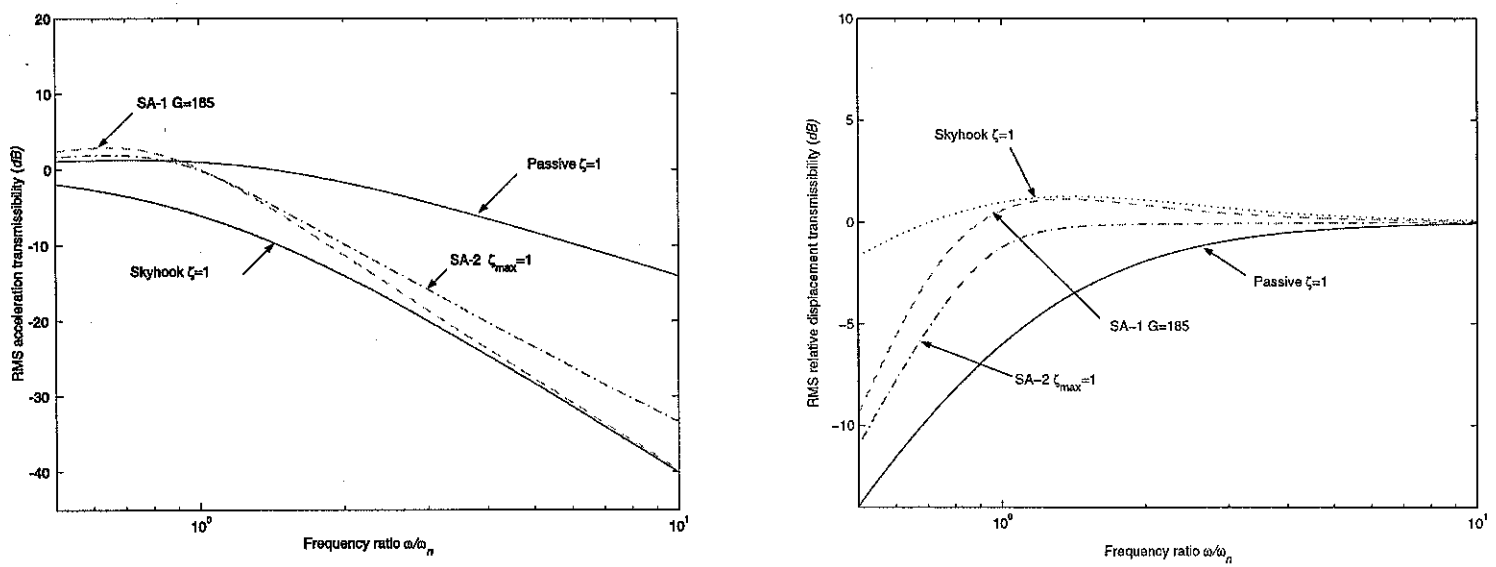

(d)

Figure 36 Comparison of the transmissibility of SA-1 and SA-2 SDOF system (a) $\zeta_{\max} = 0.25$; (b) $\zeta_{\max} = 0.50$; (c) $\zeta_{\max} = 0.707$; (d) $\zeta_{\max} = 1.0$

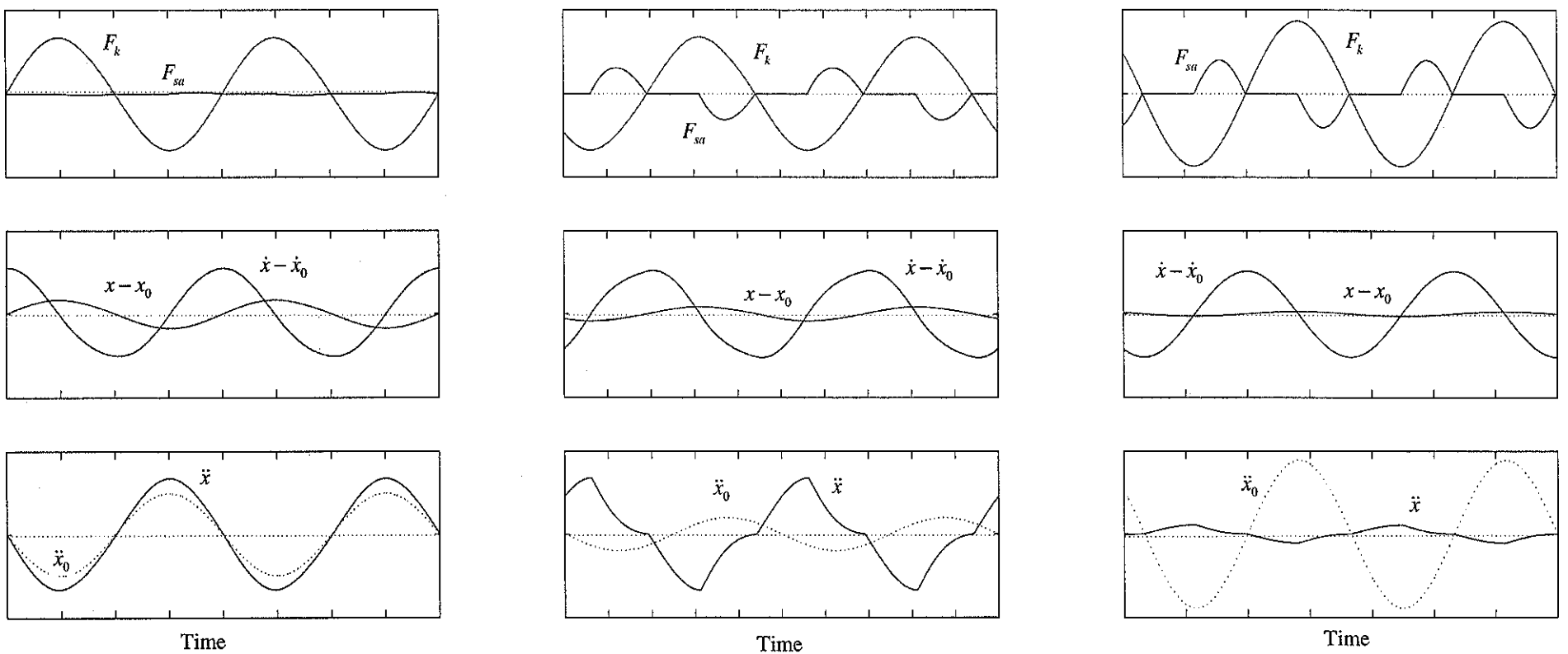

Figure 37 Steady-state response of SA-3 SDOF system at (a) $\omega/\omega_n = 0.5$; (b) $\omega/\omega_n = 1$; (c) $\omega/\omega_n = 3$

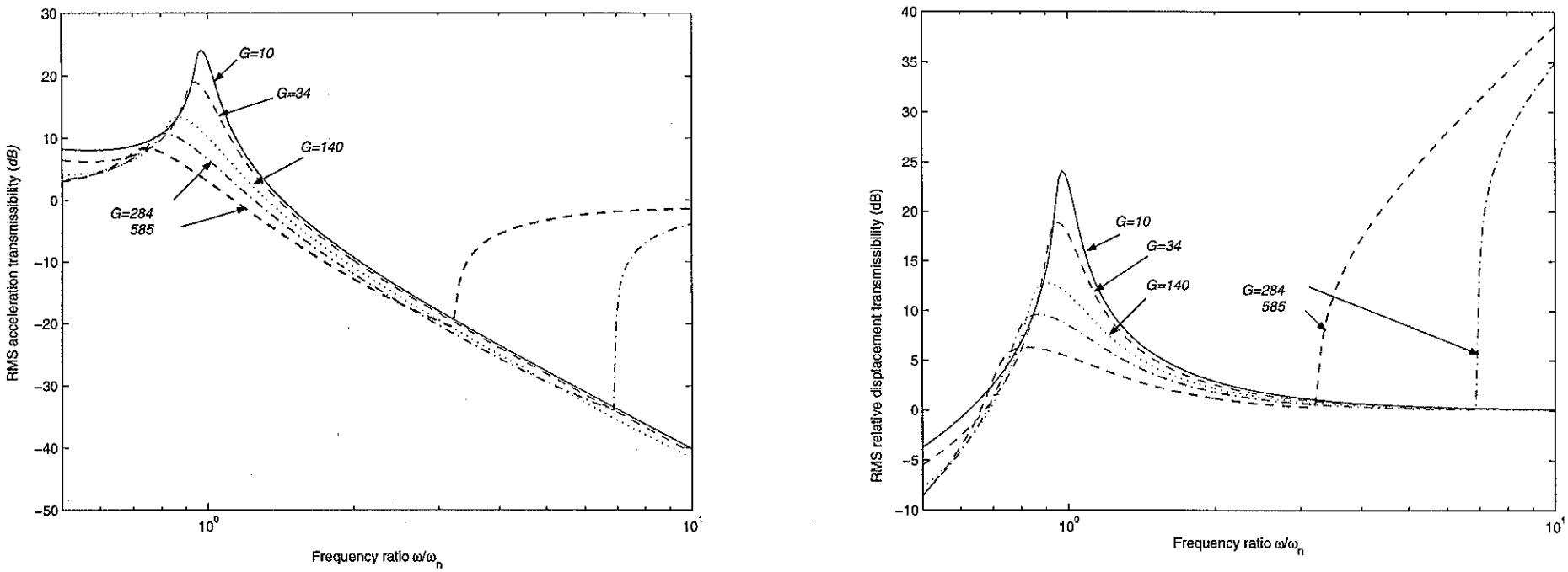

(a) (b)

Figure 38 Transmissibility of SA-3 SDOF system (a) acceleration transmissibility; (b) relative displacement transmissibility

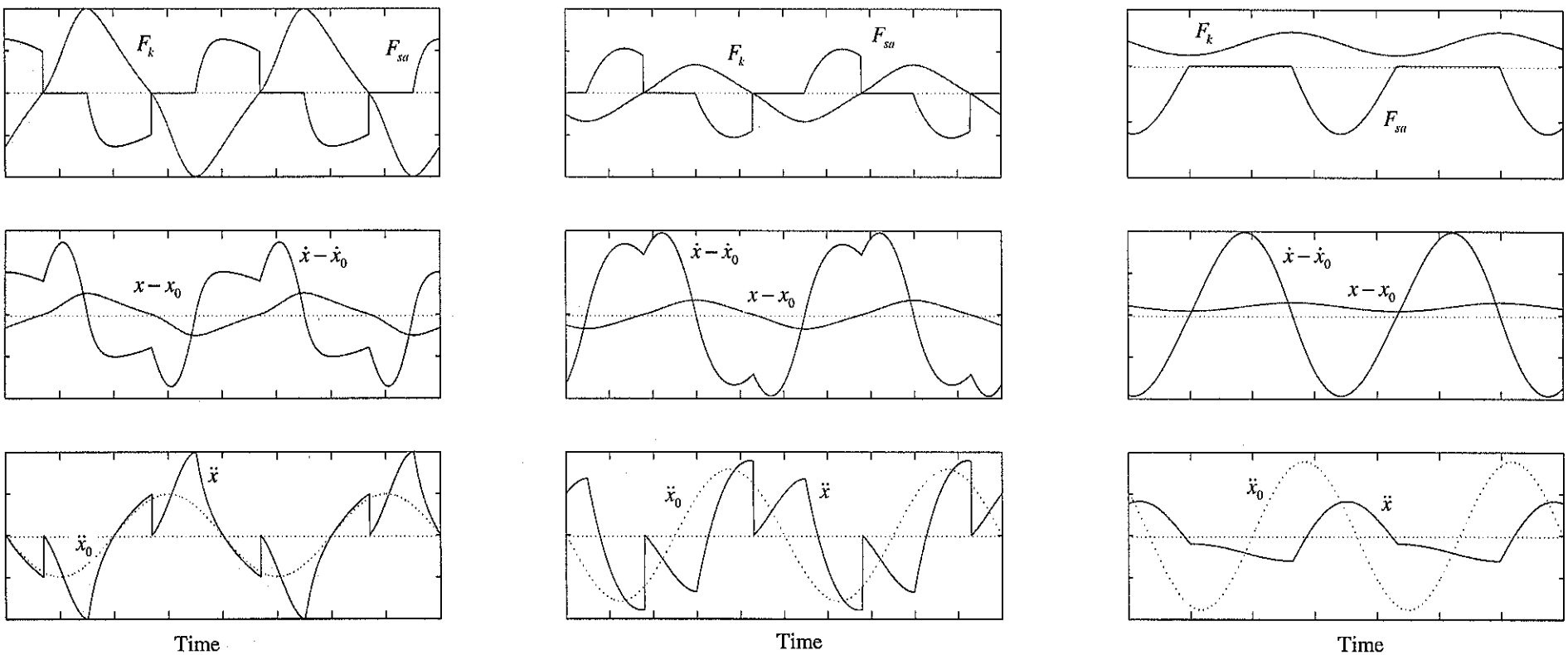

Figure 39 Steady-state response of SA-4 SDOF system at (a) $\omega/\omega_n = 0.5$; (b) $\omega/\omega_n = 1$; (c) $\omega/\omega_n = 3$

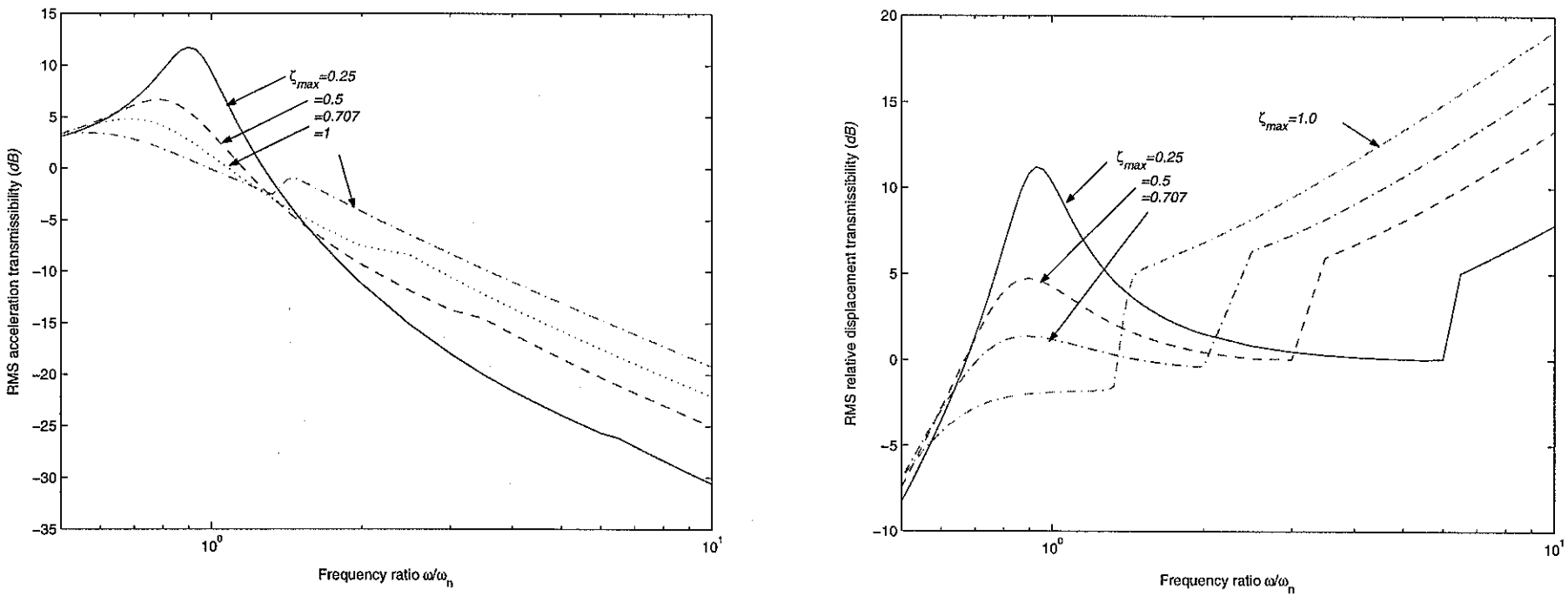

(a) (b)

Figure 40 Transmissibility of SA-4 SDOF system (a) acceleration transmissibility; (b) relative displacement transmissibility

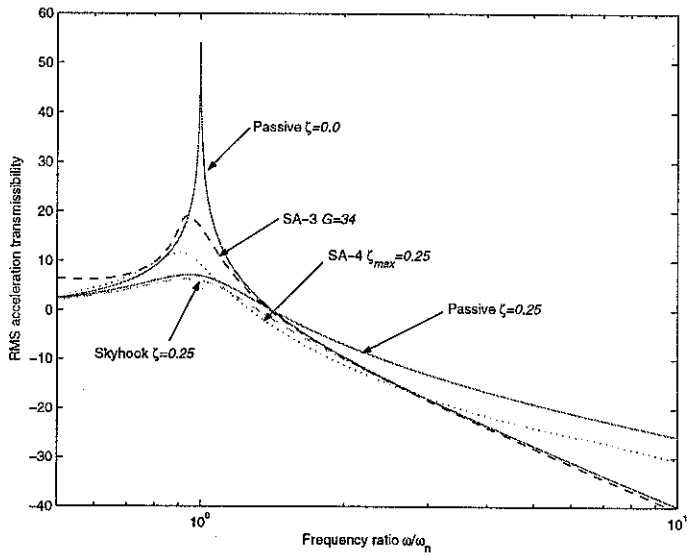
RMS acceleration transmissibility
Frequency ratio ω/ω_n
Passive ζ=0.0
SA-3 G=34
SA-4 ζ_max=0.25
Passive ζ=0.25
Skyhook ζ=0.25

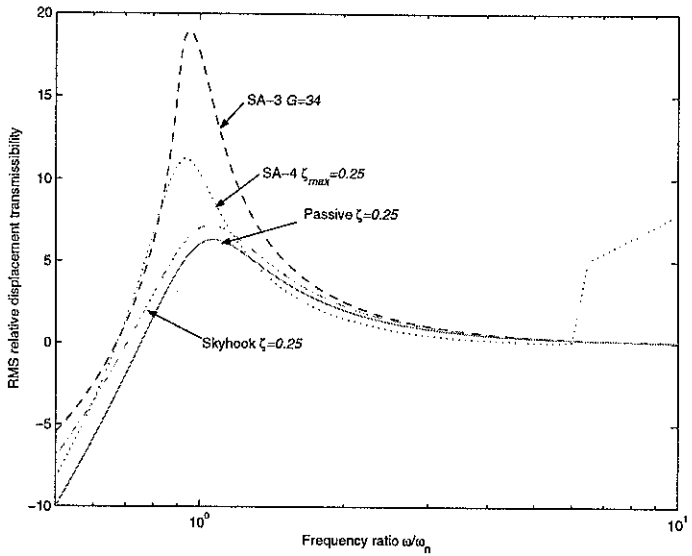
RMS relative displacement transmissibility
Frequency ratio ω/ω_n
SA-3 G=34
SA-4 ζ_max=0.25
Passive ζ=0.25
Skyhook ζ=0.25

(a)

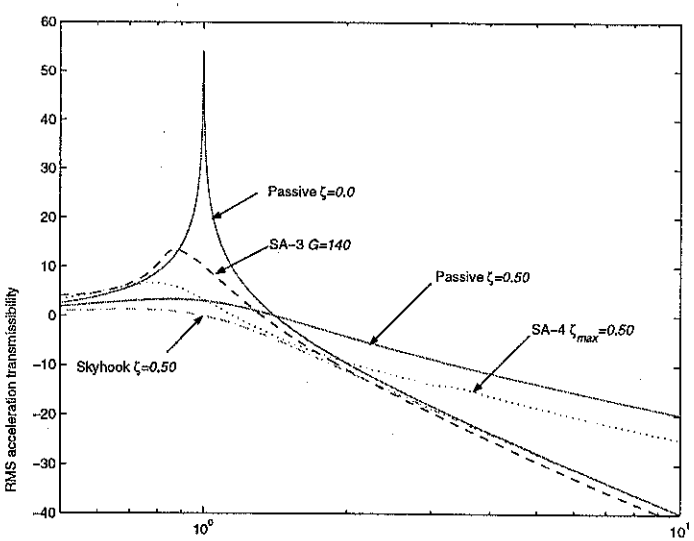
RMS acceleration transmissibility
Passive ζ=0.0
SA-3 G=140
Passive ζ=0.50
SA-4 ζ_max=0.50
Skyhook ζ=0.50

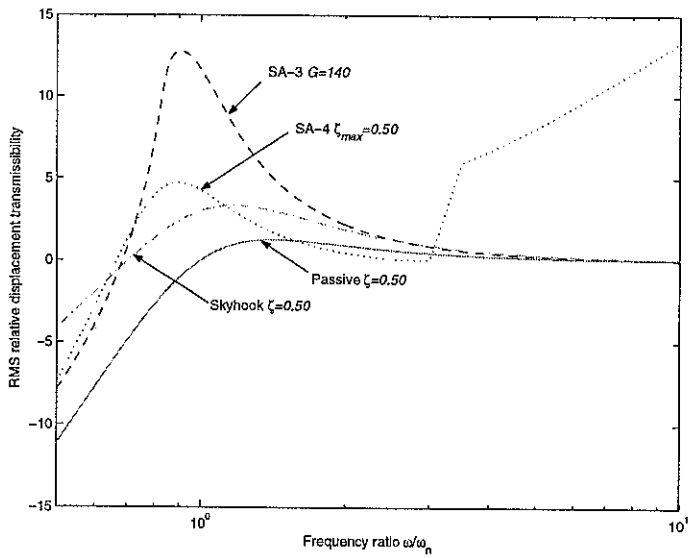
RMS relative displacement transmissibility
Frequency ratio ω/ω_n
SA-3 G=140
SA-4 ζ_max=0.50
Passive ζ=0.50
Skyhook ζ=0.50

(b)

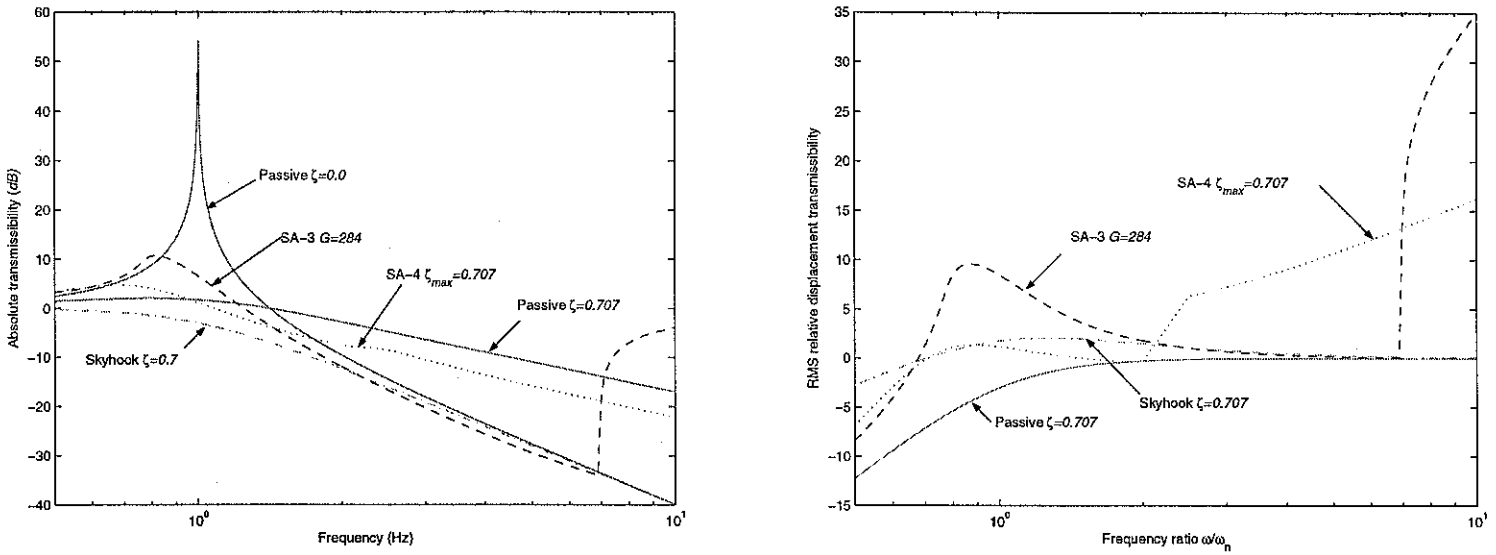

(c)

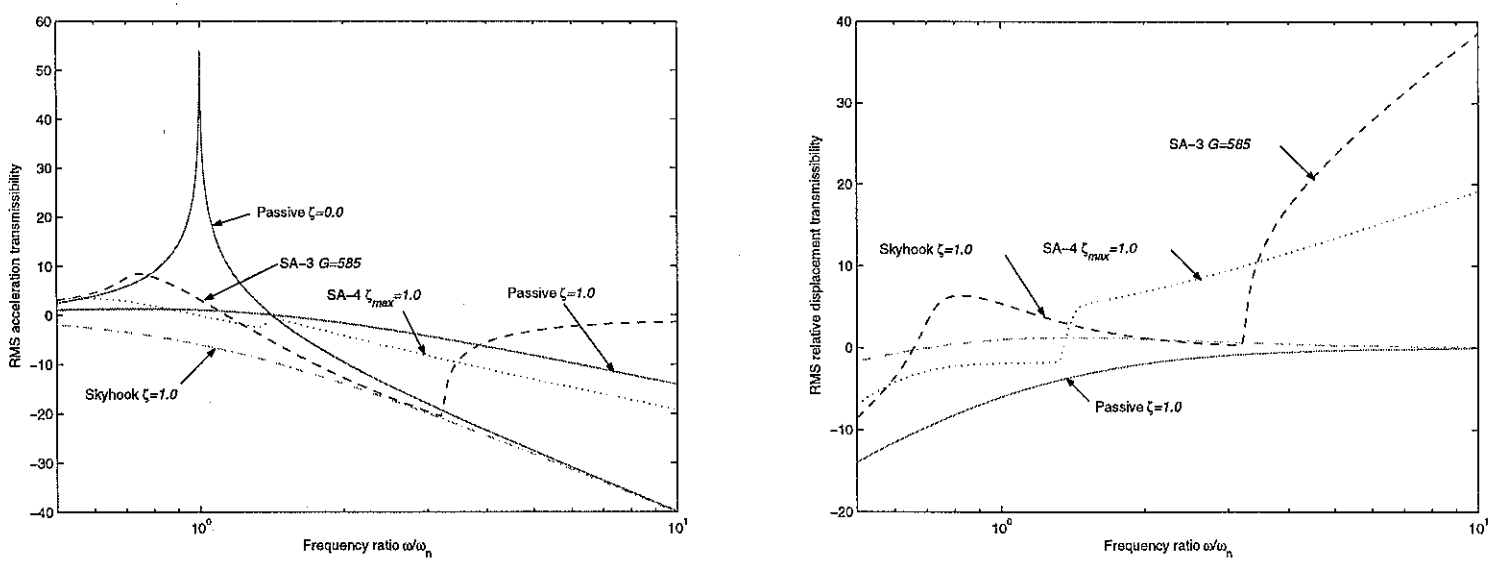

(d)

Figure 41 Comparison of the transmissibility of SA-3 and SA-4 SDOF system (a) $\zeta_{max} = 0.25$; (b) $\zeta_{max} = 0.50$; (c) $\zeta_{max} = 0.707$; (d) $\zeta_{max} = 1.0$

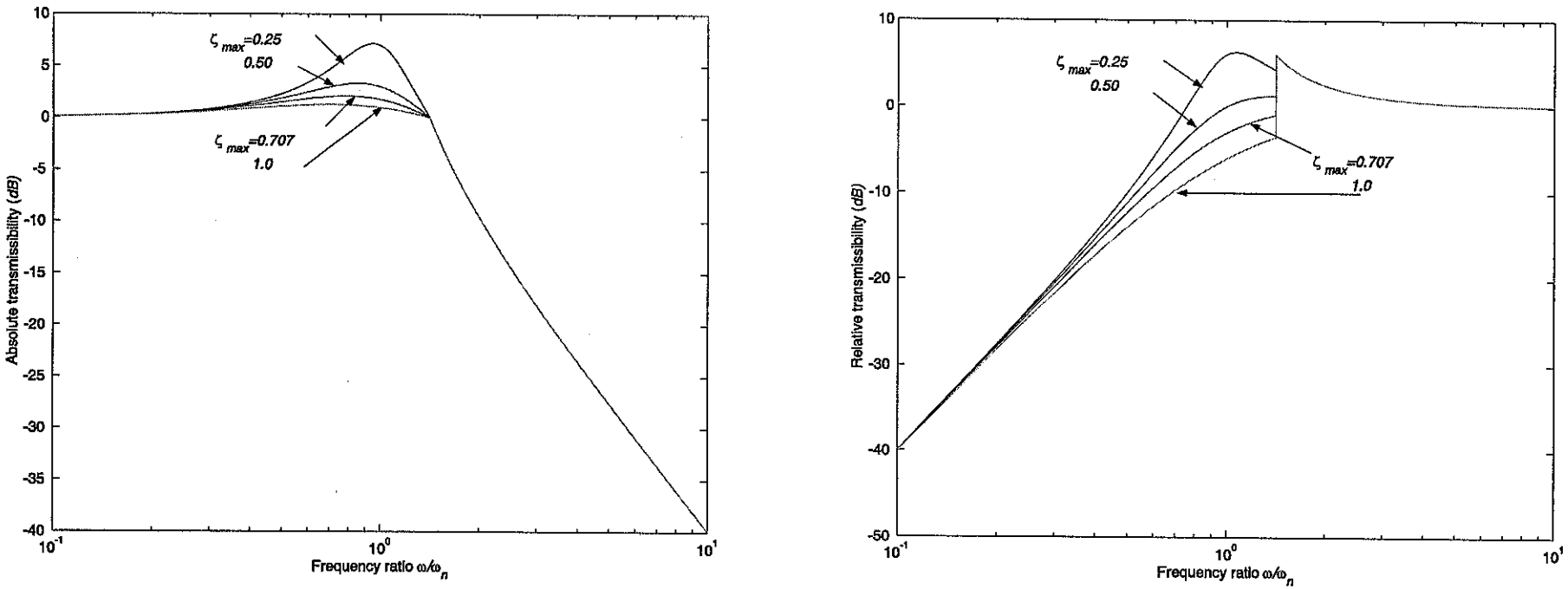

(a) (b)

Figure 42 Transmissibility of SA-5 system (a) acceleration transmissibility; (b) relative displacement transmissibility

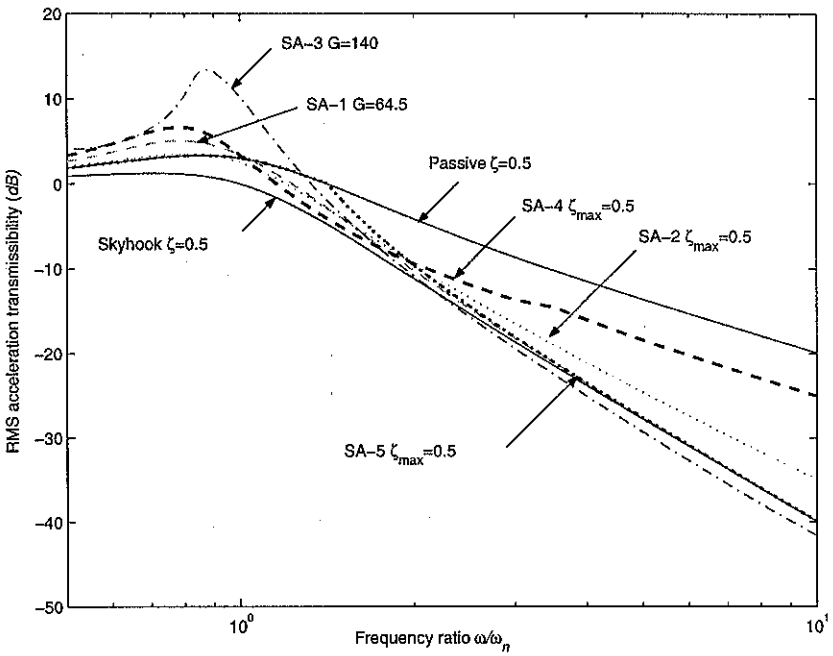
SA–3 G=140
SA–1 G=64.5
Passive ζ=0.5
SA–4 ζmax=0.5
SA–2 ζmax=0.5
Skyhook ζ=0.5
SA–5 ζmax=0.5
RMS acceleration transmissibility (dB)
Frequency ratio ω/ωn

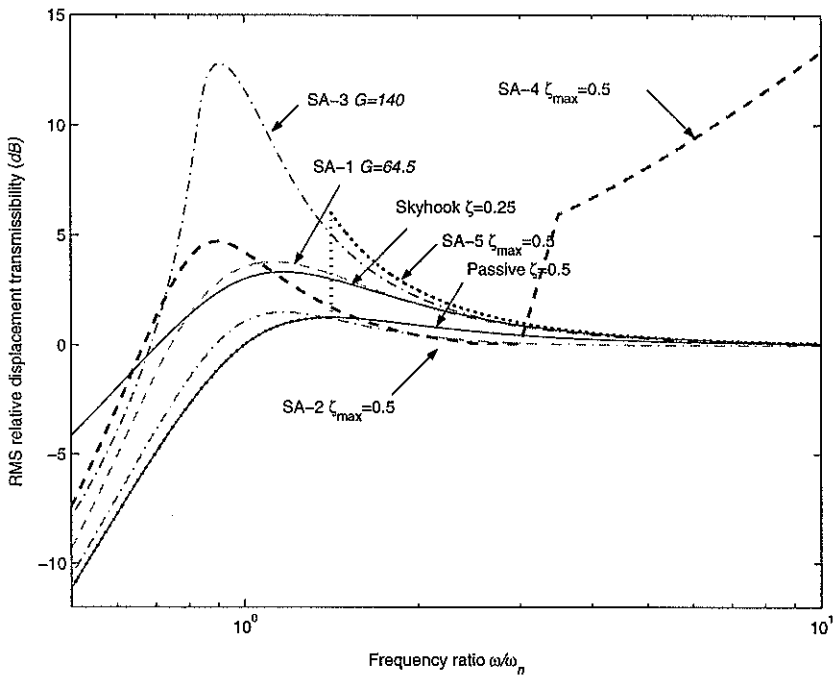
SA–3 G=140
SA–4 ζmax=0.5
SA–1 G=64.5
Skyhook ζ=0.25
SA–5 ζmax=0.5
Passive ζ=0.5
SA–2 ζmax=0.5
RMS relative displacement transmissibility (dB)
Frequency ratio ω/ωn

(a)

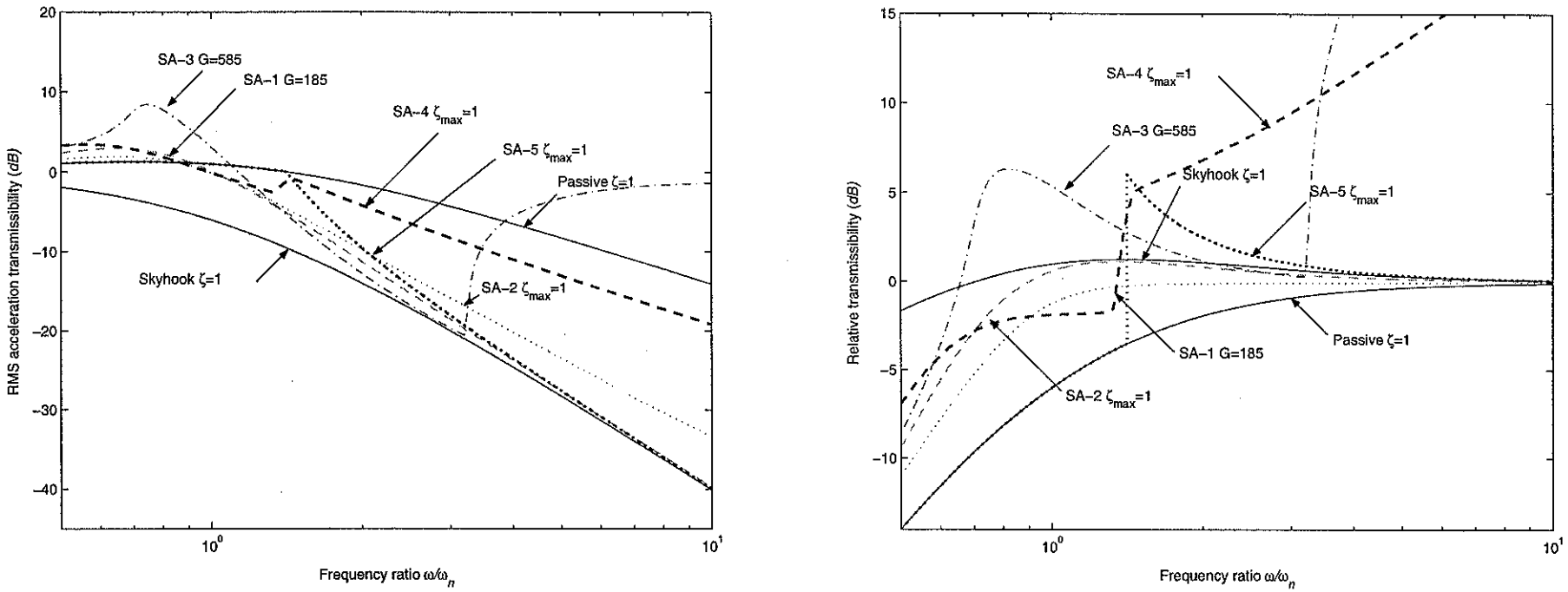

(b)

Figure 43 Comparison of the transmissibility of SDOF system with different types of dampers (a) moderate damping; (b) critical damping

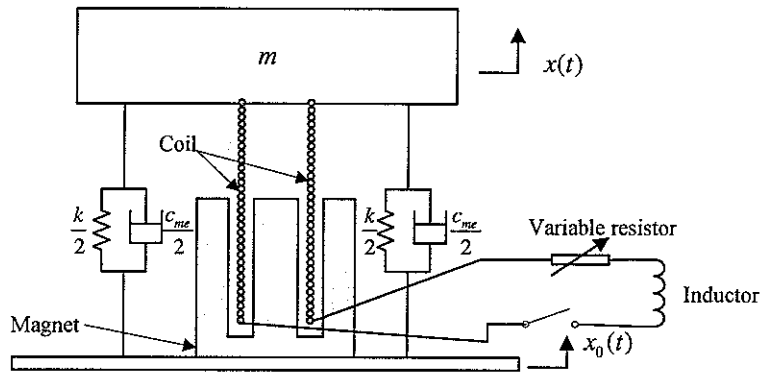

Figure 44 Model of base isolation system using an electromechenical damper

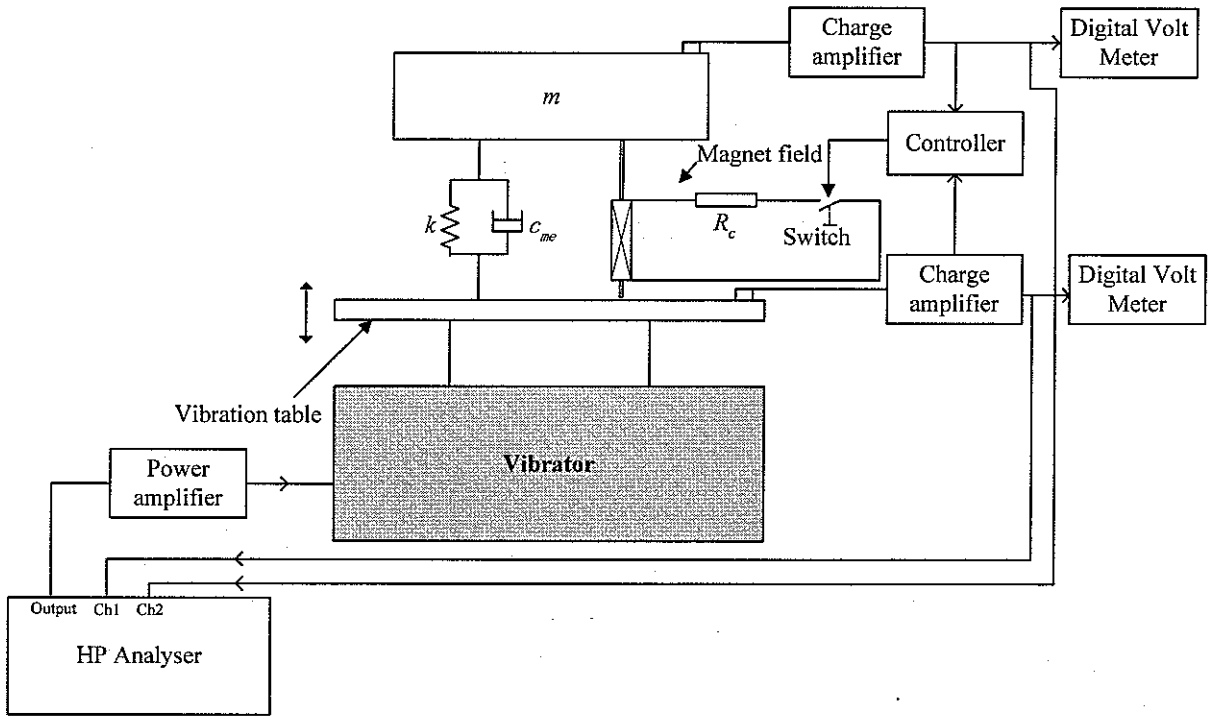

Figure 45 Schematic of the experimental setup

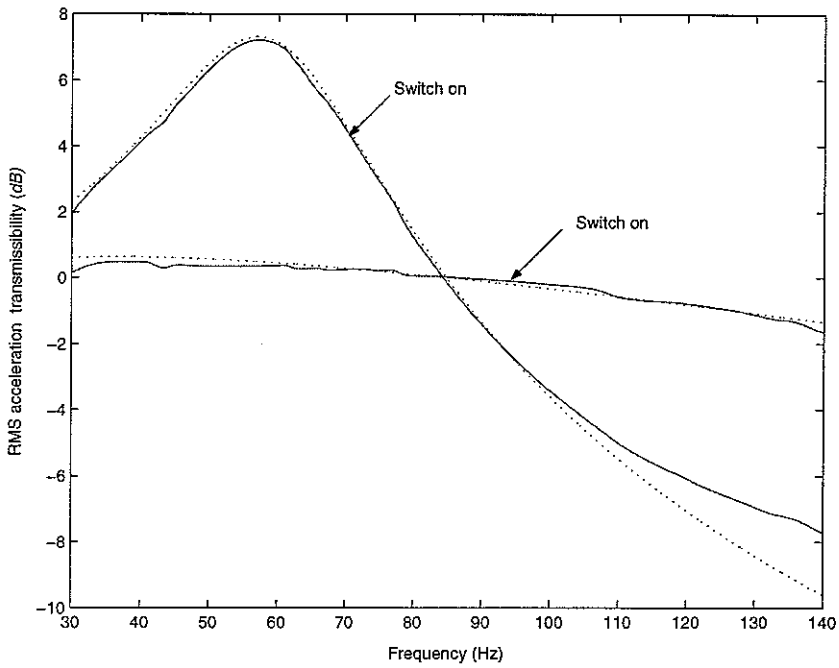

Figure 46 Measured rms acceleration transmissibility and comparison with theoretical results (—, measured results; ..., theoretical results)

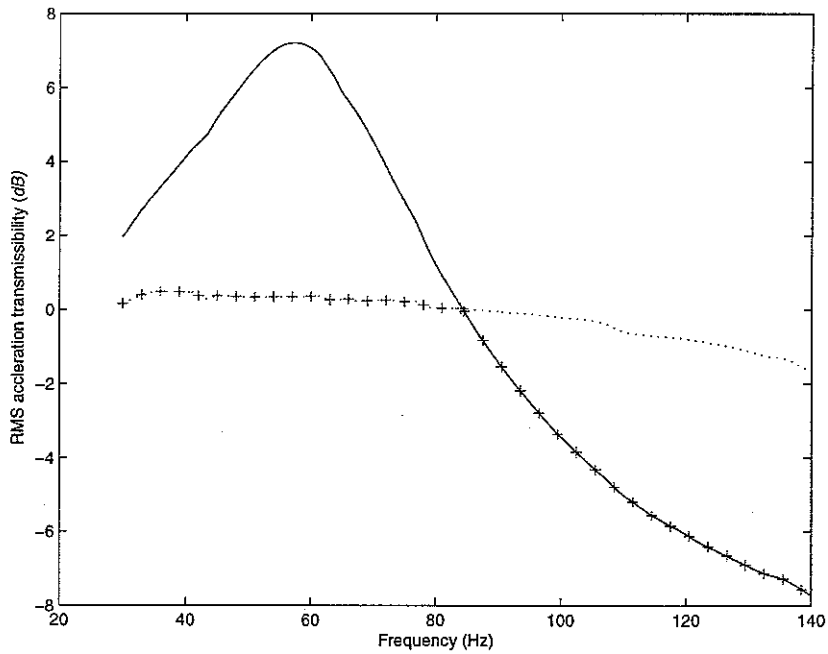

Figure 47 Acceleration transmissibility of SA-5 control algorithm (—, switch off ; ..., switch on; +, SA-5)

Appendix A

Isolation Properties of Semi-Active Dampers

From the results in section 5, it can be seen that semi-active damper is capable of providing better isolation across the whole spectrum as compared to a passive damper. The primary purpose of this section is to investigate thoroughly the isolation properties of semi-active systems. Specifically the following question will be answered: Why are semi-active dampers able to isolate at frequencies well below that which is possible with a passive damper, even though, similar to passive damper, they do not add any energy to the system?

To answer this question, consider a base excited SDOF system. The response of a passive system to a harmonic base-excitation, such as

$$x_0 = X_0 e^{i\omega t} \tag{A.1}$$

is given by

$$x = X_0 \left| H(\omega) \right| e^{i(\omega t - \phi)} \tag{A.2}$$

where

$$\left| H(\omega) \right| = \left[\frac{1 + \left(2\zeta \frac{\omega}{\omega_n} \right)^2}{\left[1 - \left(\frac{\omega}{\omega_n} \right)^2 \right]^2 + \left(2\zeta \frac{\omega}{\omega_n} \right)^2} \right]^{\frac{1}{2}} \tag{A.3}$$

and

$$\phi = \tan^{-1} \left(\frac{2\zeta \left(\frac{\omega}{\omega_n} \right)^3}{1 - \left(\frac{\omega}{\omega_n} \right)^2 + \left(2\zeta \frac{\omega}{\omega_n} \right)^2} \right) \tag{A.4}$$

The variables $\left| H(\omega) \right|$ and ϕ represent the transmissibility amplitude and phase shift between the input and output. ξ and ω_n are damping ratio and natural frequency of the system, respectively.

The behavior of the system for different damping ratios and input frequencies is shown in Figure A.1. It can be seen that increasing the damping reduces the resonance response, but it deteriorates the isolation performance in the isolation range where $\omega/\omega_n > \sqrt{2}$. This represents the well-known compromise between better control of resonance and less vibration isolation due to damping. The phase diagram in Figure A.2 indicates that increasing damping contributes to a lower phase difference (i.e. stronger coupling) between the base and the sprung mass. Further discussions on this subject can be found in most vibration text books, for example [17].

To determine the reason for the above, and also why semi-active dampers are able to isolate at frequencies far below the fixed frequency of system with passive dampers, the transmissibility equation for the system in Figure 6 is derived. Unlike the passive system, it is not possible to derive the transmissibility equation for the semi-active system because the damping coefficient is time dependent. Alternatively, we consider its equivalent where the damper is connected between the mass and an imaginary sky, as shown in Figure 5.

For this system, the transmissibility amplitude and phase are:

$$H(\omega) = \frac{1}{\left\{\left[1-\left(\frac{\omega}{\omega_n}\right)^2\right]^2 + \left[2\zeta\left(\frac{\omega}{\omega_n}\right)\right]^2\right\}^{1/2}} \tag{A.5}$$

$$\phi = \tan^{-1}\frac{2\zeta\frac{\omega}{\omega_n}}{1-\left(\frac{\omega}{\omega_n}\right)^2} \tag{A.6}$$

The transmissibility and phase of the skyhook damper are shown in Figure A.3 and Figure A.4. Comparing equations of (A.5)and (A.6) provides the insight as follows. The transmissibility amplitudes have the same denominators but different numerators. For a passive system, the numerator is a function of damping ratio, ζ, where as for a semi-active system, it is a constant. Table A.1 shows the effect of ζ on transmissibility in different frequency ranges for a passive system. The table is derived from evaluating the numerator and denominator of equation (A.3), which shows that the frequency range in which amplification, direct transmission and attenuation occurs is independent of the damping ratio ζ.

Examining equation (A.5)-(A.6) shows that a skyhook damper yields completely different results. The numerator is a constant, and therefore the transmissibility is relative to unity depends whether the denominator is less than, greater, or equal to 1. Evaluating the denominator for one of the three possibilities will allow us to make conclusions on the effect of ζ on the transmissibility magnitude. Consider the frequency range where some isolation is achieved. For this to happen, the frequency ratio must be such that:

$$\left[1-\left(\frac{\omega}{\omega_n}\right)^2\right]^2+\left[2\zeta\left(\frac{\omega}{\omega_n}\right)\right]^2 \geq 1 \tag{A.7}$$

which will reduce to

$$\left(\frac{\omega}{\omega_n}\right)^2 \geq 2-4\zeta^2 \tag{A.8}$$

The above equation shows that for semi-active system, as ζ increases, attenuation occurs at lower frequencies, unlike a passive system in which the isolation is independent of ζ. Two special cases exist in the equation, the first of which is when $\zeta=0$, the equation reduces to $\frac{\omega}{\omega_n} \geq \sqrt{2}$. This indicates that when no damping is present, isolation stars at $\omega=\sqrt{2}\omega_n$, the fixed frequency of passive system. For $\zeta>0$, isolation stars at frequencies smaller than $\sqrt{2}\omega_n$, thus we can conclude for a given ζ, a semi-active system behaving as a skyhook system can always provide better isolation performance than passive ones.

The second case is when

$$2-4\zeta^2=0$$

or

$$\zeta=\frac{\sqrt{2}}{2}=0.707 \tag{A.9}$$

This is the minimum damping ratio at which the semi-active system provides isolation at all frequencies. Therefore, it is possible to tune a semi-active system such that it can provide isolation across the whole frequency.

The passive representation of the semi-active system assumes that the off-state damping is zero. In practice, however, it is not possible and may not desirable. In most cases, c_{off} is a

small portion of the on-state damping. Therefore, in reality, the passive representation of the semi-active system dampers appears as shown in Figure A.5.

This modifies the transmissibility equation to:

$$|H(\omega)| = \left[\frac{1 + \left[2\zeta_{off} \frac{\omega}{\omega_n} \right]^2}{\left[1 - \left(\frac{\omega}{\omega_n} \right)^2 \right]^2 + \left[2(\zeta_{on} + \zeta_{off}) \left(\frac{\omega}{\omega_n} \right) \right]^2} \right]^{1/2} \tag{A.10}$$

$$\phi = \tan^{-1} \left[\frac{2 \left[(\zeta_{on} + \zeta_{off}) \frac{\omega}{\omega_n} - \zeta_{off} \frac{\omega}{\omega_n} + \zeta_{off} \left(\frac{\omega}{\omega_n} \right)^3 \right]}{1 - \left(\frac{\omega}{\omega_n} \right)^2 + 4(\zeta_{on} + \zeta_{off}) \zeta_{off} \left(\frac{\omega}{\omega_n} \right)^2} \right] \tag{A.11}$$

where

$$\zeta_{on} = \frac{c_{on}}{2m\omega_n}; \zeta_{off} = \frac{c_{off}}{2m\omega_n} \tag{A.12}$$

Figure A.6 and A.7 show the transmissibility and phase angle of the skyhook system with off-state damping. Comparing Figure A.6 with Figure A.3 shows that the insertion of off-state damping has two effects compared to the system without off-state damping: (1) it reduces the RMS acceleration ratio at and around the natural frequency; (2) it increases the RMS acceleration ratio at frequencies greater that natural frequency.

Table A.1 Effect of ζ on transmissibility in frequency ranges for a passive SDOF

$\frac{\omega}{\omega_n}$	$\left[1 - \left(\frac{\omega}{\omega_n} \right)^2 \right]^2$	$\lvert H(\omega) \rvert$	
<1	<1	>1	Amplification
=1	=0	>1	Amplification
$1<\bullet<\sqrt{2}$	<1	>1	Amplification
$=\sqrt{2}$	=1	=1	Direct transmission
$>\sqrt{2}$	>1	<1	Isolation

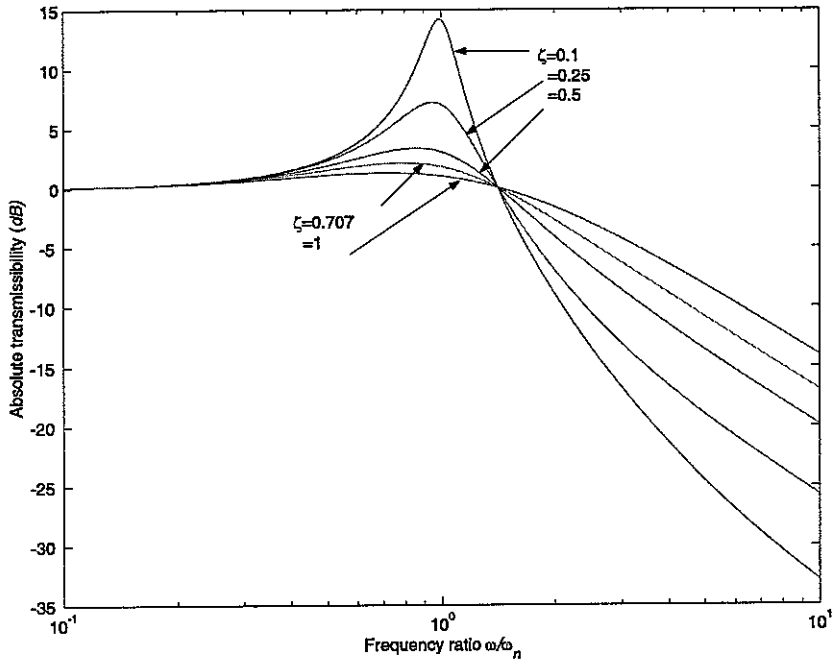

Figure A.1 Acceleration transmissibility of passive SDOF system

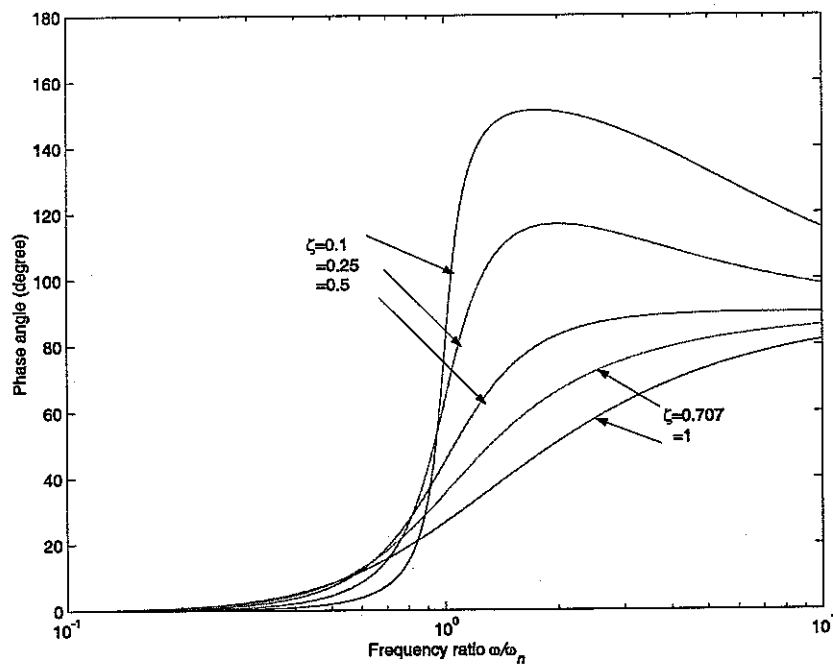

Figure A.2 Transmissibility phase of passive SDOF system

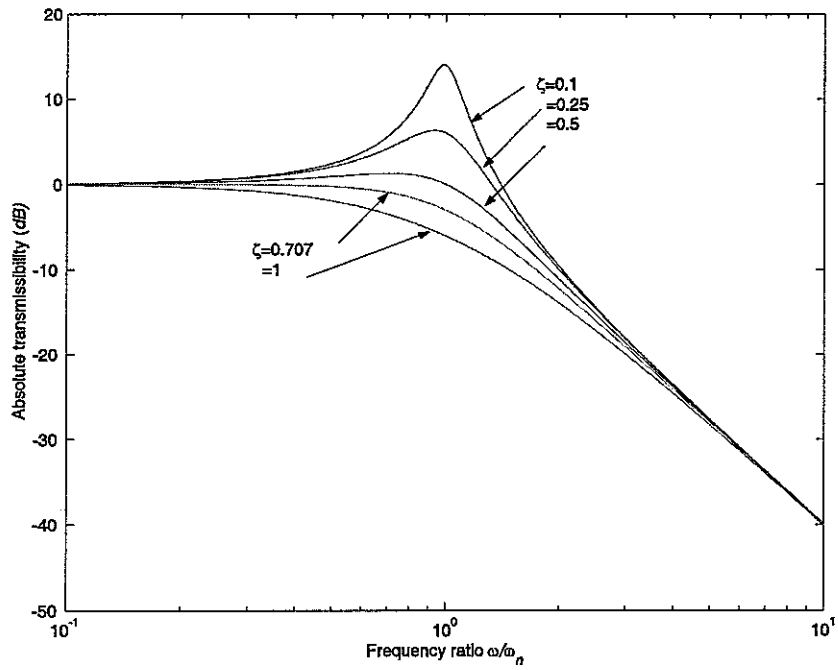

Figure A.3 Acceleration transmissibility of skyhook damper system

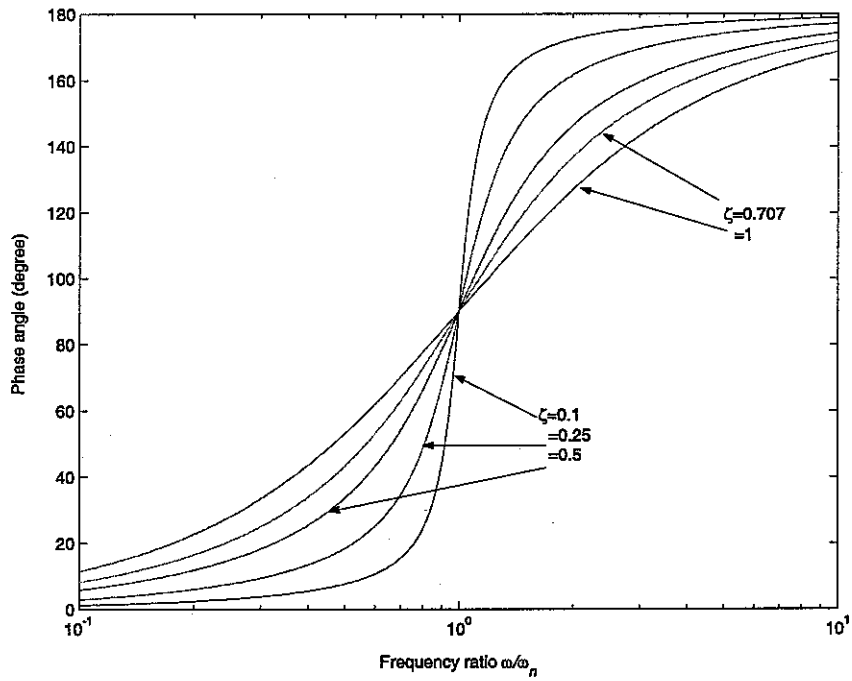

Figure A.4 Transmissibility phase of skyhook system

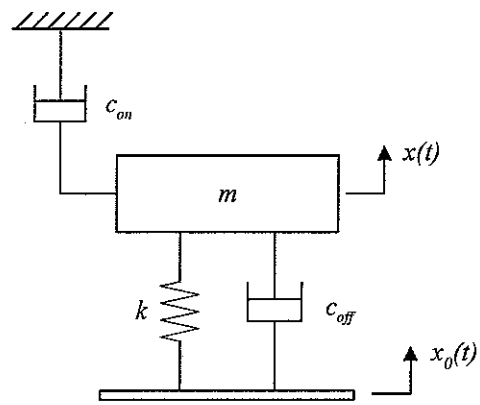

Figure A.5 Actual representation skyhook system

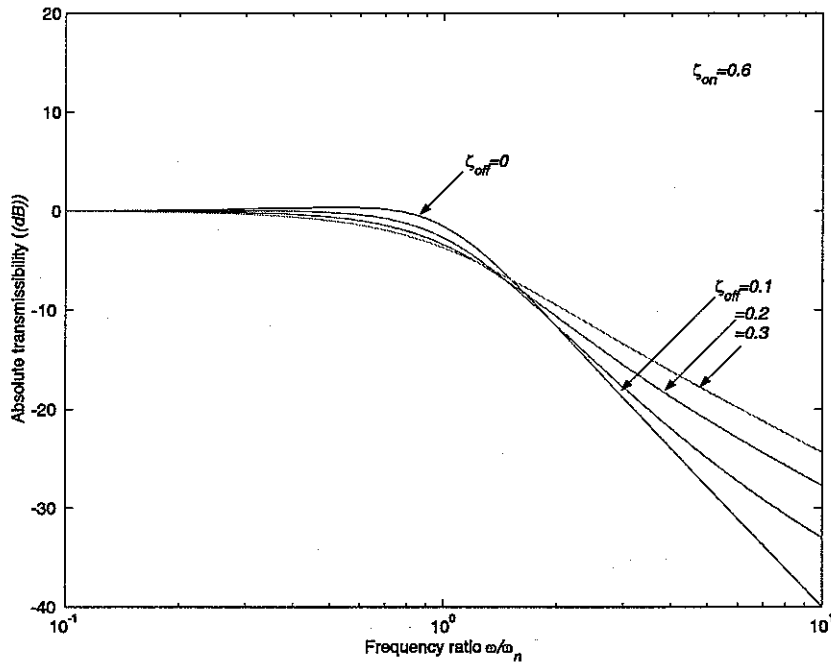

Figure A.6 Absolute transmissibility of actual skyhook damper system

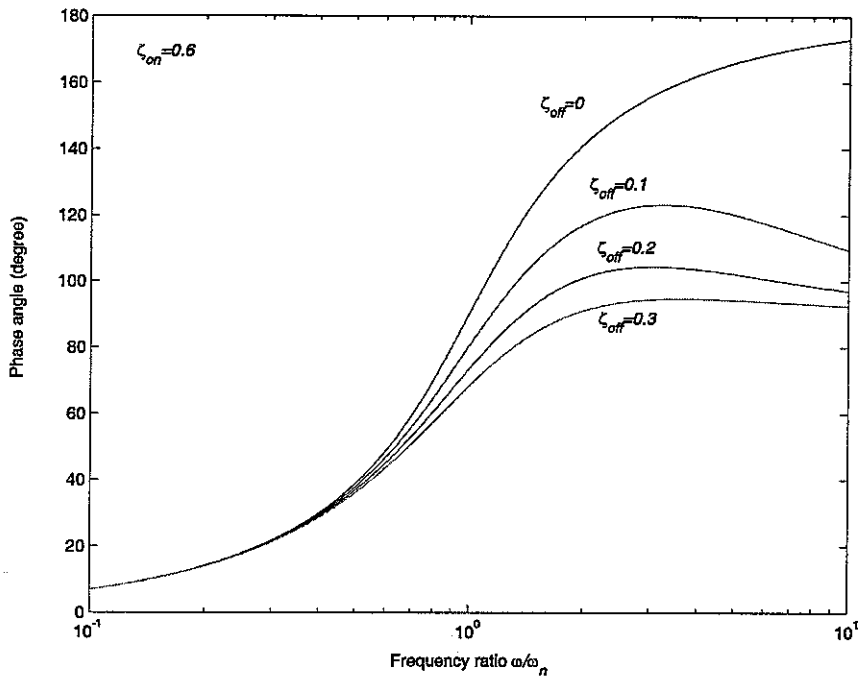

Figure A.7 Transmissibility phase of actual skyhook damper system

Appendix B

List of Equipments Used for the Experiment

Equipment	Serial Number	Quantity
HP 35655A Analyser	2911A01088	1
Derritron Vibrator Type VP.4	325	1
TPA series Professional Power Amplifier	8252	1
Colossus 12 MB Loudspeaker Driver	14314	1
B&K 4393 Accelerometer	1697354 1697154	2
B&K 2635 Charge Amplifier	943130 1474190	2
Wavetek DM25XT Digital Meter	60405182	1
HM 303-6 Analog Oscilloscope	25620	1
Carling Switch	9403	1

Appendix C

Specifications for Colossus 12MB Loudspeaker Driver

Mounting information:	
Overall Diameter	*330.2 mm*
Width Across Flats	309.5 mm
Depth	137 mm
Weight	7.8 kg
Electro mechanical specifications:	
Impedance	*8 Ω*
Resonance	*55 Hz*
Moving Mass inc. Air Load	*59 g*
BL Product	*18.3 N/A*
Flux Density	*1.16 Tesla*
Magnetic Gap Depth	*9 mm*
Coil Winding Height	*18 mm*
Voice Coil Length	*21.8 m*
Voice Coil Diameter	*77 mm*